BAŞKENT UNIVERSITY
INSTITUTE OF SCIENCE
DEPARTMENT OF MOLECULAR BIOLOGY AND GENETICS
MASTER OF SCIENCE IN
MOLECULAR BIOLOGY AND GENETICS

COLLAGEN/KERATIN/ALGINATE HYDROGEL FOR AN IN VITRO THREE-DIMENSIONAL CO-CULTURE OF FIBROBLASTS AND KERATINOCYTES

BY

KAAN YILDIRIM

MASTER OF SCIENCE THESIS

ANKARA-2025

BAŞKENT UNIVERSITY
INSTITUTE OF SCIENCE
DEPARTMENT OF MOLECULAR BIOLOGY AND GENETICS
MASTER OF SCIENCE IN
MOLECULAR BIOLOGY AND GENETICS

COLLAGEN/KERATIN/ALGINATE HYDROGEL FOR AN IN VITRO THREE-DIMENSIONAL CO-CULTURE OF FIBROBLASTS AND KERATINOCYTES

BY

KAAN YILDIRIM

MASTER OF SCIENCE THESIS

ADVISOR
ASSIST. PROF. DR. ÖZGE ERDEMLİ

ANKARA-2025

BAŞKENT UNIVERSITY
INSTITUTE OF SCIENCE

This study, which was prepared by Kaan YILDIRIM, for the program of Master of Science with Thesis (English), has been approved in partial fulfillment of the requirements for the degree of MASTER OF SCIENCE in MOLECULAR BIOLOGY AND GENETICS Department by the following committee.

Date of Thesis Defense: 07/02/ 2025

Thesis Title: Collagen/Keratin/Alginate Hydrogel for an In Vitro Three-Dimensional Co-Culture of Fibroblasts and Keratinocytes

Examining Committee Members	**Signature**
Assoc. Prof. Dr. Bengi YILMAZ ERDEMLİ, University of Health Sciences	……
Assist. Prof. Dr. Özge ERDEMLİ, Başkent University	……
Assoc. Prof. Dr. Ömer AKTÜRK, Kırıkkale University	……

APPROVAL
Prof. Dr. Dilek ÇÖKELİLER SERDAROĞLU
Director, Institute of Science
Date: … / … / ……..

BAŞKENT UNIVERSITY

INSTITUTE OF SCIENCE

YÜKSEK LİSANS / DOKTORA TEZ ÇALIŞMASI ORİJİNALLİK RAPORU

Tarih: 20/ 02/ 2025

Öğrencinin Adı, Soyadı : Kaan YILDIRIM

Öğrencinin Numarası : 22120293

Anabilim Dalı : Moleküler Biyoloji ve Genetik

Programı : Moleküler Biyoloji ve Genetik Tezli Yüksek Lisans (İngilizce)

Danışmanın Unvanı/Adı, Soyadı : Dr. Öğr. Üyesi Özge Erdemli

Tez Başlığı : Collagen/Keratin/Alginate Hydrogel for an In Vitro Three-Dimensional Co-Culture of Fibroblasts and Keratinocytes

Yukarıda başlığı belirtilen Yüksek Lisans tez çalışmamın; Giriş, Ana Bölümler ve Sonuç Bölümünden oluşan, toplam 82 sayfalık kısmına ilişkin, 20 / 02 / 2025 tarihinde tez danışmanım tarafından Turnitin adlı intihal tespit programından aşağıda belirtilen filtrelemeler uygulanarak alınmış olan orijinallik raporuna göre, tezimin benzerlik oranı % 17'dir. Uygulanan filtrelemeler:

1. Kaynakça hariç
2. Alıntılar hariç
3. Beş (5) kelimeden daha az örtüşme içeren metin kısımları hariç,

"Başkent Üniversitesi Enstitüleri Tez Çalışması Orijinallik Raporu Alınması ve Kullanılması Usul ve Esaslarını" inceledim ve bu uygulama esaslarında belirtilen azami benzerlik oranlarına tez çalışmamın herhangi bir intihal içermediğini; aksinin tespit edileceği muhtemel durumda doğabilecek her türlü hukuki sorumluluğu kabul ettiğimi ve yukarıda vermiş olduğum bilgilerin doğru olduğunu beyan ederim.

Öğrenci İmzası:…….

ONAY

Tarih: 20 / 02 / 2025

Öğrenci Danışmanı

Dr. Özge ERDEMLİ

…….

To my dearest family and most precious friends

Kaan YILDIRIM

Ankara – 2025

ACKNOWLEDGEMENTS

I would like to express my heartfelt gratitude to all those who supported me throughout my thesis journey.

First and foremost, I am deeply grateful to my respected advisor, Assist. Prof. Dr. Özge Erdemli, for her invaluable guidance, patience, and encouragement. Her expertise and unwavering support have been instrumental in shaping this research. I also extend my appreciation to my thesis committee members, Assoc. Prof. Dr. Bengi Yılmaz Erdemli and Assoc. Prof. Dr. Ömer Aktürk, for their insightful feedback and constructive criticism.

During my thesis study, I had the privilege of receiving valuable support and insightful guidance from Prof. Dr. Özlem Darcansoy İşeri, Assist. Prof. Dr. Başak Kandemir, Assoc. Prof. Dr. Ceyhun Kayıhan for which I am truly grateful.

Most importantly, I would like to express my deepest gratitude to my dearest parents Işınsun Aksel and Burhan Yıldırım for their unconditional love, patience, and encouragement throughout this process.

I would also like to acknowledge my dear friends and lab mates Rümeysa Işıl Özdemir, Yasemin Pazarçeviren, Batuhan Ünal, Buse Öncel, Öykü Irmak Dikkatli, Efe Mıhçı for their unwavering support, friendship, collaboration, and for bringing joy and positivity to this journey.

I am grateful to Başkent University for their support and for providing the necessary facilities that contributed to the successful completion of my study.

The study was partially supported by Scientific and Technological Research Council of Turkey (TUBITAK) under the 1002 - B Emergency Support Module (Grant Number: 124M231). I would also like to thank TUBITAK for their support.

ABSTRACT

Kaan YILDIRIM

COLLAGEN/KERATIN/ALGINATE HYDROGEL FOR AN IN VITRO THREE-DIMENSIONAL CO-CULTURE OF FIBROBLASTS AND KERATINOCYTES

Başkent University Institute of Science

Department of Molecular Biology and Genetics

2025

Due to the high demand for advanced biomaterials in tissue engineering, research has focused on biomimetic hydrogels and three-dimensional (3D) co-culture systems to enhance tissue formation. The aim of this study was to examine the potential of Collagen/Keratin/Alginate (Col/Ker/Alg) hydrogel as a tissue scaffold for fibroblast and keratinocyte 3D co-culture. Collagen and keratin were extracted from bovine *Achilles* tendons and human hair waste, respectively, and characterized using Fourier Transform Infrared Spectroscopy (FTIR) and Sodium Dodecyl Sulfate-Polyacrylamide Gel Electrophoresis (SDS-PAGE). FTIR spectra confirmed the presence of characteristic peaks of keratin and collagen, while SDS-PAGE analysis showed collagen bands at 130, 110, 250, and 300 kDa and keratin bands at 39–45 and 50–55 kDa. Hydrogels with varying calcium chloride cross-linking conditions (0.10 M, 0.50 M, and 1.0 M) were produced and examined for morphology, swelling capacity, *in vitro* degradation behavior, total protein release and porosity. Hydrogels cross-linked with 0.50 M and 1.0 M exhibited more uniform structures, while hydrogels cross-linked with 0.50 M exhibited the highest water uptake. Hydrogels cross-linked with 0.50 M had a more open and interconnected cross-sectional structure. Degradation studies revealed that the hydrogel cross-linked with 0.10 M exhibited significant weight loss, whereas the hydrogel cross-linked with 1.0 M showed lower weight loss due to stronger cross-linking. Protein release studies indicated that all hydrogels exhibited a burst protein release in the first 6 hours. The hydrogel cross-linked with 0.50 M exhibited the highest protein release after Day 2. Preliminary cell culture studies demonstrated that the all-hydrogel groups promoted fibroblast cell viability for 9 days. Based on physicochemical and biological characterizations, the Col/Ker/Alg hydrogel cross-linked with 0.50 M was chosen as the optimal scaffold for 3D co-culture studies due to its higher water uptake capacity, porous structure, and ability to support cell viability. Micro-patterned 3D-printed stamps were designed and subsequently utilized to create channel

formations selective to cells, enhancing biomimicry at the microscale. The hydrogel matrix was seeded with human dermal fibroblasts (HDF-a) and keratinocytes (HaCaT) in a co-culture system and the viability and proliferation were monitored via resazurin reduction for 21 days and fluorescence imaging for 7 days. The results showed that Col/Ker/Alg hydrogel provides a suitable 3D microenvironment for cell proliferation and viability, which indicates the potential of this composite as a new biomaterial for skin tissue engineering research.

KEYWORDS: Collagen, Keratin, Alginate, Hydrogel, 3D Co-culture

ÖZET

Kaan YILDIRIM

FİBROBLAST VE KERATİNOSİT HÜCRELERİNİN IN VİTRO ÜÇ BOYUTLU KO-KÜLTÜRÜNDE KOLAJEN/KERATİN/ALJİNAT HİDROJELİ

Başkent Üniversitesi Fen Bilimleri Enstitüsü

Moleküler Biyoloji ve Genetik Anabilim Dalı

2025

Doku mühendisliğinde ileri biyomalzemelere olan yüksek ilgi nedeniyle, araştırmalar biyomimetik hidrojel ve üç boyutlu (3B) ko-kültür sistemlerine odaklanarak doku oluşumunu artırmayı amaçlamaktadır. Bu çalışmanın amacı, Kolajen/Keratin/Aljinat (Col/Ker/Alg) hidrojelinin fibroblast ve keratinosit 3B ko-kültürü için doku iskelesi olarak potansiyelini incelemektir. Kolajen ve keratin sırasıyla sığır Aşil tendonları ve insan saç atıklarından ekstrakte edilmiş ve Fourier Dönüşümlü Kızılötesi Spektroskopisi (FTIR) ve Sodyum Dodesil Sülfat-Poliakrilamid Jel Elektroforezi (SDS-PAGE) kullanılarak karakterize edilmiştir. FTIR spektrumları, keratin ve kolajene ait karakteristik piklerin varlığını doğrularken, SDS-PAGE analizi kolajen bantlarının 130, 110, 250 ve 300 kDa'da, keratin bantlarının ise 39–45 ve 50–55 kDa aralığında olduğunu göstermiştir. Farklı kalsiyum klorür çapraz bağlama koşulları (0,10 M, 0,50 M ve 1,0 M) ile hidrojeller üretilmiş ve morfoloji, şişme kapasitesi, *in vitro* bozunma davranışı, toplam protein salımı ve gözeneklilik açısından incelenmiştir. 0,50 M ve 1,0 M ile çapraz bağlanmış hidrojeller daha düzenli yapılar sergilerken, 0,50 M ile çapraz bağlanmış hidrojel en yüksek su alım kapasitesine sahip olmuştur. Bu hidrojel, diğer gruplara kıyasla daha açık ve birbirine bağlı bir iç kesit yapısı göstermiştir. Bozunma çalışmaları, 0,10 M ile çapraz bağlanmış hidrojelin önemli ölçüde ağırlık kaybına uğradığını, 1,0 M ile çapraz bağlanmış hidrojelin ise daha güçlü çapraz bağlanma nedeniyle daha düşük ağırlık kaybı gösterdiğini ortaya koymuştur. Protein salım çalışmaları, tüm hidrojellerin ilk 6 saat içinde ani bir protein salımı gerçekleştirdiğini göstermiştir. 0,50 M ile çapraz bağlanmış hidrojel, ikinci günden sonra en yüksek protein salımına sahip olmuştur. Ön hücre kültürü çalışmaları, tüm hidrojel gruplarının 9 gün boyunca fibroblast hücre canlılığını desteklediğini göstermiştir. Fizikokimyasal ve biyolojik karakterizasyonlara dayanarak, 0,50 M ile çapraz bağlanmış Col/Ker/Alg hidrojeli, daha yüksek su alma kapasitesi, gözenekli yapısı ve hücre canlılığını

destekleme yeteneği nedeniyle, 3B ko-kültür çalışmaları için optimal doku iskelesi olarak seçilmiştir. Mikro-ölçekte biyomimikriyi artırmak için mikro desenli 3B baskılı kalıplar tasarlanmış ve hücrelere seçici kanal oluşumları sağlamak amacıyla kullanılmıştır. Hidrojel matrisi, insan dermal fibroblastları (HDF-a) ve keratinositler (HaCaT) ile bir ko-kültür sisteminde ekilmiş ve hücrelerin canlılığı ve proliferasyonu 21 gün boyunca resazurin indirgenmesi ve 7 gün boyunca floresan görüntüleme ile izlenmiştir. Sonuçlar, Col/Ker/Alg hidrojelinin hücre proliferasyonu ve canlılığı için uygun bir 3B mikroçevre sağladığını, dolayısıyla bu hidrojelin deri doku mühendisliği araştırmaları için yeni bir biyomalzeme olma potansiyeline sahip olduğunu göstermektedir.

ANAHTAR KELİMELER: Kolajen, Keratin, Aljinat, Hidrojel, 3B ko-kültür

TABLE OF CONTENTS

LIST OF TABLES

Page

LIST OF FIGURES

Page

LIST OF SYMBOLS AND ABBREVIATIONS

3D	Three Dimensional
APS	Ammonium persulfate
BCA	Bicinchoninic acid assay
DMEM	Dulbecco's Modified Eagle Medium
EDC	1-Ethyl-3-(3-dimethyl aminopropyl) carbodiimide
EDTA	Ethylenediamine tetraacetic acid
FBS	Fetal Bovine Serum
FTIR	Fourier Transform Infrared
HaCaT	Immortalized Human Keratinocytes
HDF-a	Human Dermal Fibroblasts-Adult
NHS	N-Hydroxysuccinimide
PBS	Phosphate Buffered Saline
SDS-PAGE	Sodium Dodecyl Sulfate Polyacrylamide Gel Electrophoresis
SEM	Scanning Electron Microscopy
TCP	Tissue Culture Plate
TEMED	N, N, N', N'-Tetra methyl ethylene diamine
UV	Ultraviolet

1. INTRODUCTION

Tissue engineering is a rapidly evolving area that integrates concepts from various disciplines to generate bioartificial substitutes or stimulate tissue regeneration, ultimately aiming to restore or enhance tissue and organ function. In recent decades, this field has received considerable attention due to its promise in addressing key medical challenges, including organ failure, traumatic injuries and degenerative diseases. Beyond the limited availability of organ transplant donors and immune-related challenges, conventional medicine therapies such as organ transplantation and prosthetic implants constrained by their inability to fully replicate specific functional properties of native tissues [1]. Tissue engineering has addressed these challenges by utilizing cells, biomaterials, and biochemical factors to create engineered tissues that closely mimic their native counterparts.

The creation of scaffold systems as three-dimensional (3D) structural templates plays a crucial role in tissue engineering by promoting cellular adhesion, proliferation, and differentiation. These scaffolds serve as temporary frameworks for new tissue growth, gradually degrading and integrating into the host over time [2]. Choosing appropriate biomaterials is crucial in the design of the scaffold, as they must be biocompatible, biodegradable, and possess suitable mechanical properties while interacting with biological environments in a controlled manner. Various natural and synthetic biomaterials, such as collagen, keratin, alginate, polylactic acid (PLA), and polyglycolic acid (PGA) have been widely studied for tissue engineering applications [3]. Natural polymers, including collagen and alginate, can closely mimic the extracellular matrix (ECM), providing a suitable microenvironment for cell adhesion and differentiation [4]. In contrast, synthetic polymers provide adjustable mechanical properties, release rates, and degradation profiles, making them highly versatile for biological applications.

Skin tissue engineering has gained great attention due to the skin's fundamental role in providing a barrier against external insults, regulating temperature and enabling mechanosensory functions. The skin itself is a complex organ that has many layers (epidermis, dermis, and hypodermis) and functions to maintain physiological homeostasis.

Skin injuries or wounds, including burns, chronic wounds, and ulcers, present significant clinical challenges, necessitating advanced therapies in most cases, as conventional wound dressings and grafts may be insufficient [5]. Traditional methods for skin regeneration, such as autografts and allografts, are limited by factors including donor site morbidity, immune rejection, and scarring [6]. Tissue engineering offers a promising approach to developing bioengineered skin substitutes that can integrate with host tissue and promote functional skin restoration. However, challenges remain in achieving adequate vascularization, innervation, and long-term stability of engineered skin constructs.

In addition, cell culture approaches are also imperative in tissue engineering. Conventional two-dimensional (2D) cell culture models have been widely used for understanding cell behavior and drug responses. However, 2D cultures fail to mimic the complex 3D architecture and biochemical gradients found in native tissue. To overcome these limitations, the demand for 3D cell culture systems has grown, as they provide a more physiologically relevant environment for cellular interactions, tissue development, and drug testing. Hydrogels, other scaffold-based cell cultures, and bioreactors are increasingly used to create more physiologically relevant 3D tissue models to more accurately simulate the *in vivo* environments of human tissues [7]. Among these, hydrogels composed of natural or synthetic polymers have proven to be one of the most favorable due to their high-water content, biocompatibility, and ability to entrap cells within a 3D microenvironment [8]. Collagen, alginate and keratin-based hydrogels have been shown to promote cell adhesion and migration, as well as supporting differentiation, which makes them ideal for use in skin tissue engineering applications [9], [10], [11].

Another key technology in tissue engineering is co-culture systems, in which two or more different cell types are grown together to mimic the complex cellular interactions found within native tissues. Several studies have demonstrated that co-culture enhances tissue formation, improves cell-cell interactions, and facilitates stem cell differentiation into mature cell phenotypes [12], [13]. For example, co-culture of keratinocytes, fibroblasts, and endothelial cells has been shown to be advantageous for skin tissue engineering, promoting epidermis and dermis formation as well as vascularization [14], [15]. These advancements led to the development of more sophisticated engineered skin substitutes with improved structural and functional characteristics.

While great progress has been made, many challenges exist that must be overcome for tissue engineering technologies to see clinical applications. The translation of engineered tissues into clinic remains hindered by regulatory hurdles, scalability limitations, and high production costs [16]. These challenges are likely to be improved through advances in bioprinting technologies that are accelerating next-generation tissue engineering solutions [17]. As a complementary approach, recent studies on 3D co-culture systems suggest their potential to enhance the functional outcomes of tissue engineering strategies. This method holds great promise for overcoming current challenges in regenerative medicine and facilitating the creation of more effective and clinically viable replacements.

The aim of this thesis is to develop and characterize a collagen/keratin/alginate hydrogel and assess its potential for application in an *in vitro* 3D co-culture system of fibroblasts and keratinocytes. Considering the growing need for new tissue scaffolds to mimic the ECM, this study focuses on optimizing a hydrogel system to enhance cell viability and proliferation. Collagen from bovine *Achilles* tendons and keratin from human hair are integrated into an alginate-based hydrogel at varying calcium chloride cross-linking conditions (0.10 M, 0.50 M, and 1.0 M), allowing for both structural and chemical characterization, thus ensuring their application in *in vitro* cell culture. In addition to developing the hydrogel's properties, such as swelling behavior, degradation, and protein release, this research introduces micro-patterned 3D-printed stamps to improve cellular organization. This study provides a preliminary examination of the hydrogel’s potential as a scaffold material for skin tissue engineering by establishing a 3D co-culture system using human dermal fibroblasts (HDF-a) and keratinocytes (HaCaT) and assessing cell viability and proliferation over time.

2. LITERATURE

2.1. Tissue Engineering

Tissue engineering is an interdisciplinary field that integrates biology, materials science and engineering principles to develop biological substitutes capable of restoring, maintaining, or enhancing tissue function [18]. It primarily employs two strategies: scaffold-based and cell-based approaches (Figure 2.1). The cell-based strategy assembles building blocks, such as cell sheets and spheroids, enabling rapid tissue formation due to high initial cell density, which minimizes reliance on cell proliferation and migration [19]. However, this approach presents challenges, including weak mechanical properties, which may cause cell damage during handling, and the immobilization time required for initial fusion and extracellular matrix (ECM) deposition [20]. In contrast, the scaffold-based strategy utilizes temporary structural templates with tunable mechanical properties and degradation profiles that facilitate cell attachment, proliferation, and 3D tissue formation, with specially designed materials playing a crucial role in its effectiveness.

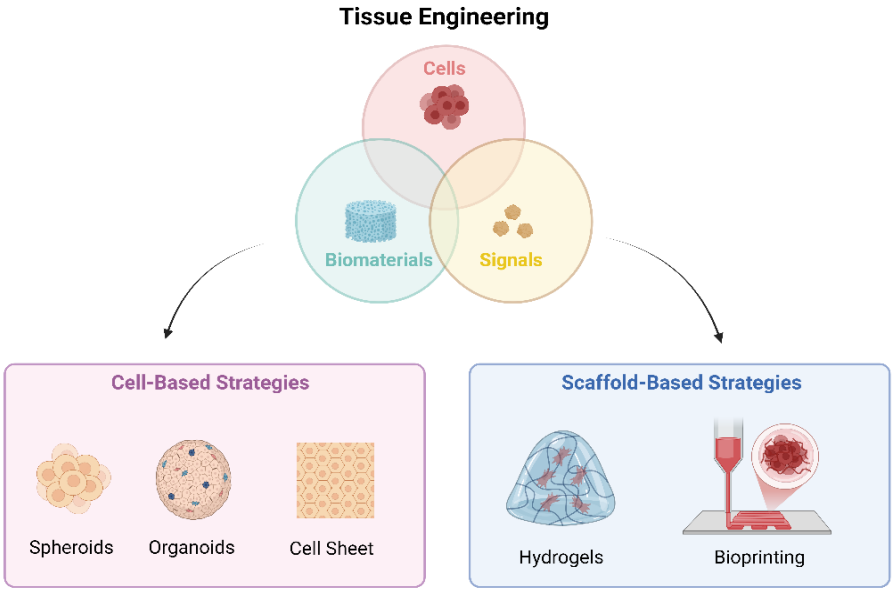

Figure 2.1. Schematic illustration of tissue engineering strategies: cell-based and scaffold-based strategies (Created with BioRender.com)

The main objective of scaffold-based tissue engineering is to regenerate tissues that closely resemble the structure and function of native tissues by incorporating cells, biomaterials, and growth factors. While cells generate the extracellular matrix (ECM) of new tissue, scaffolds offer a supportive framework that facilitates cellular activity. Growth factors are essential in stimulating and sustaining cell functions to enhance tissue regeneration [21]. The selection and optimization of these components are critical in the establishment of a microenvironment favorable to cellular proliferation and differentiation for successful tissue regeneration. This approach incorporates various strategies, including the use of human-derived, animal-derived, synthetic materials, or their combinations to produce functional tissue constructs [22]. These tissue constructs are designed to provide a suitable microenvironment to promote cell adhesion, proliferation, and differentiation, ensuring the formation of functional tissues. To produce functional tissue structures, cells are stimulated to grow on bioactive, degradable tissue scaffolds, which provide both physical and chemical cues, to guide differentiation and organization into 3D tissues [23].

Polymeric materials are widely used in tissue engineering due to their versatile properties, including biocompatibility, biodegradability, and ease of processing. These materials promote cell growth and regeneration of the tissue while degrading, enabling the seamless integration of newly formed tissues with their surrounding environment. Furthermore, to facilitate 3D tissue organization, these materials are fabricated into 3D scaffolds, which are precisely engineered in terms of structural and mechanical properties to provide the specific functional requirements of the target tissue [24].

Scaffolding plays a crucial role in tissue engineering by providing a 3D temporary structural framework essential for cell attachment, proliferation, and the development of new tissue. The choice of tissue scaffold materials, derived from either natural or synthetic sources, is essential, as they must show biocompatibility, biodegradability and appropriate mechanical properties to support the target tissue [25]. These biomaterials replicate the mechanical and biological properties of the native ECM, creating a three-dimensional environment that supports cell adhesion, growth, and functional tissue formation. Additionally, they facilitate the delivery of cells and bioactive factors to specific sites [26].

Biocompatible materials, including natural polymers (e.g., collagen, chitosan etc.) and synthetic polymers (e.g., polylactic acid (PLA), polyglycolic acid (PGA) etc.), are widely chosen for tissue scaffold fabrication. These materials not only facilitate the cell adhesion and growth but are also biodegradable, enabling the gradual integration of the engineered tissue into the host body [27]. For example, poly(lactic-co-glycolic acid) (PLGA) and collagen have garnered considerable attention because of their biocompatibility and suitability for specific tissue engineering applications [28].

Natural polymers like collagen, gelatin, and alginate are widely used because of their natural biocompatibility and structural resemblance to ECM. Collagen, a primary structural protein in several tissues, promotes cellular adhesion and supports an environment conducive to tissue development [29]. On the other hand, synthetic polymers, such as PLA and PGA, offer additional advantages like controlled degradation rates and tunable mechanical properties. Especially, PLA has been widely studied for its favorable mechanical characteristics and biocompatibility [30].

Hydrogels have been widely used in tissue engineering due to their biocompatibility, degradability, oxygen and nutrient permeability, and structural stability. Hydrogels mimic the ECM by forming a 3D polymeric network, providing an ideal environment for cell encapsulation and tissue formation. Synthetic or natural polymers can be used to prepare hydrogels. Natural hydrogels are preferred over synthetic ones because they are less cytotoxic and possess more ECM-like properties [31].

Cells are fundamental components for tissue engineering, serving as the basic building blocks of engineered tissues. The selection of appropriate cell types is crucial to achieving desired tissue functions. Cellular functionality in tissue engineering relies on a diverse range of cell types, including stem cells, progenitor cells and differentiated somatic cells, which collectively contribute to the tissue development and maintenance. Stem cells have the unique ability to differentiate into multiple cell lineages, making them invaluable for regenerative medicine [32]. Their capacity to respond to particular biochemical and environmental cues aids in the regeneration of injured tissues. Stem cells can be obtained from various sources, including embryonic tissues and adult tissues (e.g., bone marrow, adipose tissue), expanding their potential therapeutic applications [33].

Growth factors are essential regulators of cell behavior in tissue engineering, playing a critical role in modulating cellular activities, promoting angiogenesis, and enhancing tissue integration [34]. Embedding bioactive elements into tissue scaffolds offers a combined strategy to enhance tissue engineering methods and address current challenges in the field. By integrating growth factors into the tissue scaffolds or delivering them in a controlled manner, tissue engineers can precisely guide cellular activities to promote the regeneration of specific tissue types.

In summary, tissue engineering offers exciting possibilities, including the development of functional grafts for tissue repair, the study stem cell behavior in 3D models, and the use of engineered tissues as models for understanding physiology and disease [35]. It also serves as a powerful tool for studying cell differentiation and tissue development in controlled environments, which is essential for understanding disease mechanisms, testing drugs, and developing human disease models. These 3D models offer a promising alternative to traditional animal testing, addressing ethical concerns while providing more physiologically relevant platforms for drug discovery and biomedical research.

2.2. Skin Tissue and Skin Tissue Engineering

The skin serves as a protective barrier between the body's internal systems and the external environment and is the largest organ in the human body. It accounts for approximately 15% of an adult's total body weight and defends against physical, chemical, and biological threats [36]. The skin consists of three primary layers: the epidermis, dermis, and hypodermis (also known as the subcutaneous layer).

The epidermis is the outermost layer, primarily composed of keratinocytes, which undergo continuous proliferation, differentiation, and keratinization [37]. This layer plays a crucial role in maintaining the skin's barrier function, preventing water loss, and protecting deeper tissues from environmental insults such as pathogens, physical abrasions, and ultraviolet (UV) radiation [38], [39]. The structural organization of the epidermis, including its layered stratification and keratin production, significantly contributes to its barrier

properties. Additionally, the epidermis contains melanocytes, which produce melanin, playing a key role in the pigmentation of skin and protection against UV radiation [40].

Beneath the epidermis lies the dermis, a layer rich in connective tissue that contains cells, blood vessels, and nerve endings. It is significantly thicker than the epidermis and provides structural support to the skin. The dermis is composed of dense connective tissue, primarily composed of collagen and elastin fibers, which provide tensile strength and elasticity [41]. This layer is rich in blood vessels, sensory nerve endings, and skin appendages, including hair follicles, sebaceous glands and sweat glands. The presence of these structures allows the dermis to play a vital role in thermoregulation and sensation. The sweat glands and sebaceous glands allows the regulation of body temperature and the maintenance of skin hydration [42]. Furthermore, the dermal layer is responsible for the mechanical properties of the skin, including strength and elasticity, and sensory perception via specialized receptors [43].

The hypodermis, or subcutaneous layer, is the deepest layer of the skin, consisting mainly of loose connective tissue and adipose cells. It serves as an energy reservoir, provides thermal insulation, and assists in the protecting underlying muscles and bones [44]. While not technically part of the skin, hypodermis plays a important role in connecting the skin to underlying tissues, allowing for mobility while maintaining protective barrier properties [45]. Composed of connective tissue and adipose fat, the hypodermis acts as an insulator, reducing heat loss and protecting muscles and organs from mechanical injury [46].

In addition to its protective role, skin tissue holds considerable promise in the fields of regenerative medicine and tissue engineering. In recent years, the progress in tissue engineering has led to the development of bioconstructs designed for skin regeneration, offering promising solutions for the treatment of serious injuries or degenerative skin conditions [36]. A comprehensive understanding of the complex architecture and physiological functions of natural skin is essential in this field, as it provides critical insights for the design of new biomaterials. These engineered biomaterials, by imitating the structural and functional characteristics of human skin, aim to replicate its protective roles, accelerate wound healing, and facilitate tissue regeneration [45]. These innovations not only lead to

better therapeutic results for patients with skin-related health issues but also help improve the quality of life for those dealing with chronic or traumatic skin damage.

The history of skin tissue engineering has been marked by significant developments that have reshaped medical approaches and options for skin reconstruction and regeneration (Figure 2.2). Researchers began to understand the value of skin cells and healing in the 1970s. They learned that skin is made up of multiple layers, with keratinocytes and fibroblasts identified as essential cell types for these layer functions. In 1975, two independent American research groups laid the foundation for skin tissue engineering. Howard Green and James G. Rheinwald conducted *in vitro* studies on human epidermal keratinocytes. They demonstrated the feasibility of cell-based skin therapies. Simultaneously, Yannas and Burke investigated collagen degradation, leading to the development of synthetic dermal substitutes. Their contribution initiated modern skin tissue engineering and provided the foundation for improved epidermal and dermal regeneration [47]. These findings led to the initial efforts to create skin substitutes, facilitating transplants with living cells to improve tissue regeneration and wound healing. In the 1980s, the development of cultured epidermal autografts (CEAs) and cultured skin substitutes (CSSs) marked a significant milestone in wound care. CEAs were first applied in burn therapy in 1981, allowing the expansion of keratinocytes from a small skin biopsy into sheet-like structures. CSSs are autologous grafts containing both epidermal and dermal layers, forming a distinct dermal–epidermal junction [48]. These substitutes closely mimic autografted skin, reducing donor skin requirements and improving treatment outcomes for burns, chronic wounds, and dermal reconstruction. The 1990s progress of skin tissue engineering included the release of commercial products such as Epicel®, Integra®, Apligraf® and Dermagraft®- the first commercially available skin substitutes containing living cells and ECM components. These innovations marked a shift from traditional synthetic materials toward bioengineered solutions that aimed to replicate the complex structure and function of natural skin [18]. Entering the 21st century, stem cell technology further revolutionized skin tissue engineering. The development of induced pluripotent stem cells (iPSCs) offered a new approach for autologous skin cell generation, eliminating ethical concerns associated with embryonic stem cells [49]. The ability to derive skin cells from iPSCs significantly expanded research opportunities and the potential for regenerative medicine applications. In the 2010s, the introduction of 3D bioprinting marked another transformative progression of skin tissue

engineering. This advanced technology enabled the accurate, layer-by-layer assembly of biomaterials and living cells, creating intricate tissue structures that closely mimic the properties of natural skin [50]. The ability to customize the microenvironment and the spatial organization of cells has shown promising results in functional skin engineering, considerably improving clinical applications. At the same time, advancements in molecular self-assembly, polymer synthesis, and microfabrication facilitated the development of next generation "smart" biomaterials. These biomaterials are designed to respond to multiple factors such as pH, enzymes, temperature, light, and mechanical stress, making them highly attractive for medical applications [51]. By 2024, the integration of artificial intelligence, smart biomaterials, and personalized regenerative medicine has advanced the development of fully functional bioengineered skin, extending the applications beyond wound healing to cosmetic surgery, military applications, and reconstructive medicine [52].

Advancing skin tissue engineering is one of the most significant developments in medicine and cosmetics due to the growing global demand for effective skin injury treatments and aesthetic enhancements. Each year, 11 million people globally affect from only burn injuries, while chronic wounds contribute substantially to morbidity and healthcare costs [53]. Traditional approaches, such as skin grafting, often suffer from limitations due to donor shortages and graft rejection complications. Consequently, engineered skin substitutes, including dermal scaffolds and cultured skin cells, have been developed as effective alternatives to treat burns and to accelerate healing and reduce infection risks [6]. In 2022, the global wound care market was valued at USD 20.8 billion and is anticipated to grow at a compound annual growth rate (CAGR) of 5.4% between 2022 and 2027, driven by the rising incidence of skin trauma and the increasing preference for personalized and regenerative cosmetic treatments [54]. Advancements in skin tissue engineering have also influenced the cosmetic industry, where engineered biomaterials are now used to stimulate collagen production and treat skin problems such as acne, hyperpigmentation, and aging [55]. The evolution of dermal therapies, including growth factors, peptides, and bioengineered skin cells, underlines the importance of interdisciplinary nature of tissue engineering and its impact on both medical and cosmetic applications.

Over time, numerous engineered skin substitutes have been created to replicate the structure and function of native skin. These products are designed to offer coverage for

injured skin, facilitate wound healing, and restore tissue integrity. Among the clinically approved skin substitutes, Apligraf® and Dermagraft® are widely used in clinical applications to support wound healing. These products, composed of human cells and biocompatible materials, provide structural support and stimulate tissue regeneration. For example, Apligraf® is a bilayered skin substitute that has been successfully used in treating chronic venous leg ulcers and diabetic foot ulcers, while Dermagraft® is employed for diabetic foot ulcer treatment, promoting collagen synthesis and tissue regeneration.

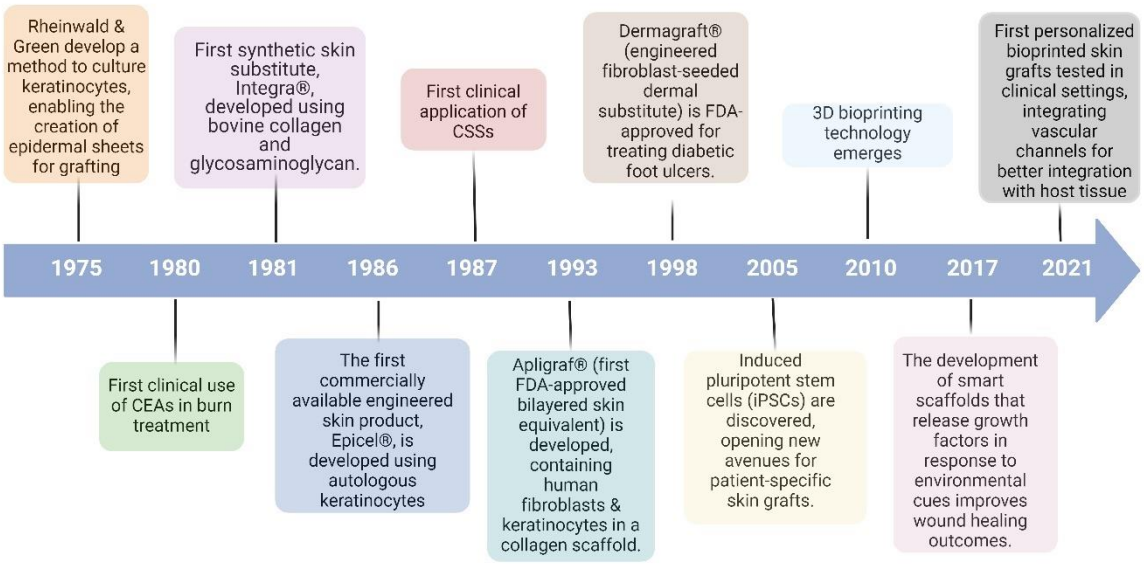

Figure 2.2. Key milestones in the progress of skin tissue engineering (CEA: cultured epidermal autograft; CSS: cultured skin substitute) (Created with BioRender.com)

In recent decades, skin tissue engineering has seen substantial progress, driven by advances in biomaterials, fabrication techniques, and regenerative medicine strategies. Skin damage, such as chronic burns or wounds, require innovative solutions to accelerate healing and restore functionality [56]. Current skin tissue engineering techniques often involve a combination of cellular and acellular approaches. One of the most promising strategies involves the use of biomaterials as tissue scaffolds, which provide the structural support for cellular attachment and proliferation. The choice of scaffolding materials plays a fundamental role in the success of skin regeneration, and ongoing research continues to

explore biomaterials that closely mimic the ECM of native skin [57]. Biocompatibility is a key criterion for selecting scaffolding materials, as it governs the interaction between the tissue scaffold and host tissue. A biocompatible scaffold minimizes adverse immune responses while promoting cellular integration and functionality [58]. This criterion dictates the interaction between the tissue scaffold and host tissue, ensuring that the scaffold integrates smoothly with the surrounding biological environment. By facilitating proper cellular adhesion, growth, and differentiation, these biomaterials contribute to long-term tissue stability and successful tissue regeneration.

One of the primary challenges in skin tissue engineering is vascularization. Proper blood supply is essential to maintain cell viability and promote tissue integration [59]. The development of thick, functional tissue requires an adequate vascular network to ensure that nutrients and oxygen reach deeper tissue layers. Without sufficient vascularization, implanted artificial tissue may fail to survive, leading to tissue necrosis and graft failure. Despite significant progress, achieving reliable vascularization remains a major challenge, especially for thicker tissue constructs that must replicate the complex network of blood vessels found in native tissue. Several strategies have been proposed to address this issue, including incorporation of angiogenic factors to stimulate blood vessel formation, designing tissue scaffolds specifically tailored to support vascular growth and bioprinting vascularized structures to mimic native tissue networks. However, even with these innovations, there remains a substantial gap in fully developing functional vascular networks within engineered tissues, particularly in large or thick constructs [60].

Skin tissue engineering holds immense promise not only in wound healing but also for various dermatological treatments and cosmetic enhancements. Clinical trials and experimental models have demonstrated the effectiveness of engineered skin substitutes, offering a viable therapeutic option for patients with severe skin injuries or diseases [61]. Furthermore, the integration of engineered skin with other tissue types presents exciting possibilities for multi-organ regeneration. For instance, composite grafts that combine skin with muscle or adipose tissue could expand treatment options for reconstructive surgery and regenerative medicine [62], [63].

2.3. Cell Culture Applications in Tissue Engineering

2.3.1. 2D and 3D Cell Cultures

Cell culture studies are fundamental to biomedical research and tissue engineering. Therefore, methodologies are continuously evolving to develop models that more accurately represent *in vivo* conditions. The traditional 2D cell culture model has been widely used for decades, providing a convenient and direct approach for studying cell behavior. In this system, cells are typically grown as a monolayer on flat surfaces, such as plastic or glass, creating a simplistic environment that fails to mimic the complex, multilayered organization of native tissues [64]. Despite its limitations, 2D culture systems offer several advantages, making them a standard method in many research areas. They are relatively simple, cost-effective, and allow for reproducible results. This makes 2D cell culture systems particularly useful in high-throughput drug screening and initial toxicity assessments, where quick and reliable data is crucial [65]. However, while 2D cultures provide benefits in terms of cost, simplicity, and reproducibility, they do not accurately mimic the complex microenvironments found within living tissues [66], [67]. The primary limitations of 2D culture systems are their inability to replicate the 3D architecture, biochemical gradients, and mechanical properties observed *in vivo* [68]. In living organisms, tissues are composed of complex biochemical gradients, physical structures, and mechanical forces that are largely absent in 2D systems. As a result, cellular activities, including cell proliferation, differentiation, and gene expressions, may differ drastically between 2D and 3D cell culture environments [67]. These limitations highlight the need for more advanced models that better mimic native tissue environments to gain a deeper and more accurate understanding of cellular processes and responses.

In contrast, 3D cell culture techniques have gained increasing attention in recent years due to their ability to mimic the *in vivo* microenvironment, thus offering a more physiologically relevant cell culture model for studying cell dynamics [69]. 3D cell culture systems use hydrogels, tissue scaffolds and bioreactors, all of which facilitate cell-cell interactions and biochemical signaling, similar to those found in native tissues [70].

Hydrogels are particularly favored due to their ability to mimic *in vivo* tissue stiffness, which can be adjusted depending on cell type. These approaches allow cells to grow in a more spatially organized manner, mimicking the architecture of native tissues. In addition, 3D cell cultures can incorporate ECM components, which play a critical role in cellular signaling and behavior, thereby further enhancing physiological relevance [71]. The comparison of 2D cell culture and hydrogel-based 3D cell culture systems is shown in Figure 2.3.

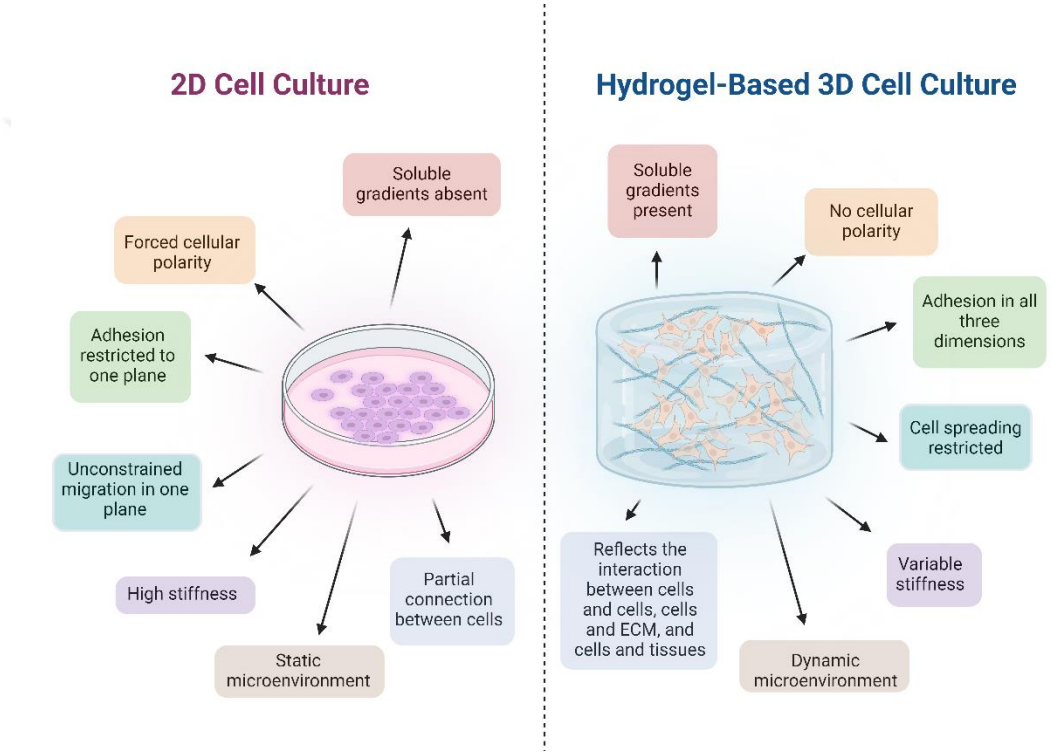

Figure 2.3. Comparison of 2D cell culture vs. hydrogel-based 3D cell culture [72], [73] (Created with BioRender.com)

The differences in cellular behavior between 2D and 3D cell culture systems influence their drug response, particularly in the context of drug resistance, a major challenge in cancer therapy. Studies comparing human breast cancer cell lines in both systems have shown that cells in 3D cell cultures exhibit greater drug resistance than those in 2D cell cultures, highlighting the importance of using 3D models in preclinical pharmacological tests to

improve the accuracy of therapeutic predictions [74]. In another study, collagen-based hydrogels were employed to develop 3D tumor models using multicellular tumor spheroids (MCTS), where cells are embedded within the collagen matrix [75]. This research demonstrated that these 3D models enhance drug screening capabilities and reveal significant differences in cell shape, density, and drug sensitivity compared to traditional monolayer 2D cell cultures, further emphasizing their relevance in cancer research. This discrepancy indicates the necessity of using 3D cell culture models in preclinical drug testing, as they provide a more accurate prediction of therapeutic effectiveness. Additionally, animal models are widely used in research to evaluate new drugs and treatments. However, advances in 3D culturing techniques have enabled researchers to create tumors and organ models for drug testing, reducing their reliance on animal models [76]. As these techniques continue to evolve and gain broader acceptance, their adoption is expected to decrease the dependence on animal testing in the future.

Despite its advantages, the application of 3D cell culture systems presents several challenges. 3D models are often technically demanding and resource-intensive, requiring specialized skills and equipment, which may not be readily available in all research facilities [77]. The complexity of experimental setup, as well as the requirement for specific biomaterials and culture conditions, can lead to higher costs and a steeper learning curve for researchers. In addition, the analysis of 3D cell culture systems is more challenging than 2D systems, as visualization techniques, such as microscopy, must be adapted to accommodate the 3D structure [78].

Both 2D and 3D culture systems have distinct advantages and limitations that affect their use in biomedical research. 2D cell cultures are convenient, cost-effective, and easy to characterize, making them ideal for high-throughput screening and preliminary research [79]. However, the risk of excessive simplification and lack of physiological relevance can lead to misleading conclusions. On the other hand, 3D cell culture systems provide a more realistic environment that better mimic *in vivo* conditions, offering invaluable ideas about cellular interactions and responses to drug treatments.

2.3.2. Cell Co-Culture Approaches

Co-culture systems in tissue engineering have developed into a crucial innovation, improving cellular interactions and enhancing the functionality of engineered tissues. Co-culture studies involve the simultaneous cultivation of two or more distinct cell types, allowing for a more accurate imitation of native tissue environment compared to traditional monoculture systems. This methodology offers a more predictive model for studying cellular behaviors and responses, ranging from simple physical mixtures of cell types to sophisticated 3D constructs that foster interactive cellular environments [80].

A key advantage of co-culture systems is their capacity to mimic the complex intercellular interactions found in native tissues, thereby improving overall tissue function. These systems serve two key roles: facilitating tissue formation through direct or indirect cellular interactions and preserving stem cell potency during expansion, often via feeder layers that secrete signaling factors. By mimicking native tissue dynamics, co-culture strategies provide advantages beyond those offered by tissue scaffolds and soluble factors, ultimately enhancing the efficiency of tissue engineering [81].

In native tissues, cellular behavior is largely influenced by neighboring cells through direct contact and soluble factors. Co-culture models have been specifically designed to mimic these interactions more accurately than monoculture systems, thereby advancing tissue engineering methodologies [82]. Furthermore, co-culture systems enable the study of intercellular signaling mechanisms, which are critical for tissue development and homeostasis, by mimicking the complex microenvironment of human tissues [83]. For example, the main advantage of co-culture approach in bone tissue engineering over monoculture approach is its ability to promote interactions between major cell types, resembling native bone tissue, while enabling real-time communication between osteoblasts and endothelial cells [83]. These interactions have been shown to stimulate angiogenic pathways, promoting a microenvironment conducive to vascularization, an essential factor for the functional integration of engineered tissues [84].

2.4. Hydrogels in 3D Cell Cultures

Hydrogels are 3D polymer networks that are hydrophilic, enabling them to absorb and retain large volumes of water or biological fluids while maintaining their structural integrity through chemical or physical cross-linking between individual polymer chains [85]. They are valuable not only for their high-water content, but also for their capacity to enable controlled release of active substances, biocompatibility, and tunable mechanical properties, making them ideal for a wide variety of applications.

Hydrogels can be classified as either natural or synthetic, each offering distinct advantages. Natural hydrogels, such as collagen, alginate, chitosan, gelatin and hyaluronic acid, are derived from biological sources and generally exhibit higher biocompatibility, biodegradability and lower cytotoxicity than synthetic hydrogels [86]. However, they have some limitations including low mechanical strength and difficulties in control due to batch variability. On the other hand, synthetic hydrogels such as poly(ε-caprolactone) (PCL), poly(lactic acid) (PLA), poly(glycolic acid) (PGA), and poly(lactide-co-glycolic acid) (PLGA) and polyethylene glycol (PEG), are produced via chemical synthesis, enabling better control over their physical, chemical, and mechanical properties [87]. Synthetic polymers are inherently more hydrophobic and chemically robust than natural polymers. Although their enhanced mechanical strength contributes to slower degradation, it also improves their durability [88]. However, hydrogels obtained from natural polymers are often preferred because of their biocompatibility and reduced toxicity.

In the field of medicine, hydrogels are widely used in drug delivery systems, wound management, and tissue engineering. Their moisture-retaining properties help maintain an optimal environment for wound healing while providing an effective barrier against infections [89]. Recent advancements have also demonstrated their potential as scaffolds in tissue engineering, offering a suitable matrix for cell attachment and growth to aid in tissue regeneration [90]. Their unique properties, which closely mimic natural ECM, along with their adjustable physical and chemical properties, are essential for optimizing the tissue scaffold design in regenerative medicine. This makes hydrogels a key focus of research and application in various tissue engineering contexts. Additionally, hydrogels can be designed to deliver therapeutic compounds in a controlled manner by encapsulating active

pharmaceutical ingredients and releasing them gradually [91]. Consequently, the literature describes many hydrogels with varying properties and purposes (Table 2.1).

Table 2.2.1. Literature examples on hydrogel types, fabrication methods, and cells used in hydrogel-based 3D culturing

Hydrogel Type	**Fabrication Technique**	**Cells**	**Features**	**Ref.**
Gelatin-Alginate	3D bioprinting	Fibroblasts, human umbilical vein endothelial cells (HUVECs), dermal papilla cells (DPCs) and epidermal cells	Biocompatibility, mechanical stability, and the ability to support cell encapsulation, proliferation, and self-aggregation, making it ideal for 3D bioprinting and hair follicle regeneration.	[92]
Alginate Chitosan Collagen	Freeze-drying	Human keratinocyte cell line (HaCaT)	High porosity, tunable pore size, excellent biocompatibility, enhanced water retention, and structural similarity to the ECM making it an ideal scaffold for skin tissue applications.	[93]
Keratin-PEG	Photo-crosslinking	Fibroblasts	Rapid gelation, tunable mechanical properties, and excellent cytocompatibility, making it suitable for 2D and 3D cell culture, microfabrication, and tissue engineering applications.	[94]
Type I Collagen	3D bioprinting	Human Dermal Fibroblasts, Keratinocytes, Melanocytes	Full-thickness biomimetic skin model with fibroblasts, keratinocytes, and melanocytes, enabling stable cell growth, dermal-epidermal structure, and freckle-like pigmentation without external stimuli.	[95]
Alginate Collagen	Enzyme-mediated crosslinking	Human amniotic mesenchymal stem cells	Improved elasticity, reduced swelling and degradation rates, enhanced cytocompatibility, and the ability to induce chondrogenic differentiation of human amniotic mesenchymal stem cells, making it a promising scaffold for cartilage tissue engineering.	[96]

The structural properties of hydrogels play a vital role in tissue engineering. Their porous nature facilitates nutrient exchange, waste removal, and cell attachment, while biochemical modifications can enhance adhesion, migration, and differentiation [97]. Beyond structural advantages, hydrogels have diverse applications across various tissue types. In skeletal tissue engineering, hydrogels have been utilized for delivering growth factors while simultaneously providing a supportive scaffold that enhances osteogenesis, thereby promoting bone regeneration [98]. Similarly, in cardiac tissue engineering, hydrogels have been employed to develop biomimetic platforms that replicate the mechanical properties of heart tissue. These advancements improve the structural integration and functional performance of cardiac cells, ultimately contributing to enhanced cardiac repair and regeneration [99]. Additionally, the incorporation of conductive materials into hydrogels has garnered significant interest in neural tissue engineering. These hybrid materials facilitate the transmission of electrical signals, which is essential for neuronal function and communication, thereby offering promising applications for neural repair and regeneration [100].

Despite their promising biomedical potential, the clinical application of hydrogels presents several challenges. Key issues include scalability, reproducibility of production, and the long-term stability of hydrogels *in vivo*, which remain significant barriers to their widespread use [101]. A major limitation of hydrogels is their slow response time, which restricts their utility in applications requiring rapid actuation, such as sensors or artificial muscles. The delayed responsiveness reduces their suitability for large-scale industrial or biomedical applications that demand high reaction efficiency [102]. To address these limitations, ongoing research focuses on the developing composite hydrogels that integrate the advantages of both synthetic and natural biomaterials. By combining the structural integrity of synthetic polymers with the bioactivity of natural components, these advanced hydrogels aim to enhance both mechanical resilience and biocompatibility [103]. Such innovations hold great promises for expanding the clinical and industrial applicability of hydrogels, paving the way for more effective and versatile biomaterials in regenerative medicine.

2.5. Collagen

Collagen is the most abundant fibrous protein in the human body, constituting approximately 30% of the total protein content. It is a vital structural component of various tissues, accounting for about 75% of the dry weight of the skin and serving as a primary element of the ECM [104]. As a key ECM component, collagen contributes to tissue resilience and mechanical strength. Collagen is found in numerous tissues, including connective tissues, skin, tendons, cornea, and cartilage. Due to its widespread presence and importance, collagen sourced from a various species, such as bovine, porcine, fish, marine sponge, shellfish, and jellyfish has been extensively studied and utilized in biomedical and industrial applications [105].

To date, 29 distinct types of collagens have been identified, all of which share a characteristic triple-helix structure, consisting of three intertwined polypeptide chains (Figure 2.4). Among these, collagen types I, II, III, V, and XI are particularly notable for their ability to form collagen fibers, which are essential for the structural integrity of tissues. The basic unit of collagen molecules consists of three alpha chains that assemble into the triple-helix configuration. Each alpha chain is composed of over a thousand amino acids arranged in a repeating tri-peptide sequence, typically following the pattern -Gly-X-Y, where glycine (Gly) occupies every third position, while X and Y represent variable amino acids [106]. This structure enables collagen fibers to withstand significant tensile stress while preserving flexibility.

Collagen has become a key material in biomedical applications because of its beneficial properties, such as biocompatibility, biodegradability, and minimal immunogenicity. Collagen-based natural biomaterials have emerged as promising candidates for tissue engineering. A notable example is the development of collagen-based hydrogels, which can be produced to mimic the mechanical and biochemical properties of native tissues [107], [108]. These hydrogels are increasingly explored for use in tissue scaffolds that support cell growth and tissue repair, highlighting collagen's potential in advancing regenerative medicine and related fields. For example, in one study, human HaCaT keratinocytes and dermal fibroblasts were seeded onto electrospun denatured collagen I microfiber scaffolds [109]. The results demonstrated that these collagen scaffolds offer

enhanced mechanical properties, including improved structural stability and reduced graft shrinkage, while also preventing immune responses. These advantages highlight the potential of collagen scaffolds in tissue engineering and regenerative medicine.

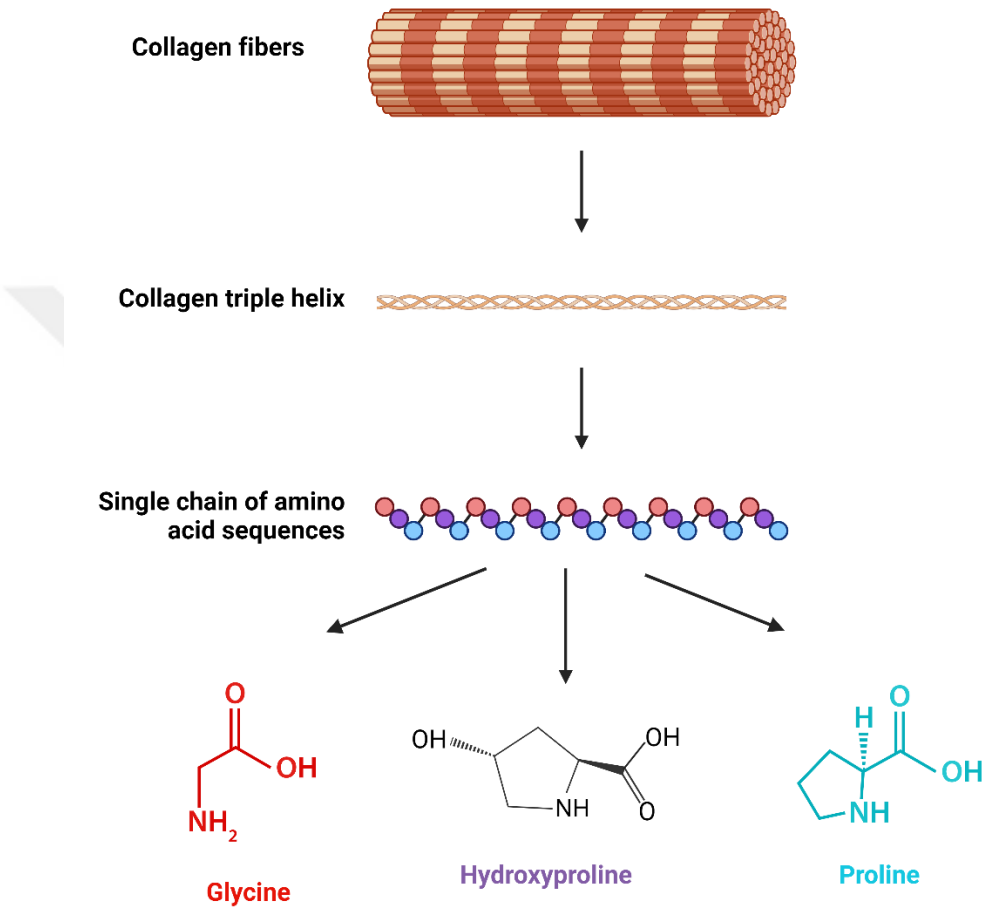

Figure 2.4. Structure of collagen (Created with BioRender.com)

2.6. Keratin

Keratin is one of the most abundant structural proteins in epithelial cells , alongside collagen, and is among the most essential biopolymers in animals [110]. As a class of fibrous structural proteins, keratin plays a fundamental role in human physiology by contributing significantly to structural integrity and the function of various tissues. It is mainly found in

epithelial cells, where it participates in several physiological processes, particularly in maintaining the integrity of the epithelial tissues [111].

The unique structural characteristics of keratin contribute to its exceptional mechanical properties, making it not only a structural scaffold but also a promising biomaterial for various biomedical applications [112]. Keratin-based materials have revolutionized modern biomaterials due to their biodegradability, biocompatibility, and mechanical durability. These versatile biopolymers, derived from sources such as wool, hair, nails, feathers, and horns, can be processed into sponges, films, and hydrogels for diverse biomedical applications [113].

Keratin proteins extracted from hair are classified as alpha- and beta- keratins. Alpha-keratins, found in the cortex of hair fibers, have an alpha-helical structure, a low sulfur content, and a molar mass of 60–80 kDa [114]. They primarily compose wool, hair, hooves, nails, horns, and the stratum corneum. Beta-keratins, which dominate the cuticle, serve a protective role and are the main component of feathers [113], [114]. In alpha-keratin, polypeptide chains adopt an alpha-helical structure, forming a coiled-coil arrangement [115]. In contrast, beta-keratin consists of pleated beta-sheets (Figure 2.5).

Keratin also plays a crucial role in wound healing and tissue regeneration. Studies indicate that keratin-based biomaterials can enhance cell proliferation and differentiation, creating an environment conducive to wound healing [116]. Additionally, several innovative biomaterial applications utilizing keratin are expanding its use in regenerative medicine. For example, keratin films have been developed for ocular surface reconstruction, demonstrating their ability to support the healing of damaged tissues [117]. The adaptability of keratin in the fabrication of films and scaffolds for cell culture is further enhanced by its compatibility with various cell types, making it highly suitable for tissue engineering [118]. Furthermore, combining keratin with other biomaterials improves mechanical strength and cellular adhesion, leading to enhanced outcomes in regenerative applications.

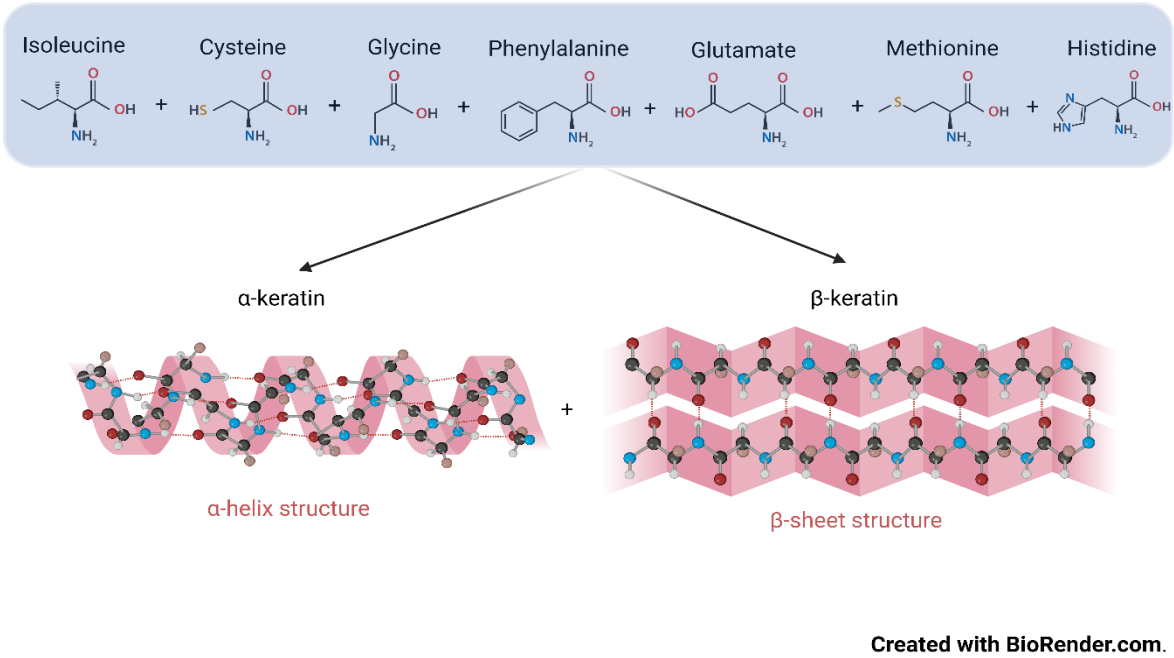

Figure 2.5. Structure of keratin (Created with BioRender.com)

2.7. Alginate

Alginate is a hydrophilic anionic polysaccharide with excellent bioactivity and biocompatibility. Primarily derived from the cell walls of brown seaweeds, alginates provide a flexible mechanical structure that protects seaweed from damage caused by strong water currents [119]. Their distinct physicochemical characteristics, such as high gelation capacity, non-toxicity, and biodegradability, have enabled their broad application in biomedical fields like drug delivery, wound healing, and tissue engineering.

Structurally, alginate is a polyanionic polysaccharide composed of α-L-guluronate (G) and β-D-mannuronate (M) units, irregularly linked by β-1,4-glycosidic bonds (Figure 2.6) [120]. The proportion and sequence of these G and M units influence the mechanical and biological properties of alginate-based materials. These characteristics enable alginate to be processed into diverse 3D scaffolding materials, including hydrogels and microcapsules, which have demonstrated efficacy in tissue repair and scaffold-based cell growth [121]. A defining property of alginate hydrogels is their ability to cross-link into matrices that mimic the ECM. This cross-linking capability grants alginate hydrogels a high water retention

capacity, ranging from 20% to 90% of their original mass, which is crucial for biocompatibility, cellular retention, and bioactive molecule delivery [122].

The biomedical applications of alginate are extensive due to its structural similarity to the natural ECM and its ability to support cell growth and differentiation. Alginate-based systems serve as vehicles for regulated release of therapeutic agents such as small-molecule drugs and proteins. Mild gelation via the additions of divalent cations, such as calcium ions (Ca^{2+}), further enhances their usability by allowing for tailored mechanical properties suited to specific biomedical needs [123]. Recent advances in alginate research have expanded its applications to include 3D tissue cultures, antibiotic adjuvants, and cell transplantation, particularly in diabetes treatment. Furthermore, alginate-based formulations are being explored for neurological disease therapies, as well as antimicrobial and antiviral treatments [124]. These ongoing developments underscore the versatility and biomedical potential of alginate-based biomaterials, positioning them as crucial components in modern therapeutic and regenerative medicine strategies.

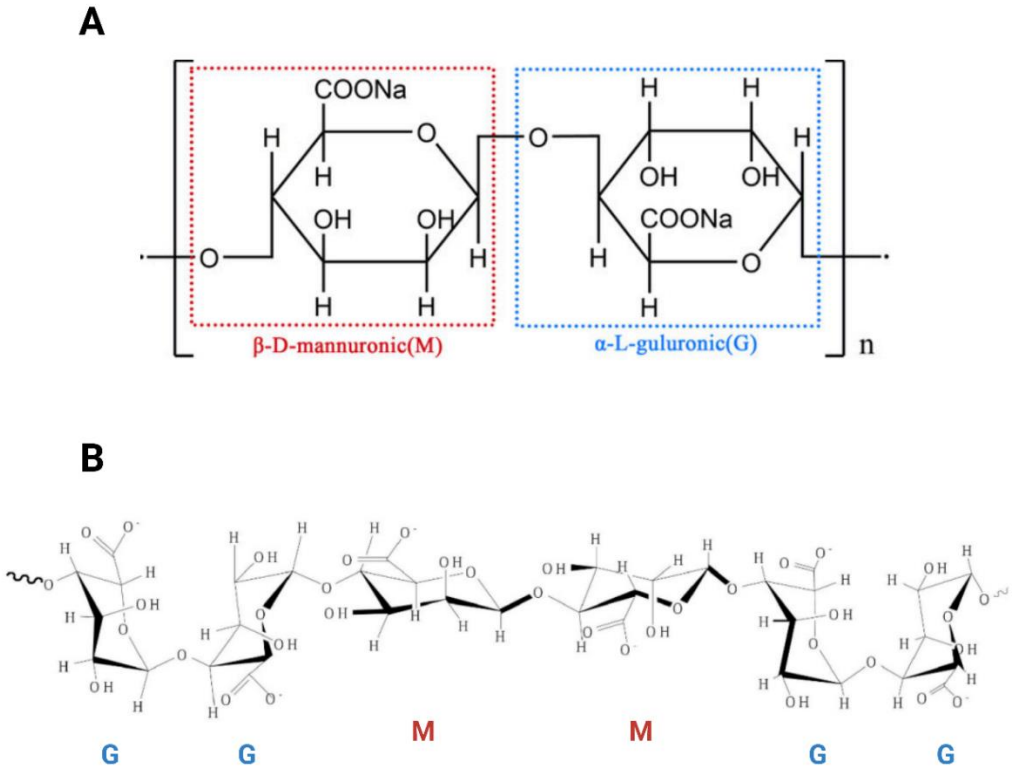

Figure 2.6. Structure of sodium alginate (A: monomers of alginate, B: chain configuration) (modified from [125] and [126] and created with BioRender.com)

3. MATERIALS AND METHODS

3.1. Materials

Materials used for protein extraction: 12-14 kDa cellulose dialysis membrane (TX0112) was purchased from BioBasic, Canada. Pepsin (10,000 N.F. U/mg) from the porcine stomach was obtained from Genaxxon, Germany. Protein Ladder, Color Prestained Protein Standard, Broad Range (10-250 kDa) was purchased from Biolabs, USA. Coomassie Brilliant Blue R-250 was provided form Serva Electrophoresis GmbH, Germany. Sodium bisulfite ($NaHSO_3$) and Urea (USP Grade) were obtained from VWR Life Science AMRESCO, USA. Collagen solution from human fibroblasts, hydrogen peroxide solution (30% w/w in H_2O), sodium sulfide (Na_2S), ammonia solution 25%, glacial acetic acid, glycerol, absolute ethanol, chloroform, methanol, sodium dodecyl sulfate (SDS), sodium hydroxide (NaOH), sodium chloride (NaCl), Sodium acetate trihydrate, ammonium persulfate (APS), tris(hydroxymethyl)aminomethane (Tris Base), tris(hydroxymethyl)aminomethane hydrochloride (Tris HCl), acrylamide, bisacrylamide(N,N-methylenebisacrylamide) and N,N,N,N-tetramethyl ethylenediamine (TEMED) were obtained from Sigma Aldrich, Germany.

Materials used for hydrogel preparation: Sodium alginate, phosphate buffered saline (PBS) tablet, sodium hydroxide (NaOH), N-(3-dimethylaminopropyl)-N′-ethylcarbodiimide (EDC), N-hydroxysuccinimide (NHS), glacial acetic acid, sodium carbonate monohydrate, methanol, copper(II) sulfate pentahydrate ($CuSO_4 \cdot 5H_2O$), magnesium chloride hexahydrate ($MgCl_2 \cdot 6H_2O$), paraformaldehyde (PFA), absolute ethanol and sodium azide (NaN_3) were provided from Sigma Aldrich, Germany. Calcium chloride dihydrate ($CaCl_2 \cdot 2H_2O$) was purchased from Multicell International Ltd., United Kingdom. Sodium potassium tartrate was obtained from Kartal Kimya, Turkey. Micro BCA reagent B was provided from Thermo Scientific, USA.

Materials used for mold preparation: Epoxy-based soybean oil resin (Eco UV Resin) was purchased from Anycubic, China.

Materials used for cell culture studies: Human dermal fibroblasts-adult (HDF-a, PCS-201-012) was obtained from ATCC®, USA. Immortalized human keratinocytes (HaCaT) was provided from Cytion, Germany. Dulbecco's Modified Eagle Medium (DMEM), high glucose, with glutamine, with sodium pyruvate and fetal bovine serum were purchased from Gibco, USA. Penicillin/streptomycin solution (100X) and tyripsin 0.25%-EDTA 0,02% in Hank's Balanced Salt Solution (HBSS) were obtained from Biowest, France. Resazurin sodium salt was purchased from Cayman Chemical, USA. Vybrant™ DiD and Vybrant™ DiO cell-labeling solutions were purchased from Invitrogen™, USA. Sterile syringe filter (0.22 μm) was obtained from Chrom Tech Inc., USA.

All chemicals used were of analytical grade and were utilized as received, without additional purification.

3.2. Methods

3.2.1. Extraction and Characterization of Collagen and Keratin

The collagen type I used in the hydrogels was extracted from bovine *Achilles* tendons provided by the Meat and Milk Board (Turkey). These tendons were stored at -20°C until the protein extraction process. For the extraction of collagen, the tendons were first cleaned to remove attached meat, washed with ethanol followed by distilled water, and then cut into 1 cm thick slices. The tendon pieces were immersed in a 100 mM NaOH solution at a solid to solvent 1:5 (w/v) ratio for six hours at room temperature to remove lipids and non-collagenous proteins [127]. The solution was replaced every two hours during this process. After NaOH pre-treatment, the tendons were washed three times with distilled water to remove the NaOH solution. The acid-enzyme hybrid method was used to break down the triple helix of collagen and dissolve its individual chains in solution [127]. For this, the tendon pieces were homogenized using a hand blender in a 700 mM acetic acid solution at a solid to solvent 1:16 (w/v) ratio and stirred with a magnetic stirrer (MS-H280-Pro SET2, DLAB, Malaysia) at 4°C for 16 h. After the step of acidification, the pepsin was added into solution at an enzyme to collagen 1:20 (w/w) ratio and the solution was magnetically agitated for 72 h at 4°C. To stop the enzymatic digestion, 200 mM sodium acetate buffer (pH 5.0)

was added to the solution. The final solution was centrifuged (SL8R, Thermo scientific, USA) at 10,000 g for 30 min at 4°C to eliminate any undigested fragments. The pH was adjusted to 7 with 6 M NaOH in the presence of 50 mM Tris buffer. For precipitation of collagen, NaCl was added with a final concentration of 2.6 M, and the mixture was stirred at 4°C for 12 h. To collect collagen, the solution was centrifuged at 10,000 g for 90 min at 4°C. After centrifugation, the supernatant was discarded, and the obtained precipitate was dissolved in 500 mM acetic acid. The dissolved collagen solution was dialyzed using a 12–14 kDa dialysis membrane in 100 mM acetic acid for 24 h at 4°C and subsequently against distilled water at room temperature for 48 h, with continuous stirring on a magnetic stirrer. After dialysis, lyophilization (LyoQuest, Telstar, Spain) was performed to obtain the collagen. Collagen extraction steps are shown in Figure 3.1.

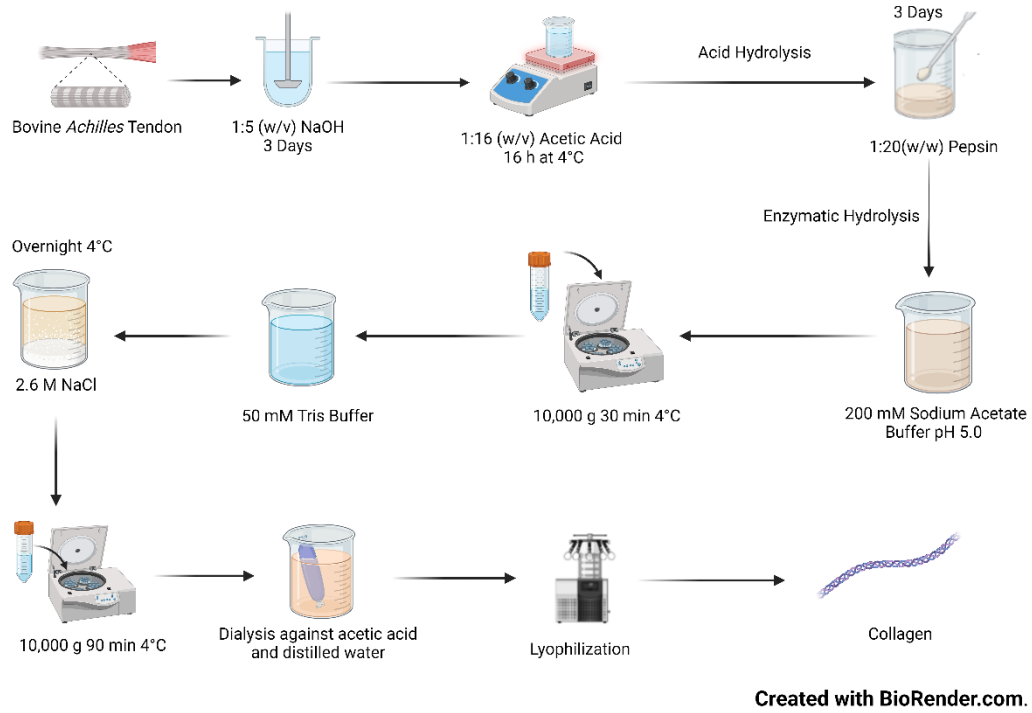

Figure 3.1. Schematic representation of collagen extraction from bovine *Achilles* tendons

Keratin used in the hydrogels was extracted from untreated waste human hair samples obtained from barbershops, using a combined method that involved reduction with sodium sulfide (Na_2S) and sulfitolysis reaction with sodium bisulfite ($NaHSO_3$) [128]. Waste hair

was cleaned with 70% (v/v) ethanol and distilled water, respectively, and then dried overnight at 40°C in an oven (Nüve, Turkey). For the delipidation process, hair samples were incubated in chloroform-methanol (2:1, v/v) solution for 6h at room temperature. Afterward, the solution was removed using Whatman Grade No. 1 filter paper and the hair was dried at 70°C for 2 h. The dried hair was decolorized by incubating in a hydrogen peroxide-ammonia solution (2:1, (v/v)) for 15 min in the dark. During this process, ultraviolet (UV) light was applied for 15 s in every minute to accelerate the reaction. Then, the decolorized hair was allowed to dry at room temperature for 24 h. For the extraction of keratin from decolorized hair, an extraction solution was prepared containing 8.0 M urea, 500 mM $NaHSO_3$, 125 mM Na_2S, and 100 mM sodium dodecyl sulfate (SDS). The dried hair was cut into small pieces using scissors, mixed with the extraction solution, and stirred on a magnetic stirrer at 50°C for 4 h. After 4 hours, the mixture was centrifuged at 10,000 g for 30 min at room temperature, and the supernatant was transferred to 12-14 kDa dialysis membrane, where it was dialyzed in distilled water for 5 days on a magnetic stirrer. The water was changed at regular intervals during the 5-day period at room temperature. After dialysis, lyophilization was applied to obtain the keratin. Keratin extraction steps are shown in Figure 3.2.

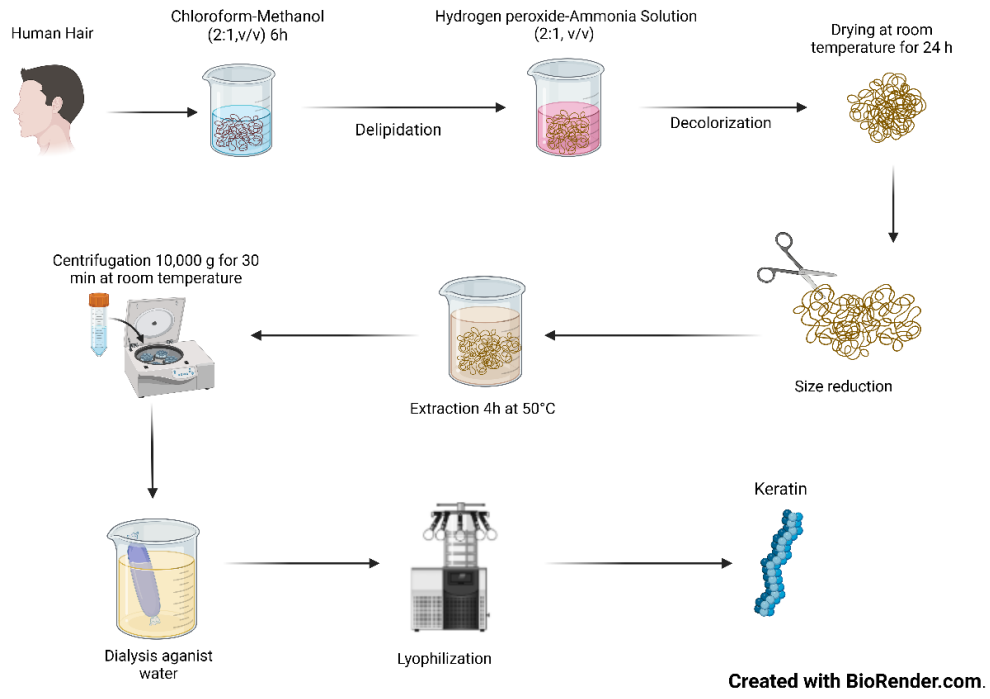

Figure 3.2. Schematic representation of keratin extraction from human hair waste

The chemical properties of the collagen and keratin obtained after lyophilization were investigated by attenuated total reflectance Fourier transform infrared spectroscopy (ATR-FTIR; Nicolet iS50, Thermo Fisher Scientific Inc., USA) in the range of 450-4000 cm^{-1}.

The extracted keratin and collagen samples were identified by Sodium Dodecyl Sulfate-Polyacrylamide Gel Electrophoresis (SDS-PAGE) according to the method described by Laemmli [129] with modifications. Keratin and collagen samples were first dissolved in distilled H_2O and 100 mM acetic acid, respectively, to achieve final concentrations of 1 mg/mL. The protein solutions were then mixed with 4X Laemmli sample loading buffer at a protein to buffer 3:1 ratio (v/v). The samples in the loading buffer were heated at 95°C for 5 min. For the SDS-PAGE analysis, a 4% stacking gel was prepared for both proteins, while separating gels of 10% and 7.5% were used for keratin and collagen, respectively. For polyacrylamide gel electrophoresis, 20 µL of each sample was loaded onto polyacrylamide gels and electrophoresed at 400A and 60V for stacking gel, followed by 100 V for the separating gel, using Mini PROTEAN® Tetra cell Electrophoresis System (Bio-Rad, China). Afterward, the gels were stained with Coomassie Brilliant staining solution for 30 min and subsequently was washed three times with distilled water and left overnight in a destaining solution. After overnight incubation, the protein bands were examined using a gel imaging system (Syngene, UK), and collagen and keratin-specific bands were identified based on the molecular weight marker.

The formulations for Laemmli sample loading buffer (4X), Coomassie Brilliant staining solution, destaining solution, as well as stacking and separating gels, are provided in Appendix A.

3.2.2. Preparation of Collagen/Keratin/Alginate Hydrogels

To prepare the Collagen/Keratin/Alginate (Col/Ker/Alg) hydrogels, equal volumes of 3% (w/v) collagen, 3% (w/v) keratin, and 3% (w/v) alginate stock solutions were prepared. Distilled water was used as a solvent for keratin and alginate, while 0.50 M acetic acid was employed for collagen. All stock solutions were stirred at 40°C on a magnetic stirrer, with a water bath ensuring uniform heat distribution. The prepared stock solutions were then mixed in a 1:1:1 volume ratio. To neutralize the mixture, 50 µL of 10 M NaOH solution was added

per mL of 0.50 M acetic acid. The mixture was stirred until fully dissolved, and a homogeneous appearance was achieved. Subsequently, the pre-gel mixture was poured into a 24-well plate in equal volumes and left for gelation at 4°C for 2 h.

The gels, with their surfaces frozen and slightly solidified, were cross-linked for at 4°C for 30 min using calcium chloride ($CaCl_2$) solutions at varying concentrations (0.10 M, 0.50 M or 1.0 M) prepared in 70% (v/v) ethanol solution. After the initial 30 min cross-linking, the gels were flipped and incubated for an additional 30 min to ensure uniform distribution of the cross-linker throughout the gels. The physically cross-linked hydrogels were incubated in absolute ethanol for 30 minutes to remove excess water and bring the polymer chains closer together. At the end of incubation, the hydrogels were rinsed three times with distilled water and left to air-dry at room temperature for 15 min. Covalent cross-linking was then performed by incubating the hydrogels overnight at 4°C in an EDC/NHS solution. The cross-linking solution was prepared by dissolving 1.150 g of EDC and 0.276 g of NHS in distilled water per gram of collagen, with the pH adjusted to 5.5 using 0.5 M acetic acid. Finally, the chemically cross-linked hydrogels were washed thoroughly with distilled water and fully dried using lyophilization. Three different hydrogel groups, differing based on the concentration of the calcium chloride cross-linker (0.10 M, 0.50 M, or 1.0 M), were used in optimization studies. A schematic representation of the hydrogel preparation process is shown in Figure 3.3.

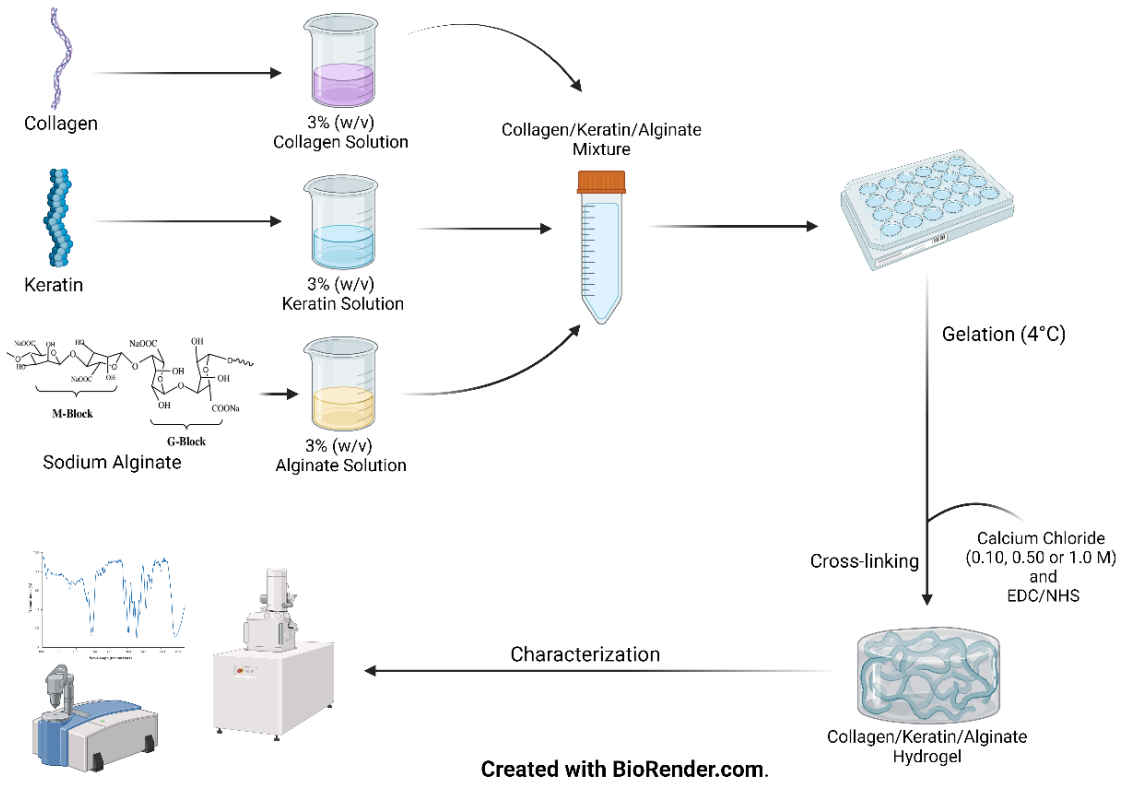

Figure 3.3. Schematic representation of the Collagen/Keratin/Alginate (Col/Ker/Alg) hydrogels

3.2.3. Characterization of Collagen/Keratin/Alginate Hydrogels

The chemical properties of Col/Ker/Alg hydrogels prepared with different concentration of the calcium chloride cross-linker (0.10 M, 0.50 M, or 1.0 M) were analyzed on Fourier transform infrared spectroscopy (ATR-FTIR, Nicolet is50, Thermo Fisher Inc., USA) from 450-4000 cm^{-1}.

The surface and cross-sectional morphology of hydrogel groups were analyzed using a scanning electron microscope (SEM, GAIA3+Oxford XMax 150 EDS, Tescan, Czech Republic). Prior to SEM imaging, the lyophilized hydrogels were coated with a carbon layer using a high-vacuum coater (EM ACE600, Leica Microsystems, Germany).

The water uptake capacity of the hydrogels in phosphate-buffered saline (PBS, 0.1 M, pH 7.4) was determined using the gravimetric method (n=4). The initial mass of the lyophilized hydrogels (m_0) was measured, and the hydrogels were then immersed in 2 mL of PBS containing Ca^{2+} ions (1 mM), Mg^{2+} ions (0.5 mM) and 0.02% (w/v) sodium azide (NaN_3) at 37°C for 72 h. At regular time points (2, 4, 6, 24, 48, and 72 h), the swollen hydrogels were removed from the PBS solution, excess PBS was removed gently with a filter paper and then were weighed (m_1). The percentage water uptake of the hydrogels was calculated according to the Equation 3.1 [130]:

$$\%\ water\ uptake = \frac{m1-m0}{m0} x\ 100 \tag{3.1}$$

The *in vitro* hydrolytic degradation behavior of the of hydrogel groups was assessed in 2 mL of PBS containing Ca^{2+} ions (1 mM), Mg^{2+} ions (0.5 mM) and 0.02% (w/v) sodium azide (NaN_3) at 37°C for 14 days (n=4). The initial mass of the lyophilized hydrogels (m_0) was measured, and the hydrogels were then immersed in PBS solution. At the end of days 2, 3, 7, and 14, the hydrogels were removed from the PBS, washed with distilled water, and lyophilized. After lyophilization, the hydrogels were weighed again (m_1), and the percentage of weight loss was determined using the following Equation 3.2 [131]:

$$\%\ weight\ loss\ = \frac{m0-m1}{m0}\ x\ 100 \tag{3.2}$$

During the *in vitro* hydrolytic degradation analysis, total protein release from the hydrogel groups was determined using the Bicinchoninic Acid (BCA) assay (n=4). At the end of 2 h, 4 h, 6 h, 1 day, 2 days, 3 days, 7 days, and 14 days, the PBS release medium was collected and replaced with fresh PBS. The collected release solutions were stored at 4°C until the BCA assay was performed. For the BCA assay, the collected release solutions were mixed in equal volumes with the BCA working solution, and the mixture was then incubated at 60°C for 1h in an oven (Bicasa, Italy). BCA working solution is prepared by mixing 25 parts of sodium carbonate monohydrate-sodium tartrate buffer solution (pH 11.25) with 24 parts of Micro BCA Reagent B, and 1 part of 4% (w/v) copper sulfate solution. After 1-h incubation, absorbance of the room temperature cooled samples was measured at 540 nm

and 630 nm using a microplate reader (ELx800 Bio-TEk Instruments Inc., USA). The 630 nm background absorbance was subtracted from the 540 nm measurement. The total protein release was calculated using a calibration curve (Appendix B) constructed with standard keratin solutions (0.5, 1, 2.5, 5, 10, 25, 50, 100, 150, 200, 250 and 300 μg/mL) prepared in PBS.

The *in vitro* degradation behavior of the Col/Ker/Alg hydrogel groups was also examined in cell culture medium at 37°C for 9 days. Dulbecco's Modified Eagle Medium (DMEM) supplemented with 10% (v/v) fetal bovine serum (FBS) and 1% (v/v) penicillin/streptomycin solution was used as a cell culture medium. At the end of day 9, the hydrogels were removed from media, washed with PBS (pH 7.2), and fixed with 4% paraformaldehyde (PFA) in PBS for 15 min at 4°C for 30 min. Following fixation, hydrogels were washed with distilled water and dehydrated using a series of ethanol solutions (30%, 50%, 70%, 80%, 96% and 100%) with each step lasting 5 minutes. Subsequently, the dehydrated hydrogels were dried at room temperature. The surface and cross-sectional morphology of dried hydrogel groups were analyzed using a SEM. Prior to SEM imaging, the lyophilized hydrogels were coated with a carbon layer using a high-vacuum coater.

The percentage porosity of the hydrogels was investigated using the liquid displacement method (n=4). The initial mass (m_0) and volume (V) of the lyophilized hydrogels were measured, and the hydrogels were then completely immersed in absolute methanol for 24 hours. After 24 hours, the hydrogels were removed from the methanol, excess methanol was removed gently with a filter paper and then were weighed (m_1). The percentage porosity of the hydrogels was calculated using the Equation 3.3 [132]:

$$\%\, porosity = \frac{m_1 - m0}{V \times \rho} \times 100 \tag{3.3}$$

ρ is the density of methanol.

3.2.4. Design of and Three-dimensional (3D) Printing Micro-Patterned Stamps

For the cell culture of fibroblast and keratinocyte cells, two distinct micro-patterned stamp designs were developed using computer-aided design (CAD) software (Autodesk® 3ds Max). The column-shaped extensions with a diameter of 500 μm on the stamp were

dimensioned according to cell type: 3 mm in length for human dermal fibroblasts-adult (HDF-a) and 1 mm in length for immortalized human keratinocytes (HaCaT). Each stamp was designed to form 19 evenly spaced channels on a circular surface with a 1 cm diameter (0.79 cm^2) on the hydrogel. An ergonomic structure was integrated into the stamp design to improve ease of handling.

The stamps were fabricated using an LCD-based resin 3D printer (Anycubic Photon Mono, China) and epoxy-based soybean oil resin. The 3D printer has a filament light source with a wavelength of 405 nm and a power of 45 W. The printer was operated using its default software settings: a layer thickness of 50 μm, with UV exposure times of 40 seconds for the first six layers and 2 seconds for all subsequent layers. At the end of the 3D-printing process, the samples were carefully removed from the printing platform and the resin residues were removed by rinsing three times with distilled water. The stamps were then dried at room temperature and cured twice for 10 minutes in a laboratory-built UV post-curing device with four 365 nm, 9 W UV lamps (total 36 W UV output) and a 360-degree rotating curing platform at 6 rpm [133]. Prior to use, the stamps were sterilized under a Class II biological safety cabinet (BiOptima, Telstar, Spain). They were washed with 70% ethanol and subsequently exposed to UV light for 30 min.

The surface morphology of micro-patterned hydrogels with deep and superficial channels created on their surface was analyzed using a SEM (GAIA3+Oxford XMax 150 EDS, Tescan, Czech Republic). Prior to SEM imaging, the lyophilized hydrogels were coated with a carbon layer using a high-vacuum coater (EM ACE600, Leica Microsystems, Germany).

3.2.5. Formation of 3D Co-Culture Environment

3.2.5.1. Cell Culture

Human dermal fibroblasts-adult (HDF-a) and immortalized human keratinocytes (HaCaT) were cultured using Dulbecco's Modified Eagle Medium (DMEM) supplemented with 10% (v/v) fetal bovine serum (FBS) and 1% (v/v) penicillin/streptomycin solution at 37°C in a 5% carbon dioxide (CO_2) in an incubator (MCO-170AICD-PE, PHCbi Corp.,

Japan). The culture media were replaced every three days, and the cells were sub-cultured at approximately 80-90% confluency by using a trypsin/EDTA solution. For both cells, the sub-culture ratio is 1:5.

3.2.5.2. In vitro cell viability

To determine the hydrogel group to be used in the formation of the 3D co-culture environment, *in vitro* cell viability of HDF-a cells on Col/Ker/Alg hydrogels, cross-linked with 0.10 M, 0.50 M, or 1.0 M $CaCl_2$, was examined. Prior to use, both sides of the hydrogels were UV-sterilized for 30 minutes under a Class II biological safety cabinet (BiOptima, Telstar, Spain).

To evaluate *in vitro* cell viability on hydrogels, a resazurin assay was performed [134], [135]. Resazurin assay is relying on the principle that living cells convert the resazurin dye (which is blue and non-fluorescent) into resorufin (a red and fluorescent compound). A 100 µL HDF-a cell suspension with a density of 5.0×10^5 cells/mL was seeded on the hydrogels, as well as on tissue culture plates (TCP) without hydrogel, which served as the control group. Cell seeded hydrogel and control group incubated in cell culture medium used in section 3.2.5.1 at 37°C in a CO_2-incubator for 1, 4 and 9 days (n=4). After each incubation period, the medium in all groups was removed and replaced with cell culture medium containing resazurin reagent solution at a ratio of 1:10 by volume. The resazurin reagent was prepared by dissolving 0.15 mg/mL of resazurin sodium salt of in PBS (pH 7.2) and sterilized by filtration through a 0.22 µm syringe filter. The samples were then incubated at 37 °C for 3 h in a CO_2-incubator. At the end of 3h, supernatants were taken from the samples into a 96-well plate and the absorbances were recorded at 540 and 630 nm utilizing a microplate reader (ELx800 Bio-TEk Instruments Inc., USA). The same procedure was also applied to hydrogel groups and TCP without cell seeding (negative control groups). The absorbance values of the hydrogel and control groups were normalized using the values obtained from excitation at the reference wavelength and the absorbance values of the negative control groups. The percentage of resazurin reduction was calculated using Equation 3.4 [136]:

$$\%\, reduction\ of\ resazurin = \frac{(O_2 \times A_1) - (O_1 \times A_2)}{(R_1 \times N_2) - (R_2 \times N_1)} \times 100 \qquad (3.4)$$

where

O_1=molar extinction coefficient of oxidized resazurin reagent at 540 nm (47619)

O_2 = Molar extinction coefficient of oxidized resazurin reagent at 630 nm (34798)

R_1 = Molar extinction coefficient of reduced resazurin reagent at 540 nm (104395)

R_2 = Molar extinction coefficient of reduced resazurin reagent at 630 nm (5494)

A_1 = Absorbance of the test sample (hydrogel group or TCP) at 540 nm

A_2 = Absorbance of the test sample (hydrogel group or TCP) at 630 nm

N_1 = Absorbance of the medium (negative control group) at 540 nm

N_2 = Absorbance of the medium (negative control group) at 630 nm

3.2.5.3. Formation and Characterization of 3D Co-Culture Environment

Both sides of the hydrogels to be used in preparing the 3D co-culture environment were UV-sterilized for 30 minutes under a Class II biological safety cabinet (BiOptima, Telstar, Spain). Using a micro-patterned sterile stamp specifically designed for HDF-a cell seeding, 3 mm channels (deep channels) were created on the hydrogels placed in 24-well plates. A 100 µL HDF-a cell suspension with a density of 2.5×10^5 or 5.0×10^5 cells/mL was seeded on the deep channel hydrogels, as well as on TCP without hydrogel, which served as a two-dimensional (2D) culture environment Cell seeded hydrogel groups and TCP groups incubated in cell culture medium used in section 3.2.5.1. overnight at 37°C in a CO_2-incubator. After incubation, 1 mm channels (superficial channels) were created on same hydrogels using a micro-patterned sterile stamp specifically designed for HaCaT cell seeding. Then, a 100 µL of HaCaT cell suspension with a density of 2.5×10^5 or 5.0×10^5 cells/mL was seeded on the superficial channel hydrogels, as well as on TCP without hydrogel. Cell seeded hydrogel groups and TCP groups incubated in cell culture medium used in section 3.2.5.1. at 37°C in a CO_2-incubator for 21 days Additionally, HDF-a and HaCaT cells were seeded separately onto the hydrogels and TCP. HDF-a and HaCaT 3D and 2D co-culture groups, and 3D and 2D culture groups seeded with only HDF-a or HaCaT are given in Table 3.1.

Table 3.1. HDF-a and HaCaT 3D and 2D co-culture groups, and 3D and 2D culture groups seeded with only HDF-a or HaCaT cells.

Group Name	Group Description
HDF-a hydrogel	HDF-a cells with a density of 5.0×10^5 cells/mL were seeded on deep channel hydrogels
HaCaT hydrogel	HaCaT cells with a density of 5.0×10^5 cells/mL were seeded on superficial channel hydrogels
HDF-a/HaCaT hydrogel 25 000	HDF-a and HaCaT cells, each with a density of 2.5×10^5 cells/mL, were seeded on hydrogels
HDF-a/HaCaT hydrogel 50 000	HDF-a and HaCaT cells, each with a density of 5.0×10^5 cells/mL were seeded on hydrogels
HDF-a TCP	HDF-a cells with a density of 5.0×10^5 cells/mL were seeded on TCP
HaCaT TCP	HaCaT cells with a density of 5.0×10^5 cells/mL were seeded on TCP
HDF-a/HaCaT TCP 25 000	HDF-a and HaCaT cells, each with a density of 2.5×10^5 cells/mL, were seeded on TCP
HDF-a/HaCaT TCP 50 000	HDF-a and HaCaT cells, each with a density of 5.0×10^5 cells/mL, were seeded on TCP

In the characterization of the 2D and 3D co-culture groups, and 3D and 2D culture groups seeded with only HDF-a or HaCaT cells, *in vitro* cell viability was monitored with resazurin assay and fluorescence analysis was performed using lipophilic Vybrant™ DiD (red) and Vybrant™ DiO (green) fluorescent cell markers.

For cell viability monitoring, 2D and 3D groups were incubated in cell culture medium used in section 3.2.5.1. at 37°C in a CO_2-incubator for 21 days (n=4). At the end of

day-1, 4, 7, 14 and 21, resazurin assay was performed as explained in Section 3.2.5.2 and the percentage of resazurin reduction was calculated using the Equation 3.4.

For the fluorescence analysis, HDF-a cells labeled with Vybrant™ DiO (green) and HaCaT cells labeled with Vybrant™ DiD (red) were seeded onto hydrogel and TCP groups given in Table 3.1. For the fluorescent labeling of cells, 5 µL of the respective cell-labeling solution was added per mL of HDF-a or HaCaT cell suspension at a density of 1×10^6 cells/mL in serum-free DMEM medium. The obtained solution mixed well by gentle pipetting and incubated for 15 min at 37°C. At the end of the incubation, the labeled cell suspensions were centrifuged at 800 rpm for HDF-a and 1500 rpm for HaCaT for 5 min. The supernatant was removed, and the labelled cells were gently resuspended in warm, complete cell culture medium.

In the fluorescence characterization of the 2D and 3D groups, fluorescently labelled cells were seeded on the 2D and 3D groups as indicated in Table 3.1. All groups were incubated in cell culture medium used in section 3.2.5.1. at 37°C in a CO_2-incubator for 7 days (n=3). At the end of 1^{st}, 4^{th} and 7^{th} days, the samples were examined using a fluorescence inverted microscope (DMi8, Leica Microsystems CMS GmbH, Germany) with a Leica CoolLED pE-300^{white} LED-based light source, a Leica CMOS camera and a LED405 filter cube (Ex: 405/60, Em: 470/40) and a FITC LP filter (Ex: 420/90, Em: 515). Fluorescent images are captured using the Leica DMi8 microscope digital camera system and the LAS X Imaging Software (Version 3.6.0.20104, Leica Microsystems CMS GmbH, Germany).

3.2.6. Statistical Analysis

All data are expressed as mean ± standard deviation. Statistical analysis was performed using IBM SPSS Statistics (Version 26.0).

For the statistical analysis of the water uptake capacity, *in vitro* degradation behavior of the hydrogels, total protein release from hydrogels, and *in vitro* cell viability: The assumption of normality was evaluated using the Shapiro-Wilk test, while the assumption of homogeneity of variances was assessed with Levene's test. Since the data did not meet the assumptions for parametric tests ($p < 0.05$ for at least one group), differences between groups

were analyzed using the Kruskal-Wallis test, followed by pairwise comparisons using the Mann-Whitney U test with Bonferroni correction. A significance level of $p \leq 0.05$ was considered statistically significant.

For the statistical analysis of percentage porosity of the hydrogels: One-Way Analysis of Variance (ANOVA) and Tukey HSD test were applied to determine the significant differences in groups. The assumption of normality was evaluated using the Shapiro-Wilk test, and the homogeneity of variance assumption was tested using Levene's test. Since both assumptions were met, a One-Way ANOVA test was conducted to examine whether there was a statistically significant difference between groups. If a significant difference was found, Tukey's HSD post-hoc test was performed to determine which groups differed from each other. A significance level of $p \leq 0.05$ was considered statistically significant.

4. RESULTS AND DISCUSSION

4.1. Extraction and Characterization of Collagen and Keratin

To prepare the Col/Ker/Alg hydrogels, collagen was extracted from bovine *Achilles* tendon, and keratin was extracted from human hair. The third component of the hydrogels, alginate, was purchased commercially. FT-IR spectra of extracted collagen and keratin with commercial alginate are shown in Figure 4.1. According to FT-IR spectrum for collagen, characteristic peaks corresponding to amide A, B, I, II and III are clearly observed in Figure 4.1.a. The broad band at around 3303 cm^{-1} can be attributed to the N-H stretching vibration of the Amide A [137]. On the other hand, the Amide B peak arises from the asymmetric stretching vibrations of the CH_2 group [137], and is observed at around 2926 cm^{-1} [138]. The absorption peaks at 1634 cm^{-1}, 1544 cm^{-1}, and 1236 cm^{-1} are attributed to the C=O stretching vibration of the amide I structure, the N-H bending and C-N stretching vibration peak of the amide II structure and the C-N stretching, N-H bending and C-H stretching vibrations of amide III, respectively [137], [139], [140]. Amide I, amide II, and amide III are directly associated with the peptide chain skeleton [137]. The peaks around 1402-1454 cm^{-1} are mainly associated with the vibrations of pyrrolidine rings in proline and hydroxyproline within the collagen structure [137], [141].

In the FTIR spectrum of extracted keratin, all the characteristic peaks specific to keratin are clearly observed (Figure 4.1.b). The broad band at 3278 cm^{-1} can be assigned to the amide A structure [142], formed by the N-H stretching in the keratin chains [143], [144]. The absorption peaks at 1648 cm^{-1}, 1541 cm^{-1} and 1196-1310 cm^{-1} belong to the amide I, amide II and amide III structures, respectively [128], [143]. The broad peak at 1648 cm^{-1} is associated with the C=O stretching vibration of the amide I structure [128], [145].The strong peak at 1541 cm^{-1} (amide II) is attributed to the N-H bending vibrations and C-N stretching vibrations [143]. The wide absorption band around 1196 cm^{-1} is associated with C-N stretching and C=O bending vibrations of amide III [128], [143]. The strong peak at 1023 cm^{-1} corresponds to the S–O symmetric stretching vibration of cysteine-S-sulfonate residues [128], [145], [146].

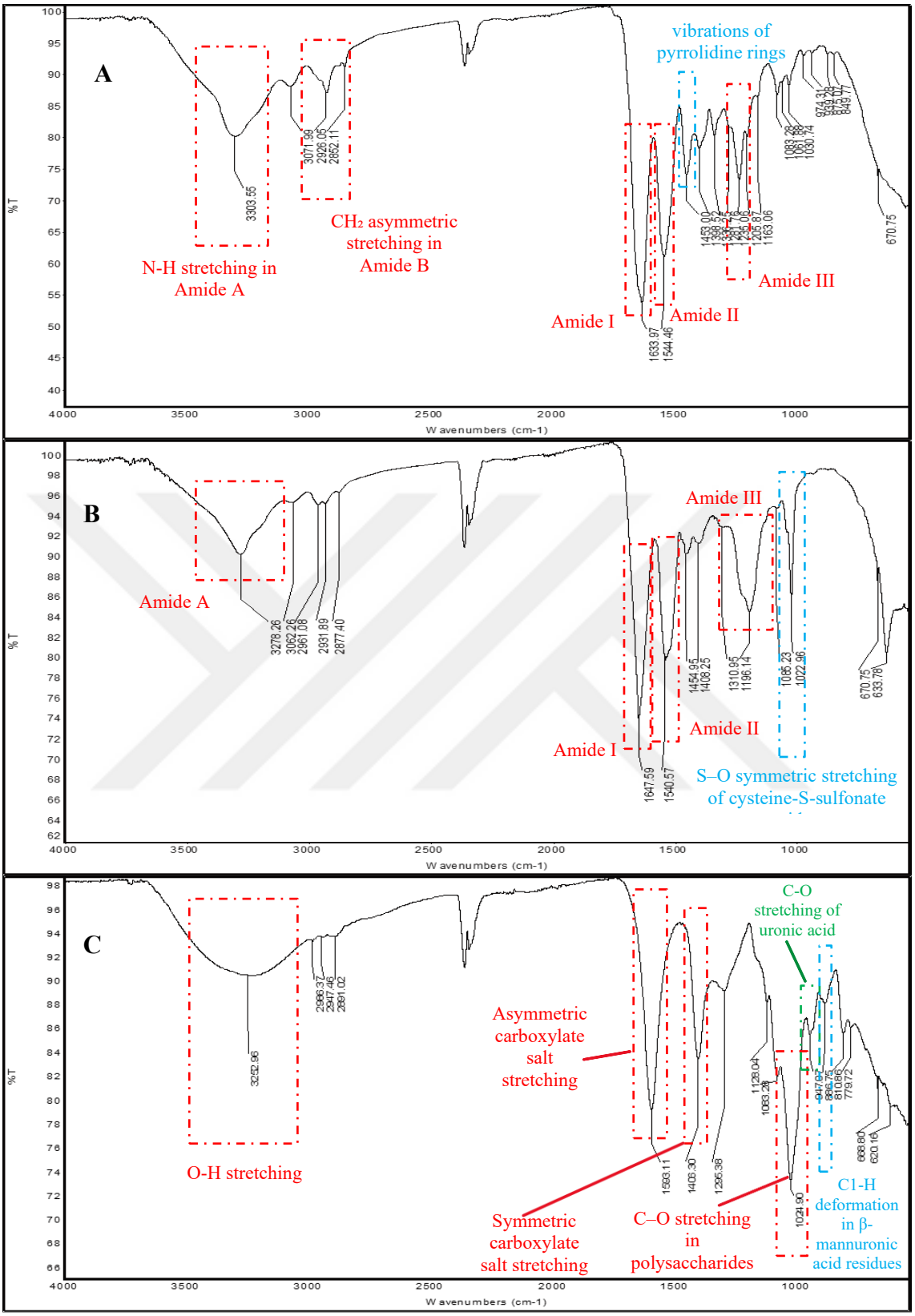

Figure 4.1. FTIR spectrum of extracted collagen from bovine *Achilles* tendon **(A)**, human hair keratin **(B)** and commercially obtained alginate **(C)**

The FTIR spectrum of sodium alginate is shown in Figure 4.1.c. The spectrum reveals characteristic peaks at 3253 cm^{-1}, corresponding to O-H stretching [147], and peaks at 1593 and 1406 cm^{-1}, which are attributed to the asymmetric and symmetric stretching vibrations of the carboxylate salt ion, respectively [148], [149]. Additionally, the peak at 1025 cm^{-1} is linked to C–O stretching within the polysaccharide structure [150]. The C-O stretching vibration of uronic acid residues is commonly associated with bands near 947 cm^{-1}, while the bands in the range of 871–883 cm^{-1} are linked to the C1-H deformation vibration of β-mannuronic acid residues [151]. The peaks at around 2300 cm^{-1} in the spectrum of collagen, keratin and alginate are generally not considered intrinsic features of these samples. Instead, they are most often attributed to instrumental artifacts or atmospheric interference that commonly affect the 2400–1900 cm^{-1} region in ATR-FTIR measurements.

The molecular weight and structural integrity of the extracted collagen and keratin were investigated by SDS-PAGE analysis. Figure 4.2.a shows an image of the SDS-PAGE gel containing different concentrations (10, 15, 20, 50 and 1000μg/mL) of collagen extracted from bovine *Achilles* tendons, a reference collagen sample (1000μg/mL) and protein ladder. One reference collagen sample was included in the test as a point of comparison: Sigma-Aldrich product collagen solution from human fibroblast (C2249). As shown in Figure 4.2.a, extracted collagen samples and reference collagen sample have alpha I (α1) and alpha II (α2) chains with molecular weights of approximately 130 kDa and 110 kDa, respectively. In addition, extracted collagen samples at 50 and 1000μg/mL concentration have beta (β) and gamma (γ) chains with a molecular weight of approximately 250 and 300 kDa, respectively. The characteristic alpha bands of type I collagen range from roughly 100 to 130 kDa, whereas the beta band is around 250 kDa [29]. SDS-PAGE analysis showed that extracted collagen samples were type I collagen. In a previous study, native collagen fibrils were extracted from bovine tendons using a modified acid-solubilized extraction and pepsin-aided method [152]. They observed that extracted native collagen fibrils have α1 and α2-chains with molecular weights of 135 and 100 kDa, respectively; β-chains with a molecular weight of 245 kDa; and γ-chains with a molecular weight higher than 250 kDa. As shown in Figure 4.2.a, reference collagen sample, prepared from the extracellular matrix secreted by normal human fibroblasts, has no beta (β) and gamma (γ) chains.

Figure 4.2.b shows an image of the SDS-PAGE gel containing different keratin samples with a 3 mg/mL concentration extracted from human hair and protein ladder. When the SDS-PAGE results of extracted keratin samples were examined, keratin samples extracted by reduction method have type I (acidic) keratins with molecular weight of between 39 - 45 kDa and type II (basic) keratin with molecular weight of 50-55 kDa [153]. In previous studies, extracted human hair keratin samples have shown α-keratin bands, which were also observed with a molecular weight between 40 and 60 kDa [128], [154].

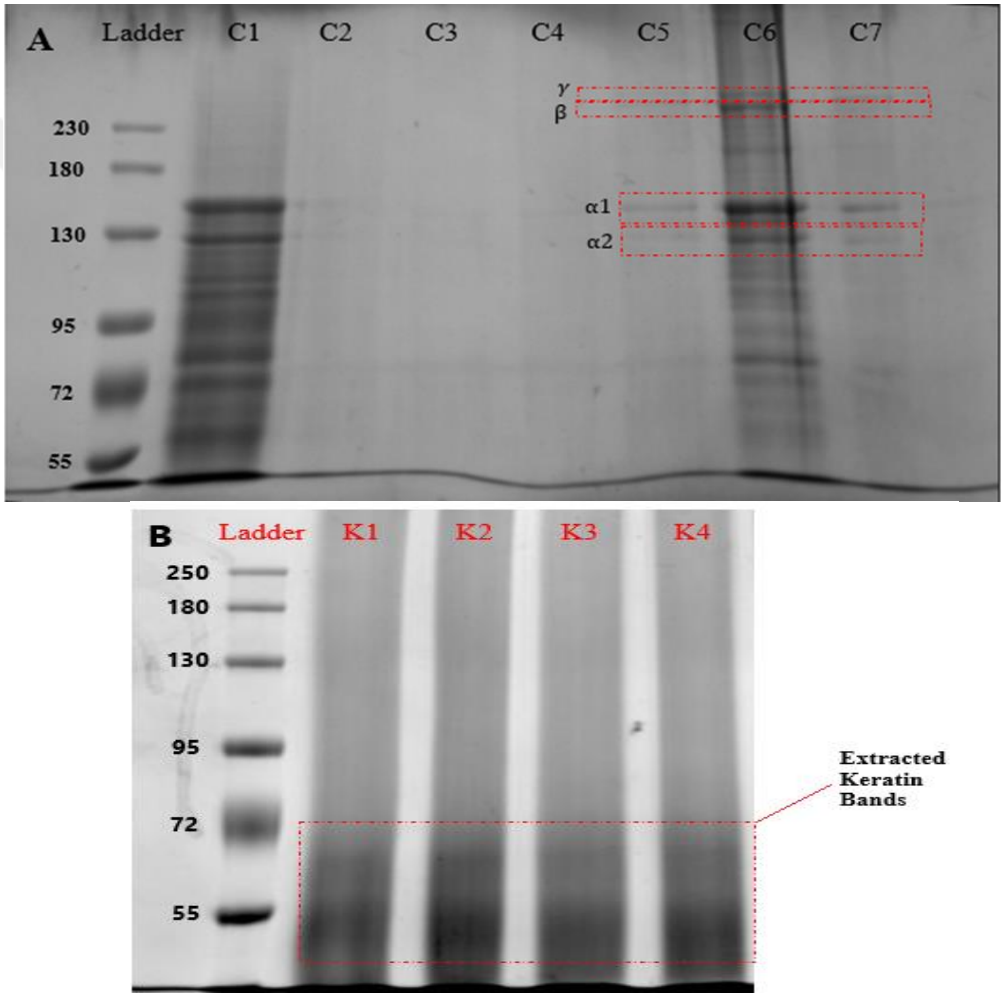

Figure 4.2. SDS-PAGE analysis of extracted collagen **(A)** and keratin **(B)**. C1: reference collagen sample (1000µg/mL); C2: extracted collagen (10 µg/mL); C3: extracted collagen (15 µg/mL); C4: extracted collagen (20 µg/mL); C5: extracted collagen (50 µg/mL); C6: extracted collagen (1000 µg/mL); C6: extracted collagen (50 µg/mL). K1-K4: extracted keratin (3 mg/mL)

4.2. Preparation and Characterization of Collagen/Keratin/Alginate Hydrogels

During the preparation of Col/Ker/Alg hydrogels, two different cross-linking strategies were used. First, the prepared hydrogel solutions were cross-linked using $CaCl_2$ solutions at varying concentrations (0.10 M, 0.50 M or 1.0 M). After that, they were further cross-linked using an EDC/NHS solution. $CaCl_2$ salt is widely used as a cross-linking agent for alginate hydrogels, as alginate readily undergoes ionic cross-linking with calcium ions through electrostatic interactions with the carboxyl groups along its polymer backbone [155]. EDC, a zero-length cross-linker, facilitates the formation isopeptide bonds between carboxyl and amine groups and is often used with NHS, which acts an EDC hydrolysis suppressor [156]. EDC/NHS is the most commonly used cross-linking agent for collagen due to its effective cross-linking ability and low cytotoxicity [157]. Three different hydrogel groups were obtained by varying the concentration of the calcium chloride cross-linker (0.10 M, 0.50 M, or 1.0 M) for subsequent optimization analyses. Macroscopic images from the hydrogel groups after lyophilization are shown in Figure 4.3. When the macroscopic images of hydrogels were examined, the structural integrity of the hydrogel cross-linked with 0.10 M $CaCl_2$ was not properly maintained, whereas the hydrogels cross-linked with 0.5 M and 1.0 M$CaCl_2$ exhibited a more uniform structure.

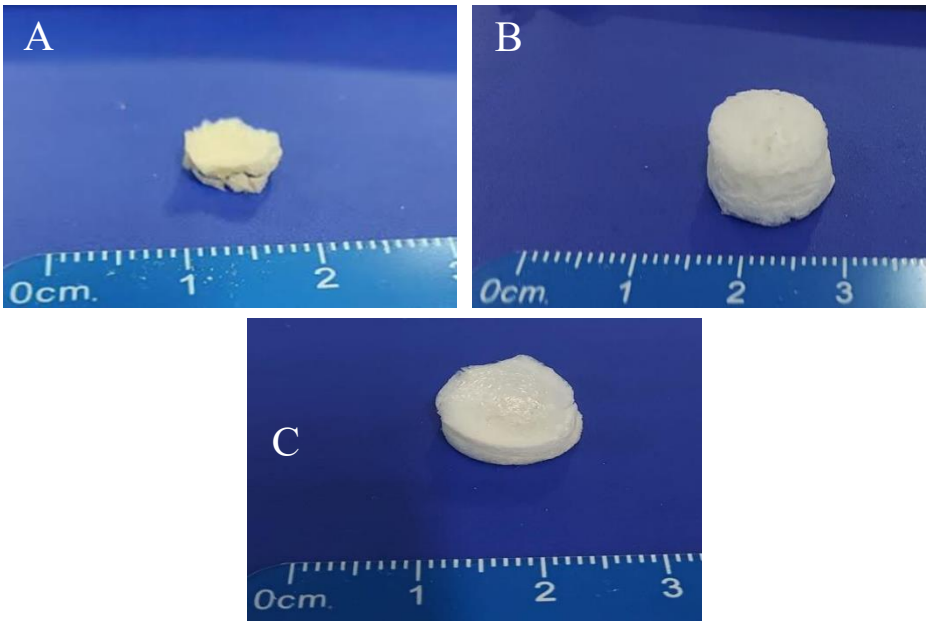

Figure 4.3. Macroscopic images from the hydrogels, cross-linked with 0.10 M **(A)**, 0.50 M **(B)**, or 1.0 M **(C)** $CaCl_2$

4.2.1. Chemical Properties of Hydrogels

The FTIR spectra of Col/Ker/Alg hydrogels cross-linked with 0.10 M, 0.50 M or 1.0 M $CaCl_2$ are given in Figure 4.4. Characteristic FTIR peaks of collagen, keratin and alginate are described in Section 4.1. were observed in the FTIR spectra of all hydrogel groups. The absorption peaks at around 3270-3283 cm^{-1} and 2850-2978 cm^{-1} are directly associated with amide A and amide B structures of protein components. The amide I is observed within the range of 1600–1700 cm^{-1}, whereas the amide II is observed at around 1538-1560 cm^{-1}. The amide III band was observed within the range of 1169-1245 cm^{-1}. The characteristic peak of alginate observed at 3253 cm^{-1} corresponds to the O-H stretching and overlaps with Amide A band of keratin and collagen. The absorption peaks around 1420 cm^{-1} are mainly associated with the vibrations of pyrrolidine rings in proline and hydroxyproline within the collagen structure, as well as the symmetric stretching vibrations of carboxylate salt ions related with alginate structure. The absorption peak at around 1023-1025 cm^{-1} corresponds to the S–O symmetric stretching vibration of cysteine-S-sulfonate residues of keratin and the C–O stretching of the polysaccharide structure of alginate. Additionally, absorption peaks related to uronic acid and β-mannuronic acid residues of alginate were observed at around 947 cm^{-1} and in the range of 871–883 cm^{-1}.

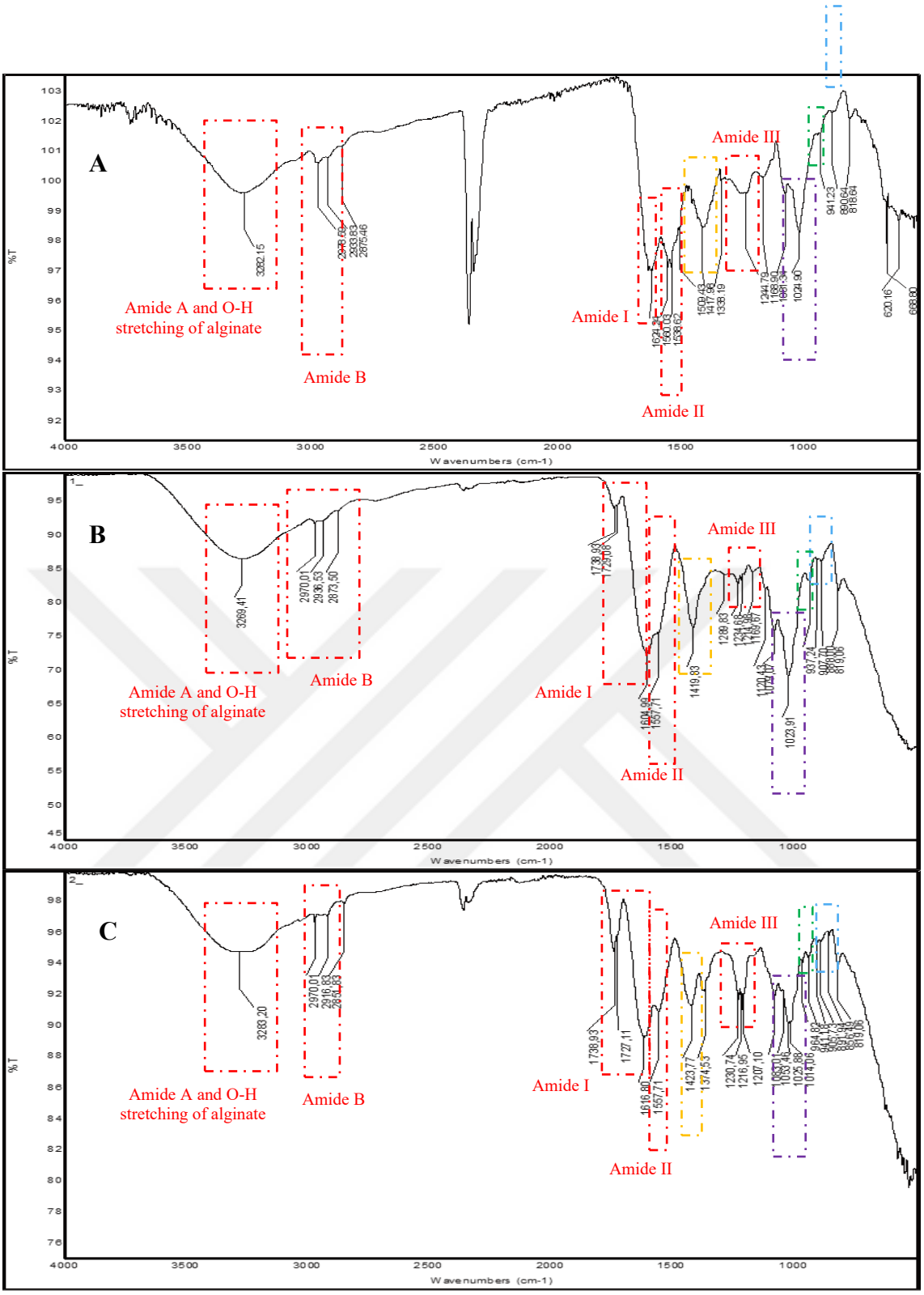

Figure 4.4. FTIR spectrum of Col/Ker/Alg hydrogels cross-linked with 0.10 M **(A)**, 0.50 M **(B)** or 1.0 M **(C)** $CaCl_2$ (Yellow label: pyrrolidine ring of collagen and carboxylate salt ion of alginate; Purple label: S-O symmetric stretching of cysteine-S-sulfonate of keratin and C-O stretching of alginate; Green label: uronic acid of alginate; Blue label: β-mannuronic acid of alginate)

4.2.2. Morphological Properties of Hydrogels

SEM images showing the surface and cross-sectional morphology of different hydrogel groups are given in Figure 4.5. When the surface morphologies were examined, there were variations in surface porosity among the groups. The surface morphology of the Col/Ker/Alg hydrogels changed with increasing $CaCl_2$ concentration. The surface of the hydrogel cross-linked with 0.10 M $CaCl_2$ was relatively smooth with minor porosity. As the concentration of $CaCl_2$ increased to 0.50 M, the surface roughness increased, with noticeable layer formations. The hydrogel cross-linked with 1.0 M $CaCl_2$ has a rough surface with visible crack structures. As the concentration of $CaCl_2$ cross-linker increased, the hydrogel surface became rougher and denser. The 0.10 M $CaCl_2$ cross-linked hydrogel had a low porous with obvious lamellar arrangements at the cross-sectional structure. The 0.50 M $CaCl_2$ cross-linked hydrogel had a more open and interconnected cross-sectional structure compared to 0.10 M $CaCl_2$ cross-linked hydrogel. The open and interconnected pores in the tissue scaffolds are important for the exchange of nutrients, gases and wastes within the hydrogel, supporting cellular functions such as cell migration and proliferation [158]. Additionally, the pores in the 0.50 M $CaCl_2$ cross-linked hydrogel were larger than those of 0.10 M $CaCl_2$ cross-linked hydrogel. The cross-sectional structure of the 1.0 M $CaCl_2$ cross-linked hydrogel was more compact and denser than that of the other hydrogels. Large, irregular fragments and breakages, which might indicate a brittle nature, were observed in the cross-sectional structure of 1.0 M $CaCl_2$ cross-linked hydrogel. This might be due to excessive $CaCl_2$ cross-linking. The results confirm that the concentration of $CaCl_2$ plays a pivotal role in determining hydrogel surface and cross-sectional morphology. Optimizing the cross-linker concentration is therefore critical for balancing porosity in hydrogels intended for tissue engineering applications. A lower concentration of $CaCl_2$ may induce reduced less cross-linking between alginate chains due to the limited availability of calcium ions required to form ionic bridges. At the lowest concentration (0.10 M), the insufficient availability of calcium ions restricted the extent of cross-linking, leading to a structure with lower porosity. This reduction in cross-linking can affect the structural stability of hydrogel as shown in Figure 4.3. In contrast, at the highest concentration (1.0 M), the increased availability of Ca^{2+} ions enhanced the cross-linking between alginate chains, leading to a more compact structure.

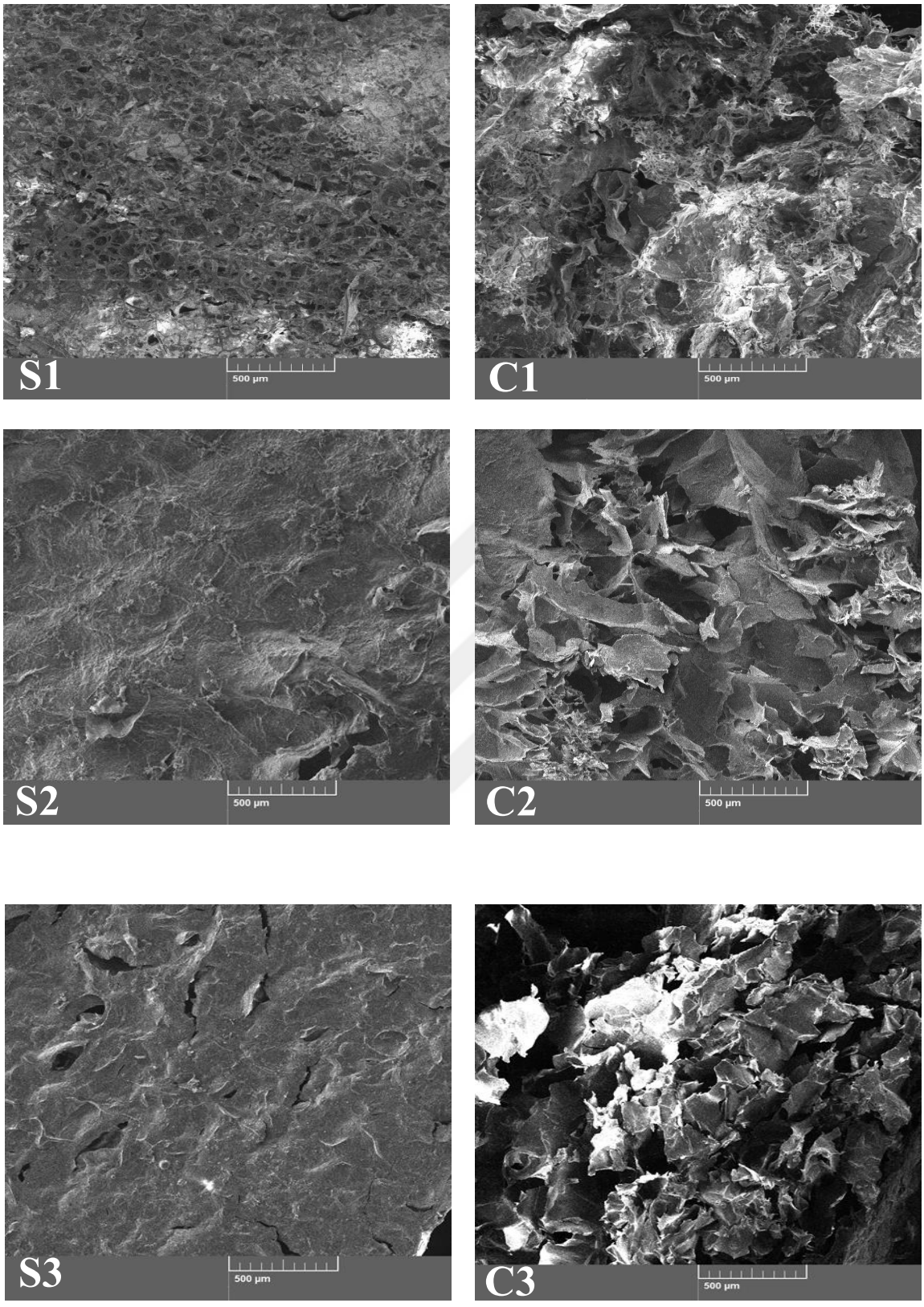

Figure 4.5. SEM images of the surfaces (S) and cross-sections (C) of Col/Ker/Alg hydrogels cross-linked with 0.10 M (S1, C1), 0.50 M (S2, C2) and 1.0 M (S3, C3) $CaCl_2$, at 100x magnification.

4.2.3. Percent Water Uptake Capacities of Hydrogels

The water uptake capacity of the hydrogels in PBS (0.1 M, pH 7.4) are shown in Figure 4.6. At 2 hours, there is no statistically significant difference between the hydrogel groups ($p = 0.055$). This indicates that the effect of $CaCl_2$ cross-linker concentration on water uptake is not yet apparent. Hydrogel cross-linked with 0.50 and 1.0M $CaCl_2$ had higher water uptake compared to those of hydrogel cross-linked with 0.10 M $CaCl_2$. In the study of Gajić *et al.*, the swelling ratio of alginate hydrogel was significantly influenced by the concentration of Ca^{2+} ions, resulting in a denser network structure [159]. Greater cross-linking of alginate chains resulted in a reduced swelling ratio and decreased water-retaining capacity. Although the Kruskal-Wallis test showed a general significant difference at the 4^{th}, 6^{th}, 24^{th},48^{th} and 72^{nd} hour, no statistically significant difference was found in pairwise comparisons since $p > 0.05$ (Table 4.1). During 72-hour incubation, the hydrogel cross-linked with 0.10 M $CaCl_2$ retained less water compared to other hydrogels due to its low-porosity structure with obvious lamellar arrangements, as seen in Figure 4.5. Because of its open and interconnected pores in the structure, the hydrogel cross-linked with 0.50M $CaCl_2$ showed the highest numerical percentage of water uptake value at the 4^{th}, 6^{th}, 48^{th} and 72^{nd} hours compared to that of other groups. The presence of open and interconnected pores might enhance better water diffusion and retention within the hydrogel. For the hydrogel cross-linked with 1.0 M $CaCl_2$, as described in Section 4.2.2, cross-linking with higher amount of calcium ions leads to fractures and cracks, which created large volumes of voids within the hydrogel. These voids may have contributed to an increased water retention capacity. In a previous study, poly(2-hydroxyethyl methacrylate) (PHEMA) and silk sericin (SS) hydrogel scaffolds with larger pores had higher degrees of swelling as larger pores allow for greater water uptake [160].

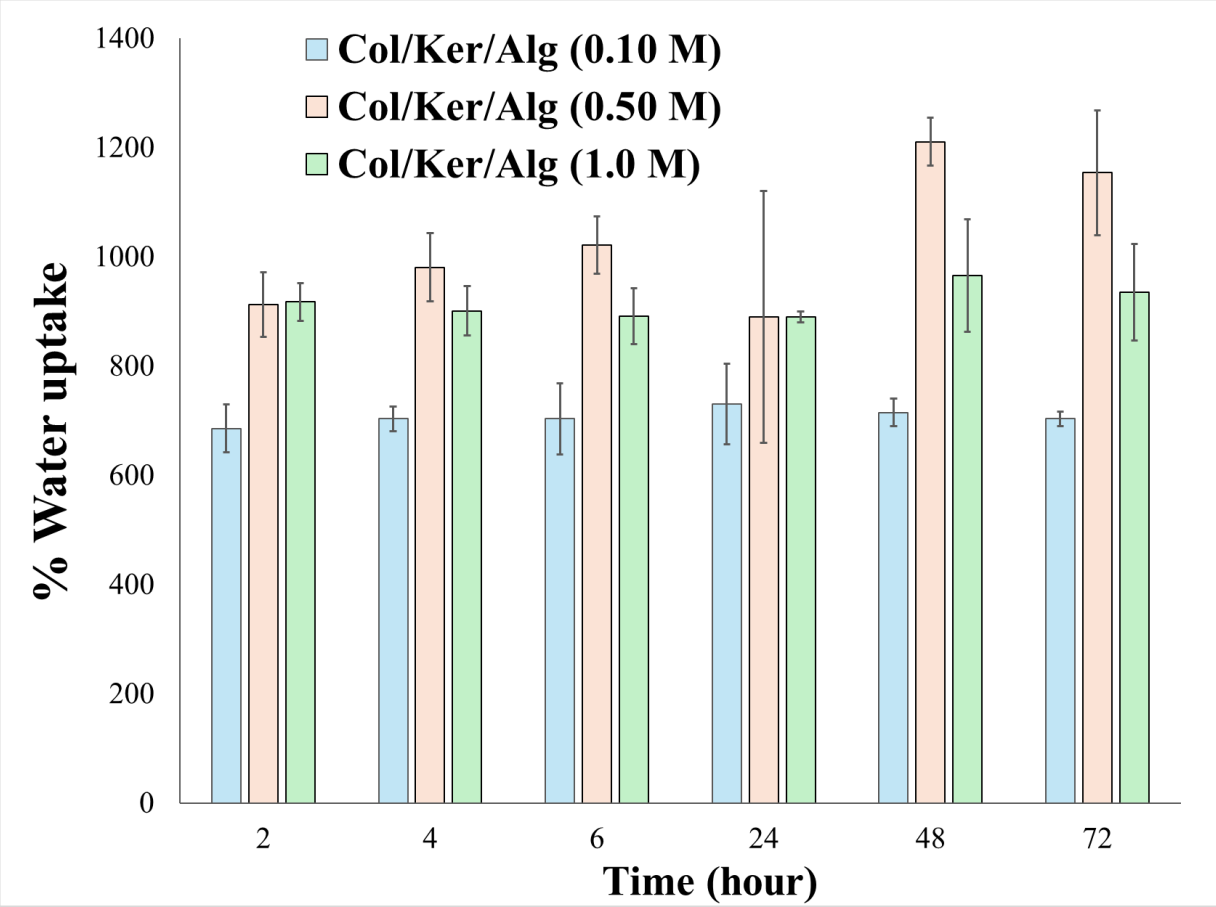

Figure 4.6. Percentage water uptake of Col/Ker/Alg hydrogels cross-linked with 0.10 M, 0.50 M and 1.0 M $CaCl_2$

Table 4.1. p values for percentage water uptake values of Col/Ker/Alg hydrogels cross-linked with 0.10 M, 0.50 M and 1.0 M $CaCl_2$ according to Mann-Whitney U test (significant difference ($p \leq 0.05$)

	4 h	**6 h**	**24 h**	**48 h**	**72 h**
Col/Ker/Alg (0.10M) vs. (0.50 M)	0.057	0.057	0.100	0.057	0.100
Col/Ker/Alg (0.10M) vs. (1.0M)	0.100	0.100	0.100	0.100	0.100
Col/Ker/Alg (0.50M) vs. (1.0M)	0.229	0.114	0.100	0.057	0.100

4.2.4. *In Vitro* Hydrolytic Degradation Behaviors of Hydrogels in PBS

The *in vitro* degradation of the hydrogels in PBS at 37°C is another important property that determines the stability of the hydrogels under physiologically relevant conditions. The *in vitro* hydrolytic degradation behaviors of the hydrogels in PBS containing Ca^{2+} and Mg^{2+} ions were given in Figure 4.7. The results indicate that hydrogels cross-linked with 0.10 M $CaCl_2$ exhibited a weight loss, while cross-linked with 1.0 M $CaCl_2$ exhibited lower weight loss among the groups. This result suggested that an increased degradation stability was observed due to stronger $CaCl_2$ cross-linking. Initially, all hydrogel formulations showed a rapid weight loss within the first two days, with the highest weight loss observed in the lowest $CaCl_2$ cross-linked group. At day-2 and day 14, a statistically significant differences ($p = 0.028$) were observed between the percentage of weight loss values of 0.50M and 1.0 M $CaCl_2$ cross-linked hydrogels (Table 4.2), indicating that the Col/Ker/Alg (1.0 M) had significantly lower degradation compared to the Col/Ker/Alg (0.50 M). At day-3, a statistically significant difference ($p = 0.028$) was observed between the percentage of weight loss values of 0.10 and 1.0 M $CaCl_2$ cross-linked hydrogels (Table 4.2). On day 7, no statistically significant differences were found among the groups (Table 4.2). The hydrogels with higher $CaCl_2$ cross-linking exhibited reduced degradation due to increased cross-linking, which provided a more stable polymeric network. In a previous study, cell-adhesive (RGD) and MMP-sensitive (VPMS↓MRGG) peptide domains incorporated hydrogel, formed from maleimide-functionalized hyaluronic acid, was developed for BMP-2 delivery [161]. The degradation rate of hydrogel decreased with increasing cross-link density. During the first two days, the 0.50 M hydrogel exhibited a lower degradation rate than the 1.0 M hydrogel. This difference may be attributed to the rough surface of 1.0 M hydrogel, which contains visible crack structures that could have led to sudden degradation during this period compared to the 0.50 M cross-linked hydrogel. However, in the following days, the situation appeared to reverse. 0.50 M cross-linked hydrogel, owing to its high-water retention capacity, may exhibit an increased degradation rate over time. In contrast, 1.0 M might demonstrate a more stable degradation kinetics. While the hydrogels cross-linked with 0.10 M and 1.0 M cross-linked hydrogels showed relatively stable weight loss over time, the 0.50 M cross-linked hydrogel may undergo continuous weight loss, a characteristic that could be advantageous in terms of biodegradability.

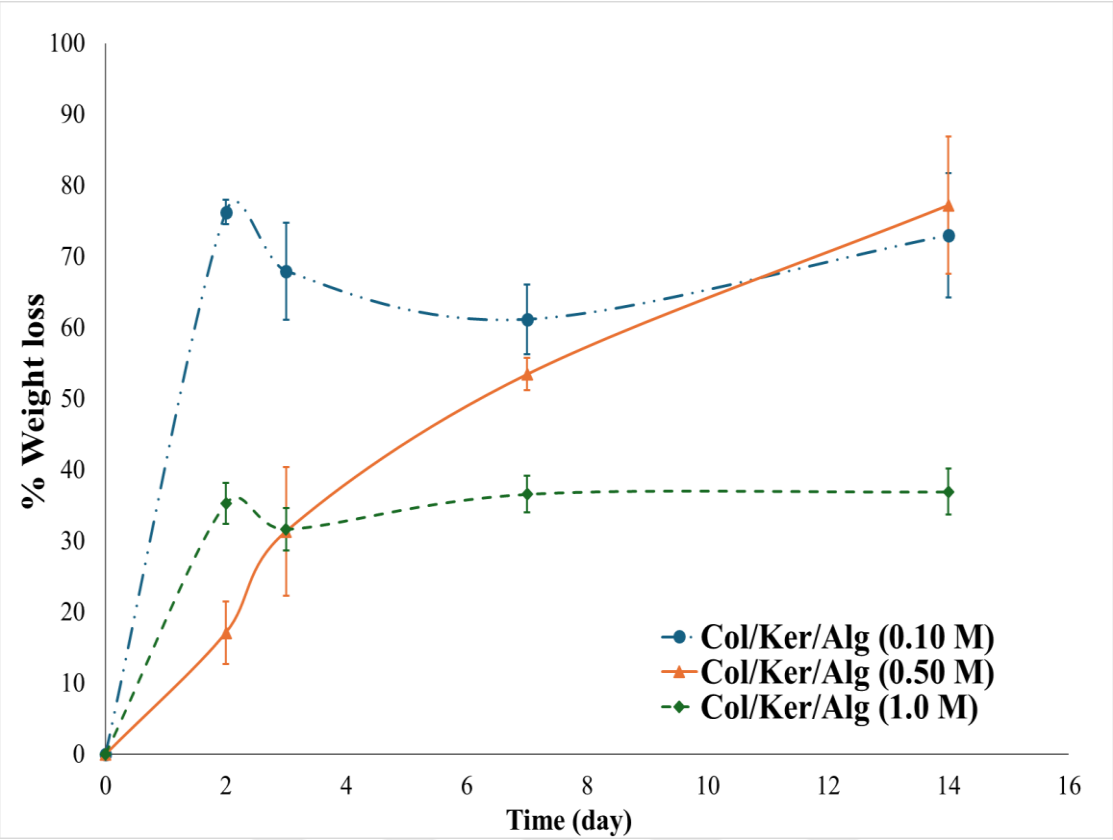

Figure 4.7. The *in vitro* hydrolytic degradation behaviors of Col/Ker/Alg hydrogels cross-linked with 0.10 M, 0.50 M and 1.0 M $CaCl_2$ (in PBS)

Table 4.2. p values for *in vitro* hydrolytic degradation behaviors of Col/Ker/Alg hydrogels cross-linked with 0.10 M, 0.50 M and 1.0 M $CaCl_2$ (in PBS) according to Mann-Whitney U test (significant difference ($p \leq 0.05$)

	2 day	**3 day**	**7 day**	**14 day**
Col/Ker/Alg (0.10M) vs. (0.50 M)	0.057	0.057	0.100	0.857
Col/Ker/Alg (0.10M) vs. (1.0M)	0.057	**0.028**	0.057	0.057
Col/Ker/Alg (0.50M) vs. (1.0M)	**0.028**	1.000	0.057	**0.028**

4.2.5. *In Vitro* Total Protein Release Profiles of Hydrogels

During the *in vitro* hydrolytic degradation analysis, the cumulative protein release profiles from the hydrogels were determined using the BCA assay. The total protein release was quantified by using a calibration curve (Appendix B) constructed with standard keratin solutions prepared in PBS. The selection of human hair keratin in this calibration curve is based on its water-soluble nature and smaller molecular size (as seen in Figure 4.2) compared to collagen, which is insoluble in water due to its extensive triple-helix structure. This structural rigidity significantly limits collagen's solubility in aqueous environments, which may affect its release behavior in PBS. Consequently, keratin's higher water solubility and smaller molecular size may facilitate its faster and greater release from the Col/Ker/Alg hydrogel, while collagen largely remained within the hydrogel matrix due to its poor water solubility and larger molecular weight. A previous study performed a comparative analysis of various sodium alginate-based hydrogel compositions, incorporating additives like gelatin or fish collagen at different concentrations [162]. The results showed that replacing gelatin with fish collagen at the same concentration resulted in materials with reduced swelling capacity, slower degradation, and lower protein release. This is attributed to the increased stability of collagen under physiological conditions, in contrast to gelatin, which is a water-soluble protein.

In vitro the percentage of cumulative release profiles of groups in PBS containing Ca^{2+} and Mg^{2+} ions were presented in Figure 4.8. During the first 6 hours, all hydrogels showed a burst release, with the 1.0 M $CaCl_2$ cross-linked hydrogel showing highest one. Until 6h, no statistically significant differences were found among the groups (Table 4.3). At 6h and Day 1, statistically significant differences were found between the 0.10 M and 1.0 M $CaCl_2$ cross-linked hydrogels and between the 0.50 M and 1.0 M $CaCl_2$ cross-linked hydrogels (Table 4.3). At 6h and Day 1, 1.0 M $CaCl_2$ cross-linked hydrogel exhibited higher protein release. As seen in Figure 4.5, 1.0 M $CaCl_2$ hydrogel had large, irregular fragments and breakages in the cross-sectional structure. These irregular fragments and breakages may have contributed to the rapid protein release. Day 3 and after, all groups were statistically significantly different from each other. (Table 4.3). After Day 2, 0.50 M $CaCl_2$ hydrogel exhibited the highest protein release, while 0.1 M $CaCl_2$ hydrogel showed the lowest protein release. As seen in Figure 4.5, 0.10 M $CaCl_2$ hydrogel showed the lowest porosity with a

smooth surface and lamellar arrangements in the cross-sectional structure. Additionally, these hydrogels had limited water uptake capacity compared to other groups (Figure 4.6). Therefore, slower water uptake may contribute to lower protein release. The highest protein release from the hydrogel cross-linked with 0.50 M $CaCl_2$ can be attributed to its higher water uptake capacity (Figure 4.6), more porous structure (Figure 4.5) and faster degradation rate (Figure 4.7) compared to other groups. Research indicates that a higher swelling rate in hydrogels results in the formation of larger pores, facilitating the transport of protein molecules from the hydrogel [163]. In a previous study showed that slowed degradation processes led to limited protein release alginate hydrogels containing gelatin or fish collagen [162].

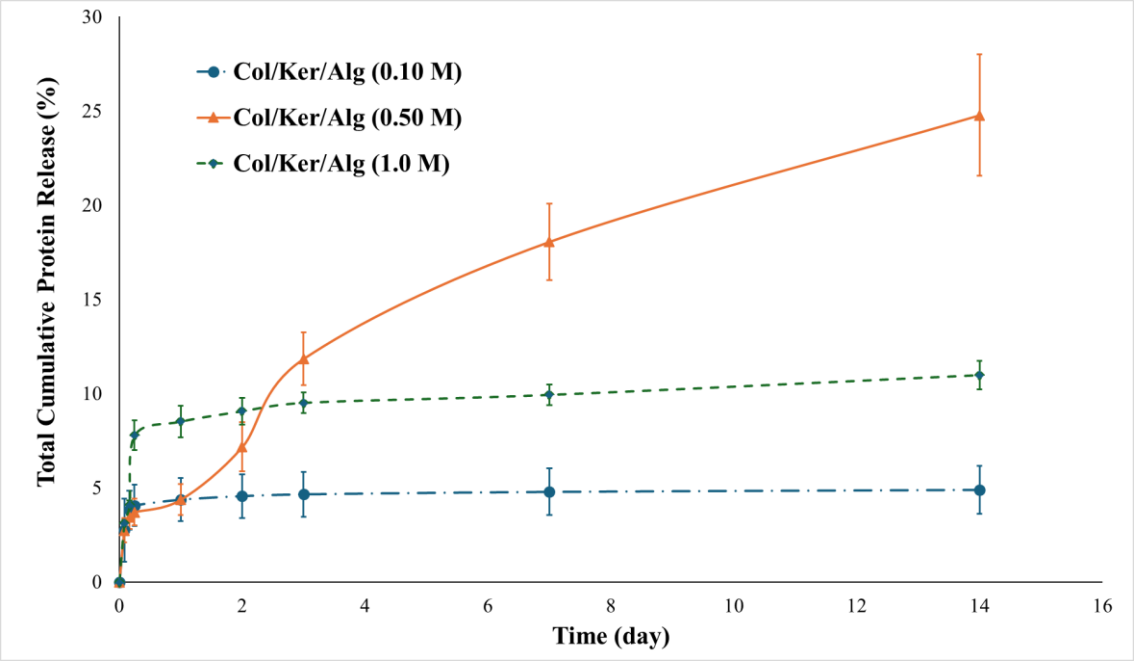

Figure 4.8. *In vitro* percentage of cumulative release profiles of Col/Ker/Alg hydrogels cross-linked with 0.10 M, 0.50 M and 1.0 M $CaCl_2$

Table 4.3. p values for *in vitro* percentage of cumulative release profiles of Col/Ker/Alg hydrogels cross-linked with 0.10 M, 0.50 M and 1.0 M $CaCl_2$ (in PBS) according to Mann-Whitney U test (significant difference ($p \leq 0.05$)

	2h	**4h**	**6h**
Col/Ker/Alg (0.10M) vs. (0.50M)	0.570	0.570	0.808
Col/Ker/Alg (0.10M) vs. (1.0M)	0.368	0.570	**0.004**
Col/Ker/Alg (0.50M) vs. (1.0M)	0.686	0.200	**0.029**

	1 day	**2 day**	**3 day**	**7 day**	**14 day**
Col/Ker/Alg (0.10M) vs. (0.50M)	1.000	**0.016**	**0.004**	**0.004**	**0.004**
Col/Ker/Alg (0.10M) vs. (1.0M)	**0.004**	**0.004**	**0.004**	**0.004**	**0.004**
Col/Ker/Alg (0.50M) vs. (1.0M)	**0.029**	0.114	**0.029**	**0.029**	**0.029**

4.2.6. *In Vitro* Degradation Behavior of the Hydrogels in Cell Culture Medium

The *in vitro* degradation behaviors of the hydrogels in cell culture medium at 37°C were given in Figure 4.9. All hydrogel groups had rougher and more irregular surfaces compared to Figure 4.5, showing evidence of structural degradation. According to Figure 4.5, 0.10 M $CaCl_2$ hydrogel showed roughest surface among the hydrogel groups. 0.50 M $CaCl_2$ hydrogel had a moderately rough surface with some porosity, whereas 1.0 M $CaCl_2$ hydrogel had the most compact surface among the groups. Higher cross-linking density (1.0 M $CaCl_2$) resulted in slow surface degradation as expected. This result is consistent with the findings in PBS, where low cross-linking resulted in faster degradation. Generally, sodium alginate in the hydrogels increases $CaCl_2$ cross-linking sites, leading to a slower degradation rate [164]. A previous study investigated sodium alginate and gelatin hydrogels, ionically cross-linked using $CaCl_2$ solutions at varying concentrations (10%, 5%, 2.5%, and 1%), in terms of mechanical properties, swelling behavior, FTIR, SEM, thermal stability, and biological characteristics [165]. They observed that hydrogels cross-linked with a 1% $CaCl_2$ solution exhibited higher weight loss compared to those cross-linked with a 2.5% $CaCl_2$ solution.

When the at the cross-sectional structure of hydrogels examined, hydrogel cross-linked with 0.10 M $CaCl_2$ showed low porosity with high lamellar structure. The presence of fragmented and lamellar structures suggested that 9-day incubation in cell culture medium adversely affected the structural integrity of the hydrogel. In the cross-sectional structure of 0.50 M $CaCl_2$ hydrogel, the interconnected pores were protected, providing a more stable structure and allowing for adequate nutrient and water exchange. The cross-sectional structure of the 1.0 M $CaCl_2$ hydrogel was denser than that of the other hydrogels. This might be due to excessive $CaCl_2$ cross-linking. Larger lamellar areas were seen at the cross-sectional structure of the 1.0 M $CaCl_2$ hydrogel.

After nine days of incubation in cell culture medium, the hydrogels showed better structural integrity compared to those incubated in PBS. PBS contained monovalent ions (e.g., Na^+, K^+) and divalent ions (e.g., Mg^{2+}, Ca^{2+}), which may compete with the cross-linking ions within the hydrogel matrix, leading to destabilization and accelerated degradation. In contrast, cell culture media are supplemented with FBS protein, which can adsorb onto the hydrogel surface, forming a protective barrier that slows down degradation. Additionally, PBS provides greater water availability, which promotes rapid swelling and hydrolytic degradation. In contrast, cell culture media contain biomolecules and nutrients that reduce the free diffusion of water into the hydrogel, thereby contributing to slower degradation rates

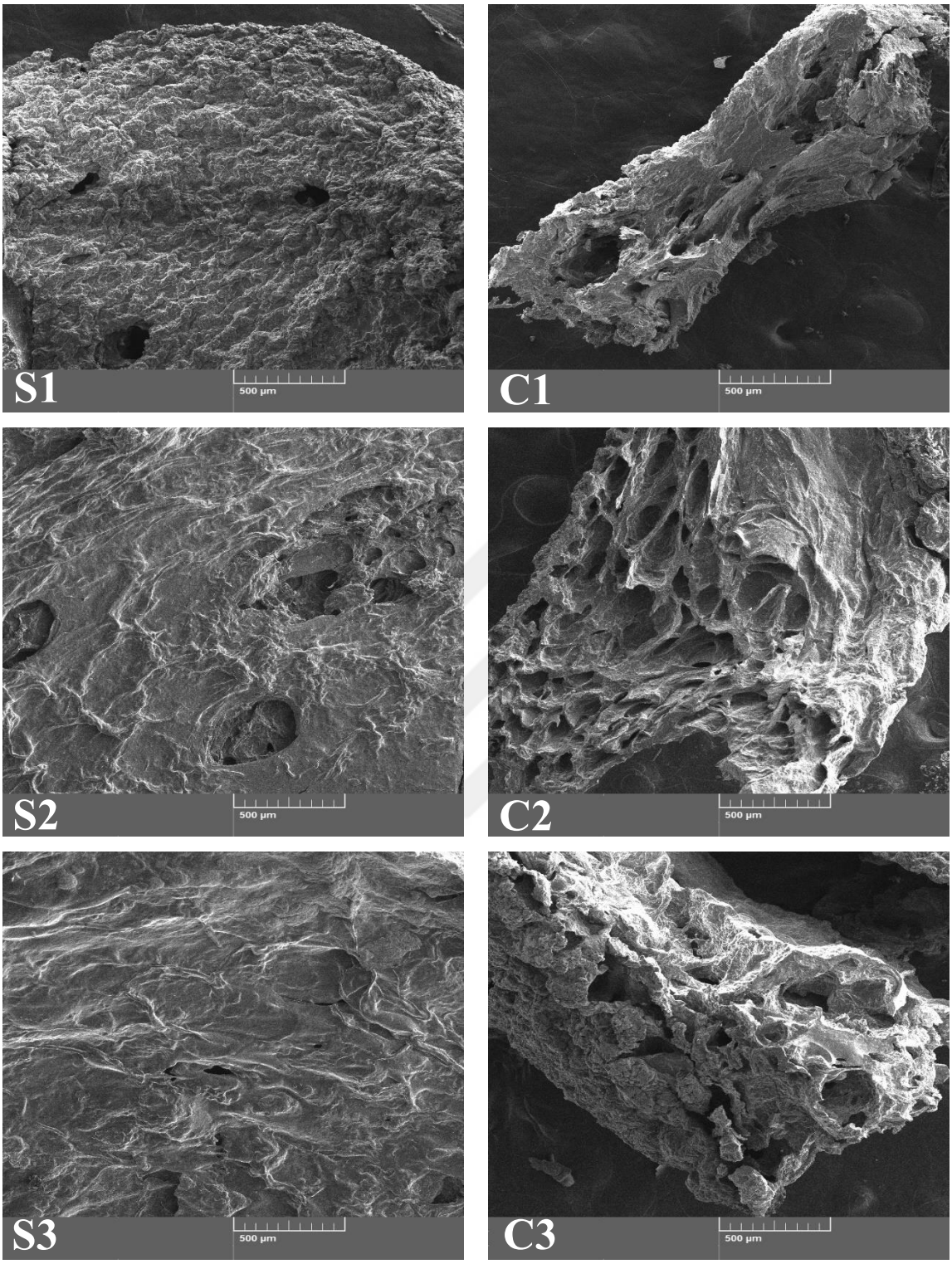

Figure 4.9. SEM images of the surfaces (S) and cross-sections (C) of Col/Ker/Alg hydrogels cross-linked with 0.10 M (S1, C1), 0.50 M (S2, C2) and 1.0 M (S3, C3) $CaCl_2$ after 9 days of incubation in cell culture medium, at 100x magnification.

4.2.7. Percent Porosity of Hydrogels

The percentage porosity of the hydrogels was shown in Figure 4.10. Hydrogel cross-linked with 0.10 M $CaCl_2$ showed the lowest porosity, while there are no significant differences between hydrogel cross-linked with 0.50 M or 1.0 M $CaCl_2$. These findings suggest that increasing the concentration of $CaCl_2$ cross-linker had a significant effect on porosity. As seen in Figure 4.5, hydrogel cross-linked with 0.10 M CaCl2 showed the lowest porosity with a smooth surface and lamellar arrangements in the cross-sectional structure. Additionally, these hydrogels had limited water uptake capacity compared to other groups (Figure 4.6). These results were correlated with those related to percentage porosity of the hydrogels. Hydrogel cross-linked with 0.50 M had higher porosity with interconnected pores, a rougher surface morphology, and higher water uptake capacity compared to the hydrogel cross-linked with 0.10 M $CaCl_2$, as shown in Figure 4.5 and Figure 4.6. The cross-sectional structure of hydrogel cross-linked with 1.0 M $CaCl_2$ had large, irregular fragments and breakages, resulting in a higher percentage porosity than that of the hydrogel cross-linked with 0.10 M $CaCl_2$.

Increasing the concentration of a crosslinking agent typically results in a denser polymer network with smaller and fewer pores as explained in Section 4.2.2. In many systems, a higher crosslinker concentration reduces overall porosity by restricting the mobility and spacing of polymer chains, thereby limiting the free volume available for pore formation. For instance, studies on superporous hydrogels have demonstrated that as crosslinker concentration increases, swelling capacity decreases, which directly correlates with reduced porosity [166]. Similarly, research on HEMA-based copolymers found that using crosslinkers with more reactive groups (i.e., a higher effective crosslinking concentration) formed denser, more compact networks with lower porosity [167].

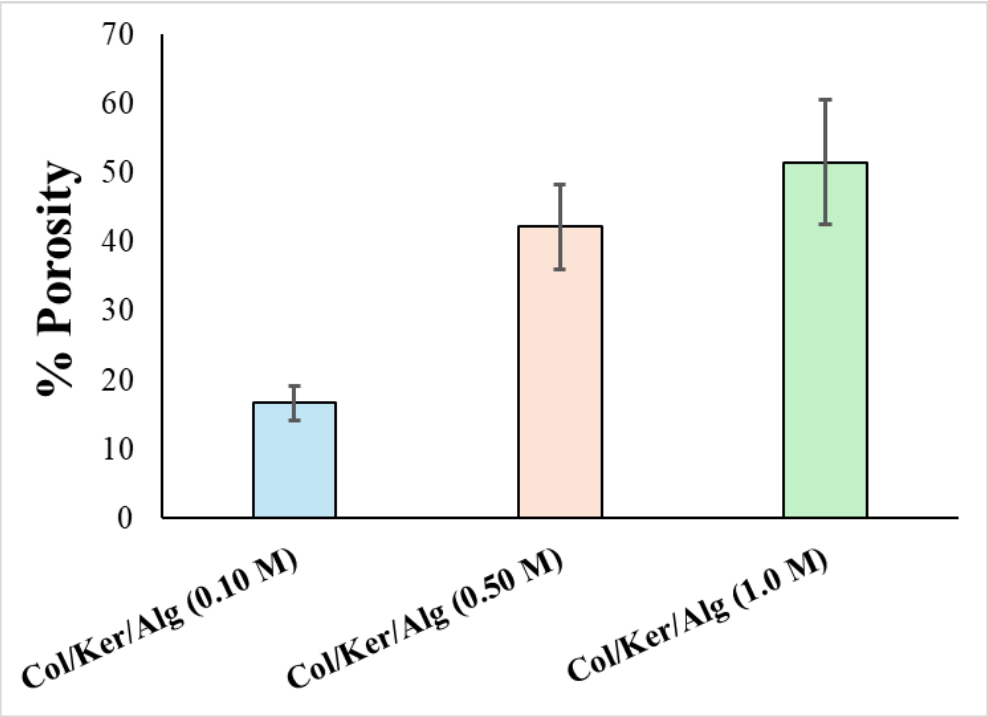

Figure 4.10. The percentage porosity of Col/Ker/Alg hydrogels cross-linked with 0.10 M, 0.50 M and 1.0 M $CaCl_2$

Table 4.4. p values for percentage porosity of Col/Ker/Alg hydrogels cross-linked with 0.10 M, 0.50 M and 1.0 M $CaCl_2$ according to One-Way ANOVA test (significant difference ($p \leq 0.05$)

Col/Ker/Alg (0.10M) vs. (0.50 M)	**0.0009**
Col/Ker/Alg (0.10M) vs. (1.0M)	**0.0001**
Col/Ker/Alg (0.50M) vs. (1.0M)	0.15339

4.3. 3D Printed Micro-Patterned Stamps

For the cell culture of fibroblast and keratinocyte cells, the designed micro-patterned stamps were successfully produced with a 3D printer. Figure 4.11. shows 3D-rendered models of micro-patterned stamps produced for fibroblast and keratinocyte cell seeding and photographs of the printed stamps. After the 3D printing of the stamps, measurements taken with a digital caliper showed that the design parameters were closely met. In addition, the surface and structural integrity of the resin material confirmed that the stamps could form uniform micro-patterns on the hydrogel surface. Visual assessments after the curing and sterilization processes confirmed that the stamps were suitable for use in terms of durability and surface quality.

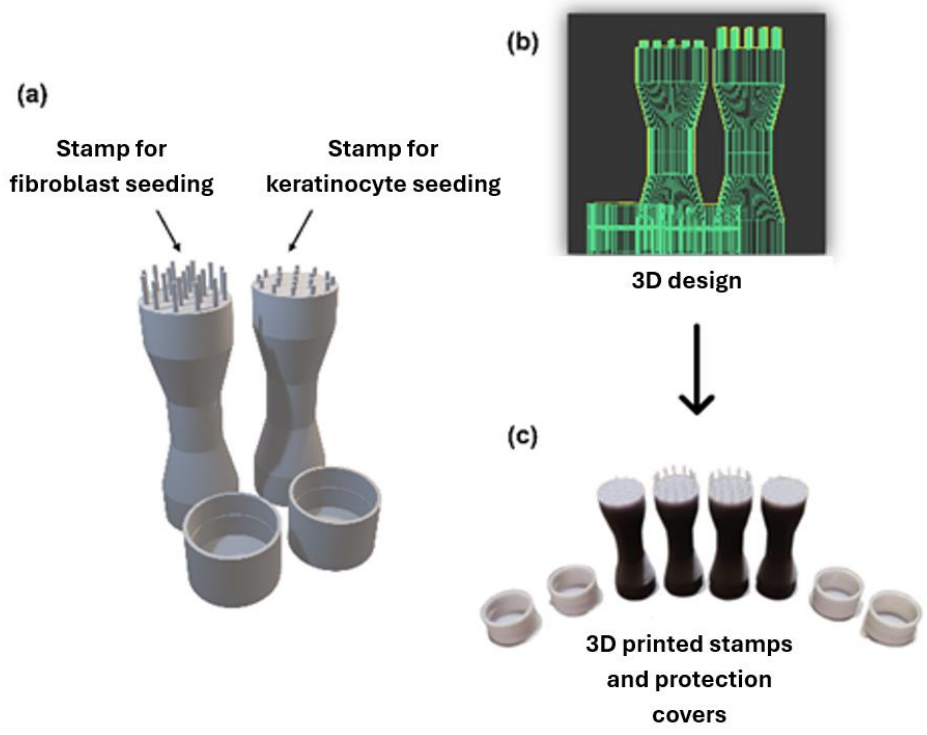

Figure 4.11. Micro-patterned stamps: **(a)** 3D stamp models and protective covers designed for seeding fibroblast and keratinocyte cells at different depths; (b) CAD design; (c) photograph of the 3D-printed stamps

The SEM images of deep and superficial channels formed using micro-patterned stamps on Col/Ker/Alg hydrogels are shown in Figure 4.12. Deep channels (Figure 4.5.a) were created on the hydrogels using the stamp designed for HDF-a cells, while superficial channels (Figure 4.5.d) were formed using the stamp designed for HaCaT cells. According to the SEM images of both groups, the diameter of the deep channels was larger than that of the superficial channels. After overnight incubation in PBS (pH 7.2) at 37°C, some of the deep channels on the hydrogel surface closed and disappeared (Figure 4.5.b). Figure 4.5.c shows the SEM image of the hydrogels used in the co-culture study, where the channels were formed as explained in Section 3.2.5.3. During the channel formation, deep channels were initially formed using the stamp designed for HDF-a cells. Then the hydrogels were then incubated overnight in PBS (pH 7.2) at 37°C. After that, superficial channels were formed using the stamp designed for HaCaT cells. Although some of the deep channels partially closed, the superficial channels remained visible. In addition, during the channel formation on the hydrogel surface, porous structures also formed between the channels compared to Figure 4.5. The presence of a porous structure between the channels suggests that the hydrogels can provide nutrients, gases, waste and fluid exchange during 3D co-culture.

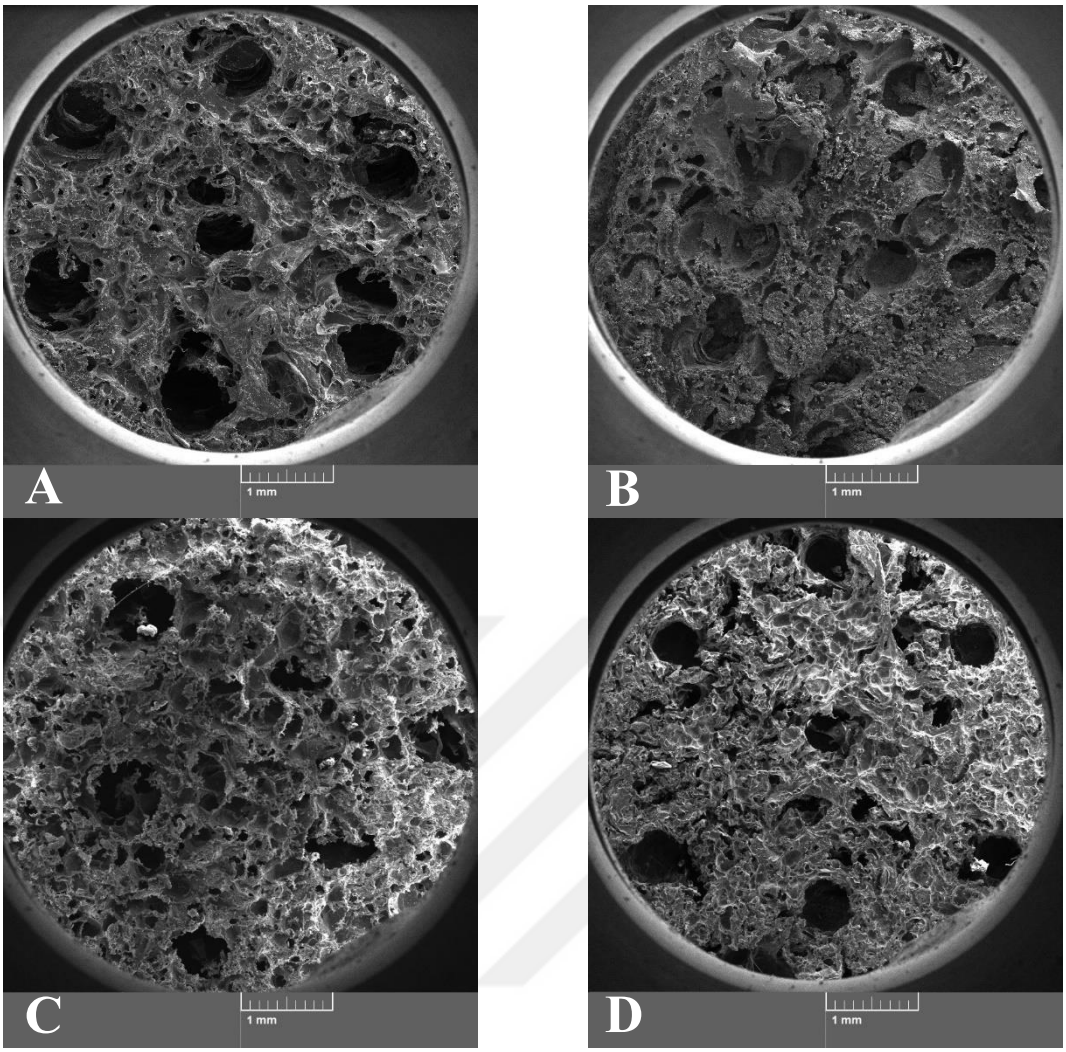

Figure 4.12. SEM images of the surfaces of micro-patterned hydrogels with deep and superficial channels created using stamps. **(A)** Group with deep channels created using the stamp designed for HDF-a cells, **(B)** Group with deep channels created using the stamp designed for HDF-a cells and incubated overnight in PBS (pH 7.2) at 37°C. **(C)** Group with deep channels created using the stamp designed for HDF-a cells, incubated overnight in PBS (pH 7.2) at 37°C, and then superficial channels created using the stamp designed for HaCaT cells. **(D)** Group with superficial channels created using the stamp designed for HaCaT cells.

4.4. Characterization of 3D Co-Culture Environment

To determine the hydrogel group to be used in the formation of the 3D co-culture environment, in addition to physicochemical characterizations, *in vitro* cell viability of HDF-a cells on Col/Ker/Alg hydrogels, cross-linked with 0.10 M, 0.50 M, or 1.0 M $CaCl_2$, was examined by using the resazurin assay (Figure 4.13). At the end of Day 1, HDF-a cells cultured on Col/Ker/Alg hydrogels cross-linked with 0.10 M $CaCl_2$ showed the highest viability (88.6 ± 5.9 %), significantly higher than that of cells cultured on TCP and cells cultured on other hydrogel groups (Table 4.4). 2D cultured cells (TCP) and cells cultured on hydrogels cross-linked with 1.0 M $CaCl_2$ had the lowest viabilities (61.6 ± 0.9 % and 60.8± 6.1 %, respectively) among the groups on Day 1. Only the viability of cells cultured on hydrogels cross-linked with 1.0 M $CaCl_2$ were not significantly different from the cells cultured on TCP (Table 4.4).

At the end of Day 4, there was no significant difference between the viability of cells cultured on hydrogels cross-linked with 0.50 M and 1.0 M $CaCl_2$ (Table 4.4). All the other groups were significantly different from each other. Again, hydrogels cross-linked with 0.10 M $CaCl_2$ showed the highest viability (108.0 ± 13.3 %), whereas 2D culture group (TCP) had the lowest viability (79.1 ± 5.8 %) among the groups on Day 4.

At the end of Day 9, cell cultured on hydrogels cross-linked with 0.10 M and 1.0 M $CaCl_2$ exhibited high cell viability (100.1 ± 7.7 % and 94.9 ± 1.3 %, respectively) among the groups. Also, cells cultured on hydrogels cross-linked with 0.50 M $CaCl_2$ had a higher cell viability (85.5 ± 2.3 %) compared to those of 2D cultured cells (TCP).

The findings suggest that the all-hydrogel groups provided an environment that supported HDF-a cell viability and proliferation over a period of 9 days. Based on protein release properties, high release of keratin and collagen into the medium may have greatly affected cell viability and proliferation of HDF-a cells.

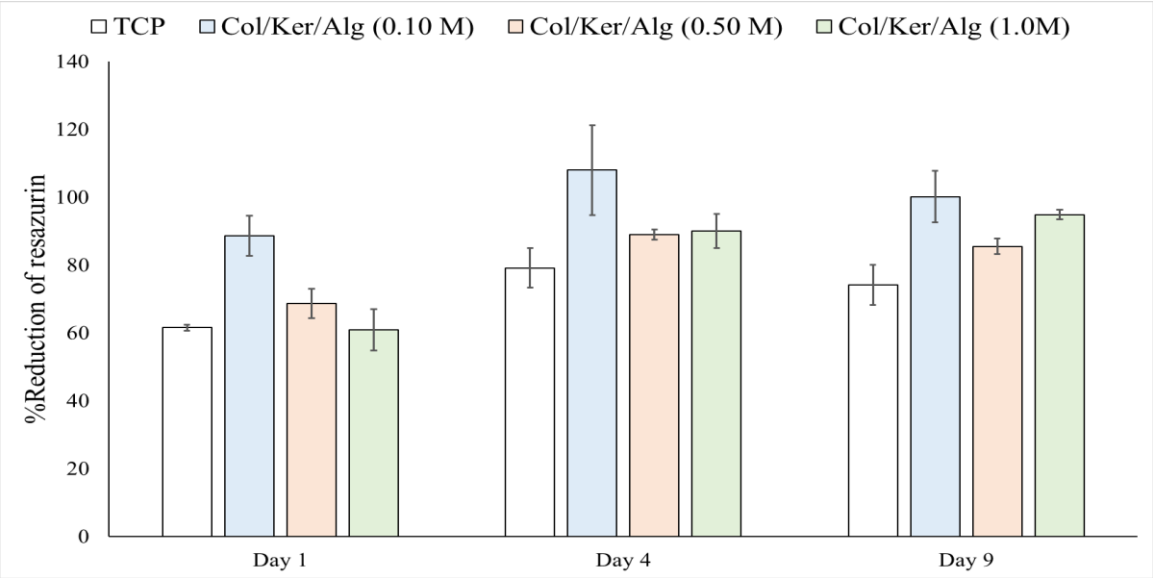

Figure 4.13. *In vitro* cell viability of HDF-a cells on Col/Ker/Alg hydrogels, cross-linked with 0.10 M, 0.50 M, or 1.0 M $CaCl_2$

Table 4.5. p values for *in vitro* cell viability of HDF-a cells on Col/Ker/Alg hydrogels cross-linked with 0.10 M, 0.50 M and 1.0 M $CaCl_2$ according to Mann-Whitney U test (significant difference ($p \leq 0.05$)

	Day 1	**Day 4**	**Day 9**
TCP vs. Col/Ker/Alg (0.10M)	**0.0014**	**0.0002**	**0.0014**
TCP vs. Col/Ker/Alg (0.50M)	**0.0025**	**0.0029**	**0.0022**
TCP vs. Col/Ker/Alg (1.0M)	0.5200	**0.0009**	**0.0002**
Col/Ker/Alg (0.10M) vs. (0.50M)	**0.0025**	**0.0004**	**0.0024**
Col/Ker/Alg (0.10M) vs. (1.0M)	**0.0025**	**0.0027**	0.3024
Col/Ker/Alg (0.50M) vs. (1.0M)	**0.0140**	0.4807	**0.0000**

According to results obtained from the physicochemical characterizations of hydrogel and *in vitro* cell viability study, Col/Ker/Alg hydrogels cross-linked with 0.50 M $CaCl_2$ were chosen for the formation of the 3D co-culture environment. This selection was primarily due to higher water uptake capacity (Figure 4.6) and more porous structure (Figure 4.5) compared to other groups, which are beneficial for cell proliferation and viability in 3D co-culture environment. In addition, the porosity in the cross-sectional structure of this hydrogel was protected at the end of a 9-day incubation in the cell culture medium (Figure 4.9). This structural integrity can ensure stability, adequate nutrient exchange, and a 3D co-culture environment conducive to cell growth.

Resazurin assay was used to monitor cell viability in the 2D and 3D co-culture groups, and 3D and 2D culture groups seeded with only HDF-a or HaCaT cells. The percentages of resazurin reduction for the groups for 21 days are given in Figure 4.14 and Figure 4.15. In addition, p-values for the values of the percentages of resazurin reduction for the 2D and 3D groups are presented in Table 4.6.

When the first day results were examined, the HDF-a hydrogel group showed the highest percentages of resazurin reduction with 62.48 ± 3.45% and the HDF-a/HaCaT hydrogel 50 000 group with 61.40 ± 2.91%. There was a statistically significant increase in the percentages of resazurin reduction of the hydrogel groups compared to the rates seen in the TCP groups with the same cell count and type. At the end of the first day, there was no statistically significant difference between the percent resazurin reduction rates of the HDF-a TCP (41.44 ± 1.29 %) and HaCaT TCP (39.29 ± 1.78 %) groups (Table 4.6). However, the percentages of resazurin reduction of the HDF-a/HaCaT TCP 50 000 group (45.81 ± 1.14 %) was statistically significant compared to the percentages of resazurin reduction of the HDF-a/HaCaT hydrogel 25 000 group (38.39 ± 2.04 %). There was no statistically significant difference between the percentages of resazurin reduction of the TCP co-culture groups and the HDF-a TCP and HaCaT TCP groups. When the first day results of the hydrogel groups were analyzed, there was no statistically significant difference between them (Table 4.6).

Fourth day results showed a statistically significant increase in the percentage percentages of resazurin reduction of the hydrogel groups compared to the TCP groups

(Figure 4.14 and Table 4.6). When TCP groups were compared among themselves, HaCaT TCP group (50.51 ± 3.51 %) had the lowest percentage resazurin reduction. At Day 4, percentage resazurin reduction of HDF-a TCP group (61.04 ± 2.75 %) was found significantly higher than those of HaCaT TCP group (50.51 ± 3.51 %) (Table 4.6). However, no statistically significant difference was observed between the other TCP groups (Table 4.6). Similarly, when comparing the hydrogel groups, there was no significant variation in the percentage resazurin reduction rates among them.

When the seventh day results were investigated, TCP co-culture groups showed the highest percentage resazurin reduction. When the TCP groups were compared among themselves, the HaCaT TCP group (59.93 ± 8.43 %) showed a statistically significant decrease in the percentage resazurin reduction compared to other TCP groups. In addition, HaCaT TCP group also had the lowest value among all groups. There was no statistically significant difference between the percentage resazurin reduction of the TCP groups except the HaCaT TCP group (Table 4.6). When the seventh day results of the hydrogel groups were analyzed, there was no statistically significant difference between them (Table 4.6).

When HaCaT TCP group and HaCaT hydrogel group were compared, it was observed that the percentage resazurin reduction of the hydrogel group (93.88 ± 8.92%) was significantly higher than that of the HaCaT TCP group (59.53 ± 8.43 %) (Table 4.6). When HDF-a TCP group and HDF-a hydrogel group were compared, no statistically significant difference was found (Table 4.6). When co-culture TCP and hydrogel groups were compared, the percentage resazurin reduction of TCP groups were significantly higher than those of hydrogel groups (Table 4.6). However, HDF-a/HaCaT hydrogel 50 000 group (87.57 ± 4.73 %) and HDF-a/HaCaT hydrogel 25 000 (85.08 ± 3.08 %) also showed high percentage resazurin reduction.

When the 14th day results were examined, there was no statistically significant difference between hydrogel groups (Table 4.6). When the TCP groups were compared among themselves, the HDF-a TCP (102.63 ± 3.86 %) showed a significant decrease in the percentage resazurin reduction compared to other TCP groups. In addition, HDF-a TCP group also had the lowest value among all groups. There was no statistically significant difference between the percentage resazurin reduction of the TCP groups except the HDF-a

TCP group (Table 4.6). When HaCaT TCP group and HaCaT hydrogel group were compared, the percentage resazurin reduction of the HaCaT TCP group (117.92 ± 2.98 %) was significantly higher than that of the HaCaT hydrogel group (82.79 ± 7.47 %) (Table 4.6). When HDF-a TCP group and HDF-a hydrogel group were compared, the percentage resazurin reduction of the HDF-a TCP (102.63 ± 3.86 %) was significantly higher than that of the HDF-a hydrogel group (85.89 ± 3.74 %) (Table 4.6). Similarly, the percentage resazurin reduction of the HDF-a/HaCaT TCP 50 000 (115.07 ± 1.90 %) was significantly higher than that of the HDF-a/HaCaT TCP 50 000 (88.43 ± 4.40 %). However, no statistically significant difference was found between HDF-a/HaCaT TCP 25 000 and HDF-a/HaCaT hydrogel 25 000 groups (Table 4.6).

When the 21st day results were examined, there was no statistically significant difference between the percentage resazurin reduction of the TCP groups except the HDF-a TCP group (Table 4.6). The HDF-a TCP (94.70 ± 8.60 %) showed a significant decrease in the percentage resazurin reduction compared to other TCP groups. There was no statistically significant difference between hydrogel groups (Table 4.6). Additionally, there was no statistically significant difference between HDF-a TCP and HDF-a hydrogel groups, nor between HDF-a/HaCaT TCP 25 000 and HDF-a/HaCaT hydrogel 25 000 groups (Table 4.6). The percentage resazurin reduction of the HaCaT TCP group (113.24 ± 4.92 %) was significantly higher than that of the HaCaT hydrogel group (96.17 ± 6.37 %) (Table 4.6). Similarly, the percentage resazurin reduction of the HDF-a/HaCaT TCP 50 000 group (112.31 ± 6.21 %) was significantly higher than that of the HDF-a/HaCaT hydrogel 50 000 group (91.65 ± 6.00 %).

The resazurin assay results demonstrated that cell viability increased over time in all groups. HaCaT and co-culture TCP groups exhibited enhanced the percentage resazurin reduction compared to other groups. When the first, fourth and seventh-day results were analyzed, the percentage of resazurin reduction increased over time in all groups. A more significant increase in resazurin reduction was observed in TCP co-culture groups compared to the groups in which the cells were alone. Notably, in the HaCaT TCP group, the percentage of resazurin reduction increased slowly compared to the other groups. On day 7, the percentage resazurin reduction of HaCaT TCP (59.93 ± 8.43 %) increased slowly compared to the TCP co-culture groups (around 101%). However, the percentage resazurin reduction

of HaCaT TCP increased rapidly after 7 days. On Day 21, there is no statistically significant difference between the percentage resazurin reduction of HaCaT TCP and TCP co-culture groups.

Since the pioneering studies of Rheinwald and Green demonstrated that fibroblasts stimulate keratinocyte proliferation in co-culture, various versions of co-culture systems have been developed to better mimic the in vivo conditions of normal skin [168]. A previous co-culture study by Gabbot and Sun showed that the attachment of HaCaT cells to the cell culture plate was further enhanced by pre-seeded HDFs [169]. In a study aimed at developing a 3D wound healing model using a type I collagen structure with fibrin-filled defects, it was demonstrated that the migration rate of keratinocytes significantly increased in the presence of fibroblasts ([170]). While keratinocytes in monoculture reached the center of the defect in seven days, this duration was reduced to three days in co-culture systems.

At the end of day 7, there was a more significant increase in the percentage resazurin reduction of the HaCaT hydrogel group (93.88 ± 8.92%) compared to the HaCaT TCP group (59.93 ± 8.43 %). However, after Day 7, a significant increase in the percentage of resazurin reduction was observed in the HaCaT TCP group compared to HaCaT hydrogel groups. In the hydrogel groups, there was no significant difference between the percentage of resazurin reduction values when HaCaT hydrogels and hydrogel co-culture groups were compared. No significant difference was found between HDF-a TCP and TCP co-culture groups at the end of the 7 days.

The percentage resazurin reduction of HDF-a hydrogels showed a significant increase compared to HDF-a TCP group during the first four days. After day 7, there is no statistically significant difference between the percentage of resazurin reduction values of the HDF-a TCP and HDF-a hydrogel groups. It is thought that the hydrogel environment supports HDF-a proliferation in the early period.

When co-culture TCP and hydrogel groups were compared, the percentages of resazurin reduction of TCP groups were lower than those of hydrogel groups until Day 7. After Day 7, the percentages of resazurin reduction of TCP groups were higher than those of hydrogel groups. However, high percentage of resazurin reduction values were also observed

in hydrogel co-culture groups. The fact that TCP co-culture groups exhibited higher reduction rates compared to hydrogel co-culture groups indicates that the higher density of cells in a smaller area in TCP medium and the increased interactions between cells in close proximity to each other increase the metabolic activity. On the other hand, since the cells were spread over larger areas due to the 3D structure and channel formation in certain regions in hydrogel groups, intercellular interactions were less than in TCP medium. At Day 14 and 21, cells seeded on hydrogel groups showed stable metabolic activity compared to their TCP counterparts. However, hydrogel groups still demonstrated higher percentage resazurin reduction values, suggesting that they provide a supportive environment for long-term culture.

HDF-a cells labeled with Vybrant™ DiO (green) and HaCaT cells labeled with Vybrant™ DiD (red) were used in the fluorescence analysis of the 3D co-culture medium of HDF-a and HaCaT cells. Fluorescence images of the hydrogel and TCP groups for 7 days are given in Figures 4.15-20. At all times, only green fluorescence staining was observed in HDF-a TCP and hydrogel groups, while only red fluorescence staining was observed in HaCaT TCP and hydrogel groups. The expected fluorescence staining was also observed in the co-culture TCP and hydrogel groups. Considering these results, the cells were properly labeled with Vybrant™ DiD and Vybrant™ DiO. It has been reported that Vybrant™ DiD and Vybrant™ DiO fluorescent labels have no effect on cell proliferation, that the degradation rates of both dyes are similar, and that the mixing effect between the dyes during the incubation period is negligible [171]. In a previous study, Vybrant™ DiD-labeled keratinocytes and Vybrant™ DiO-labeled fibroblasts were used to measure the migration of keratinocytes into fibrin-filled defects in the presence of fibroblasts within a 3D wound healing model composed of type I collagen with fibrin-filled defects [170].

At the end of the first day, it was confirmed by light microscopy images and fluorescent staining analysis that cells adhered to the surface of cell culture flasks in all TCP groups (Figure 4.15). In the hydrogel groups, cells were observed to aggregate in certain regions. When the hydrogel groups were analyzed, it was observed that the number of HDF-a cells in the hydrogel co-culture groups increased compared to the HDF-a hydrogel group. Compared to the HaCaT hydrogel group, HaCaT cells are seen in a larger area in the HDF-

a/HaCaT hydrogel 50.000 group. At the end of the fourth day, an increase in cell numbers was observed in all groups and this continued the following days.

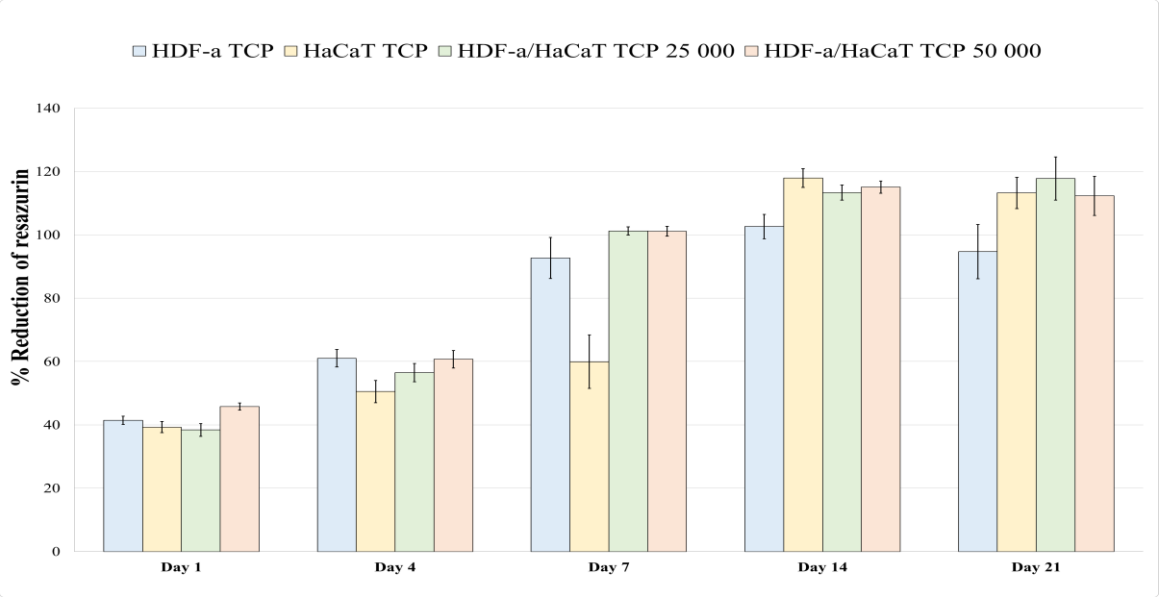

Figure 4.14. The percentages of resazurin reduction for 2D co-culture groups, as well as for 2D culture groups seeded with only HDF-a or HaCaT cells for 21 days

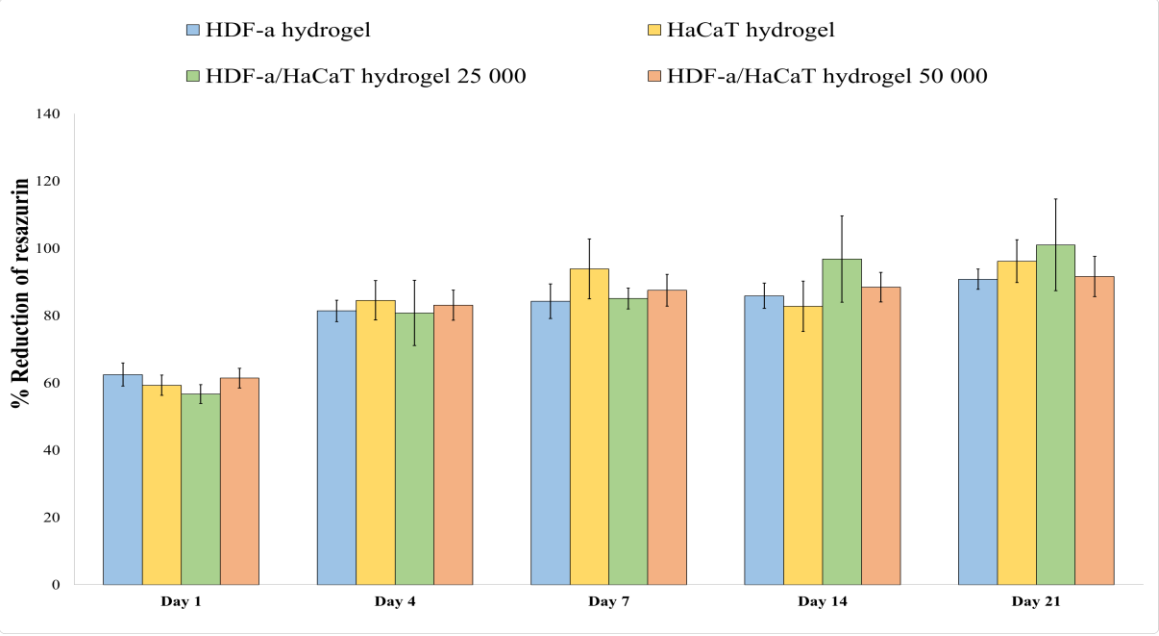

Figure 4.15. The percentages of resazurin reduction for 3D co-culture groups, as well as for 3D culture groups seeded with only HDF-a or HaCaT cells for 21 days

Table 4.6. p values for the percentages of resazurin reductions for 21 days (significant difference ($p \leq 0.05$)

	Day 1	Day 4	Day 7	Day 14	Day 21
HDF-a TCP vs. HaCaT TCP	1.0000	**0.0087**	**0.0044**	**0.0186**	**0.0186**
HDF-a TCP vs. HDF-a/HaCaT TCP 25 000	0.1958	0.2915	1.0000	**0.0044**	**0.0044**
HDF-a TCP vs. HDF-a/HaCaT TCP 50 000	**0.0087**	1.0000	1.0000	**0.0044**	**0.0087**
HaCaT TCP vs. HDF-a/HaCaT TCP 25 000	1.0000	0.2915	**0.0044**	0.2238	1.0000
HaCaT TCP vs. HDF-a/HaCaT TCP 50 000	**0.0044**	**0.0044**	**0.0044**	1.0000	1.0000
HDF-a/HaCaT TCP 25 000 vs. HDF-a/HaCaT TCP 50 000	**0.0044**	0.2915	1.0000	1.0000	1.0000
HDF-a TCP vs. HDF-a hydrogel	**0.0044**	**0.0044**	0.4133	**0.0044**	1.0000
HDF-a TCP vs. HaCaT hydrogel	**0.0044**	**0.0044**	1.0000	**0.0044**	1.0000
HDF-a TCP vs. HDF-a/HaCaT hydrogel 25 000	**0.0044**	**0.0044**	0.3543	1.0000	1.0000
HDF-a TCP vs. HDF-a/HaCaT hydrogel 50 000	**0.0044**	**0.0044**	1.0000	**0.0044**	1.0000
HaCaT TCP vs. HDF-a hydrogel	**0.0044**	**0.0044**	**0.0044**	**0.0186**	**0.0186**
HaCaT TCP vs. HaCaT hydrogel	**0.0044**	**0.0044**	**0.0186**	**0.0186**	**0.0186**
HaCaT TCP vs. HDF-a/HaCaT hydrogel 25 000	**0.0044**	**0.0044**	**0.0186**	0.5594	1.0000
HaCaT TCP vs. HDF-a/HaCaT hydrogel 50 000	**0.0044**	**0.0044**	**0.0044**	**0.0186**	0.0606
HDF-a/HaCaT TCP 25 000 vs. HDF-a hydrogel	**0.0044**	**0.0044**	**0.0044**	**0.0044**	**0.0044**
HDF-a/HaCaT TCP 25 000 vs. HaCaT hydrogel	**0.0044**	**0.0044**	1.0000	**0.0044**	**0.0044**
HDF-a/HaCaT TCP 25 000 vs. HDF-a/HaCaT hydrogel 25 000	**0.0044**	**0.0044**	**0.0186**	1.0000	0.7876
HDF-a/HaCaT TCP 25 000 vs. HDF-a/HaCaT hydrogel 50 000	**0.0044**	**0.0044**	**0.0044**	**0.0044**	**0.0186**
HDF-a/HaCaT TCP 50 000 vs. HDF-a hydrogel	**0.0044**	**0.0044**	**0.0044**	**0.0044**	**0.0044**
HDF-a/HaCaT TCP 50 000 vs. HaCaT hydrogel	**0.0044**	**0.0044**	1.0000	**0.0044**	**0.0174**
HDF-a/HaCaT TCP 50 000 vs. HDF-a/HaCaT hydrogel 25 000	**0.0044**	**0.0044**	**0.0186**	1.0000	1.0000
HDF-a/HaCaT TCP 50 000 vs. HDF-a/HaCaT hydrogel 50 000	**0.0043**	**0.0044**	**0.0044**	**0.0044**	**0.0186**
HDF-a hydrogel vs. HaCaT hydrogel	1.0000	1.0000	1.0000	1.0000	1.0000
HDF-a hydrogel vs. HDF-a/HaCaT hydrogel 25 000	0.1958	1.0000	1.0000	0.5787	0.5787
HDF-a hydrogel vs. HDF-a/HaCaT hydrogel 50 000	1.0000	1.0000	1.0000	1.0000	1.0000
HaCaT hydrogel vs. HDF-a/HaCaT hydrogel 25 000	1.0000	1.0000	1.0000	0.5787	1.0000
HaCaT hydrogel vs. HDF-a/HaCaT hydrogel 50 000	1.0000	1.0000	1.0000	1.0000	1.0000
HDF-a/HaCaT hydrogel 25 000 vs. HDF-a/HaCaT hydrogel 50 000	0.1305	1.0000	1.0000	1.0000	1.0000

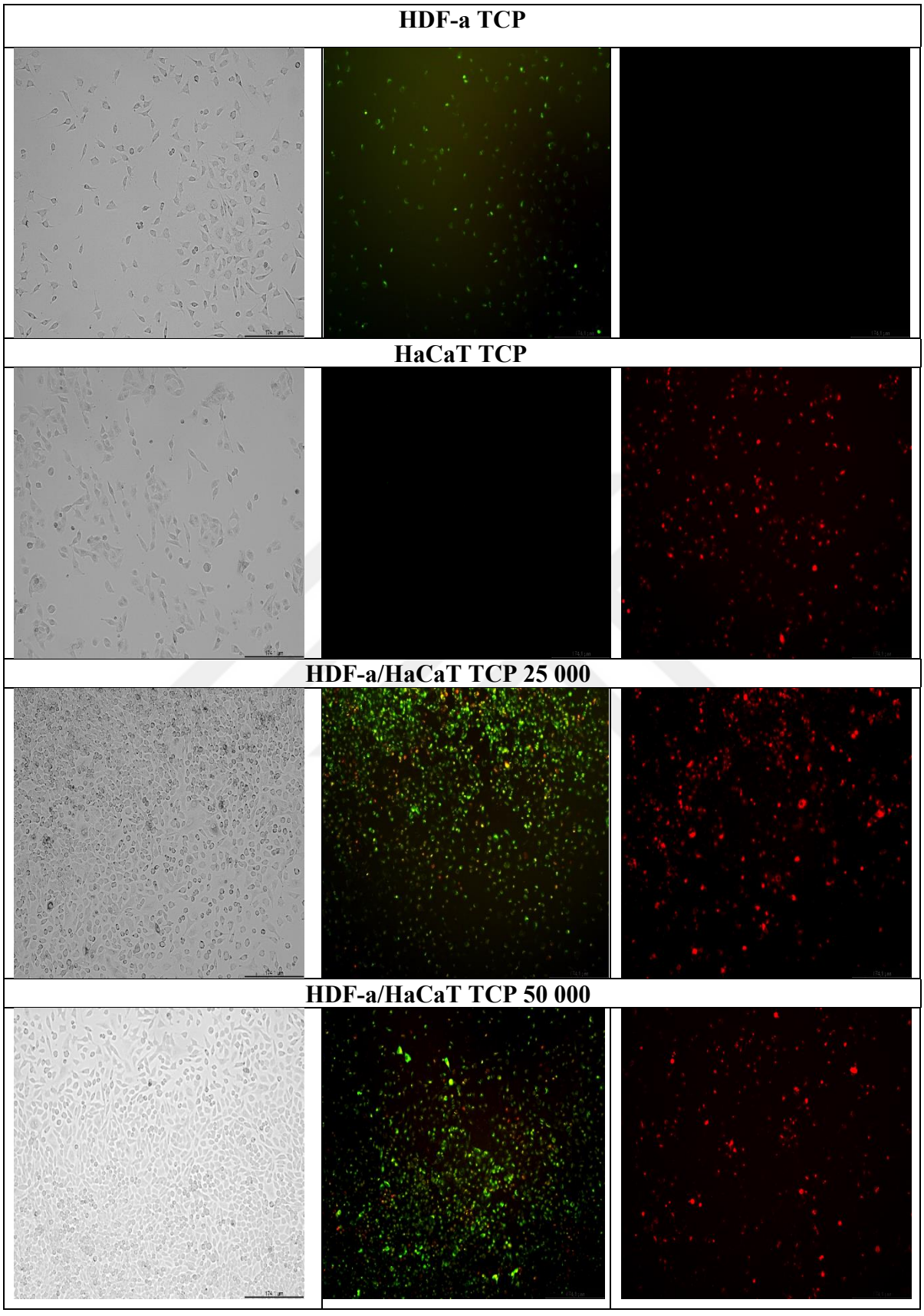

Figure 4.16. Fluorescence images of TCP groups at the end of Day 1

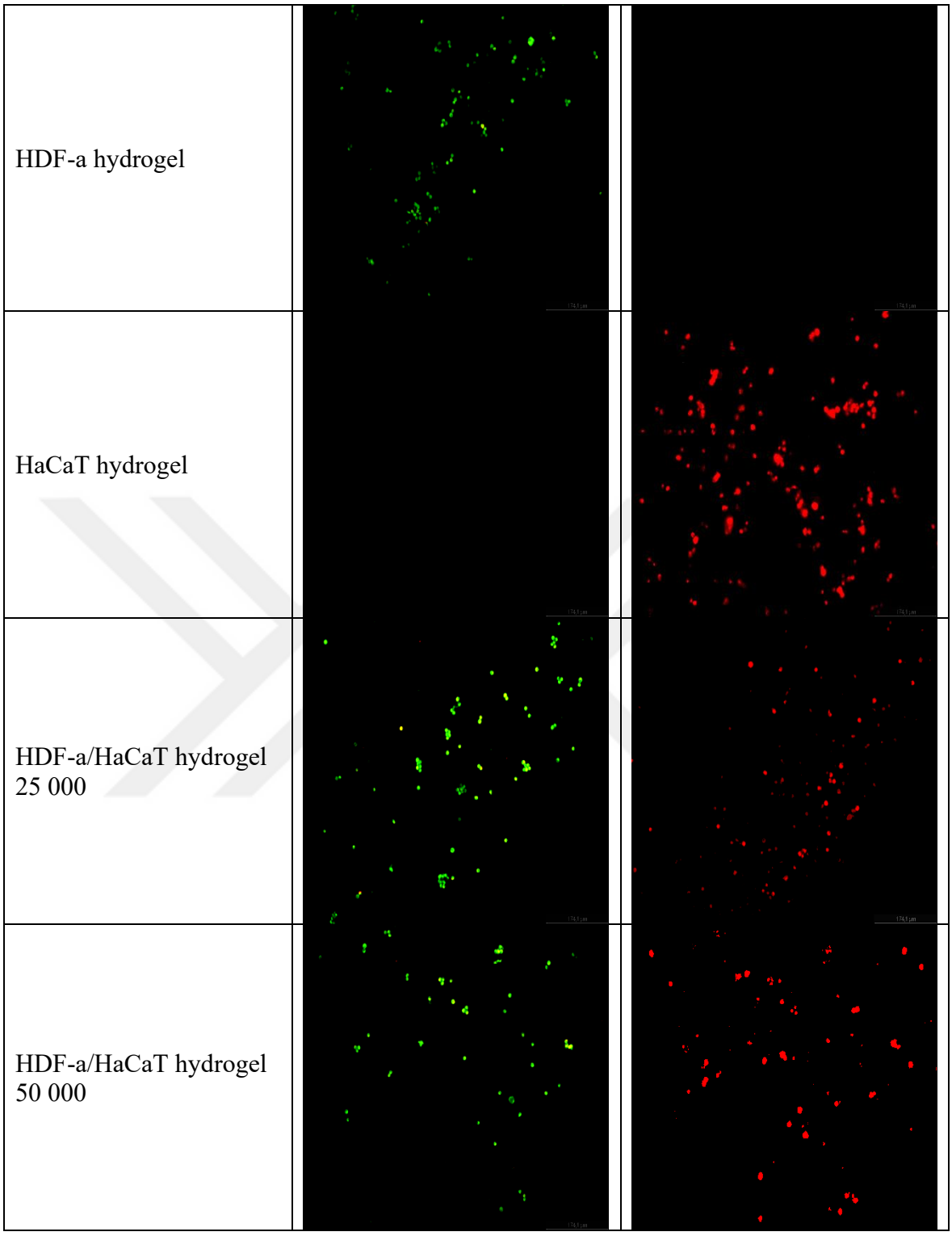

Figure 4.17. Fluorescence images of hydrogel groups at the end of Day 1

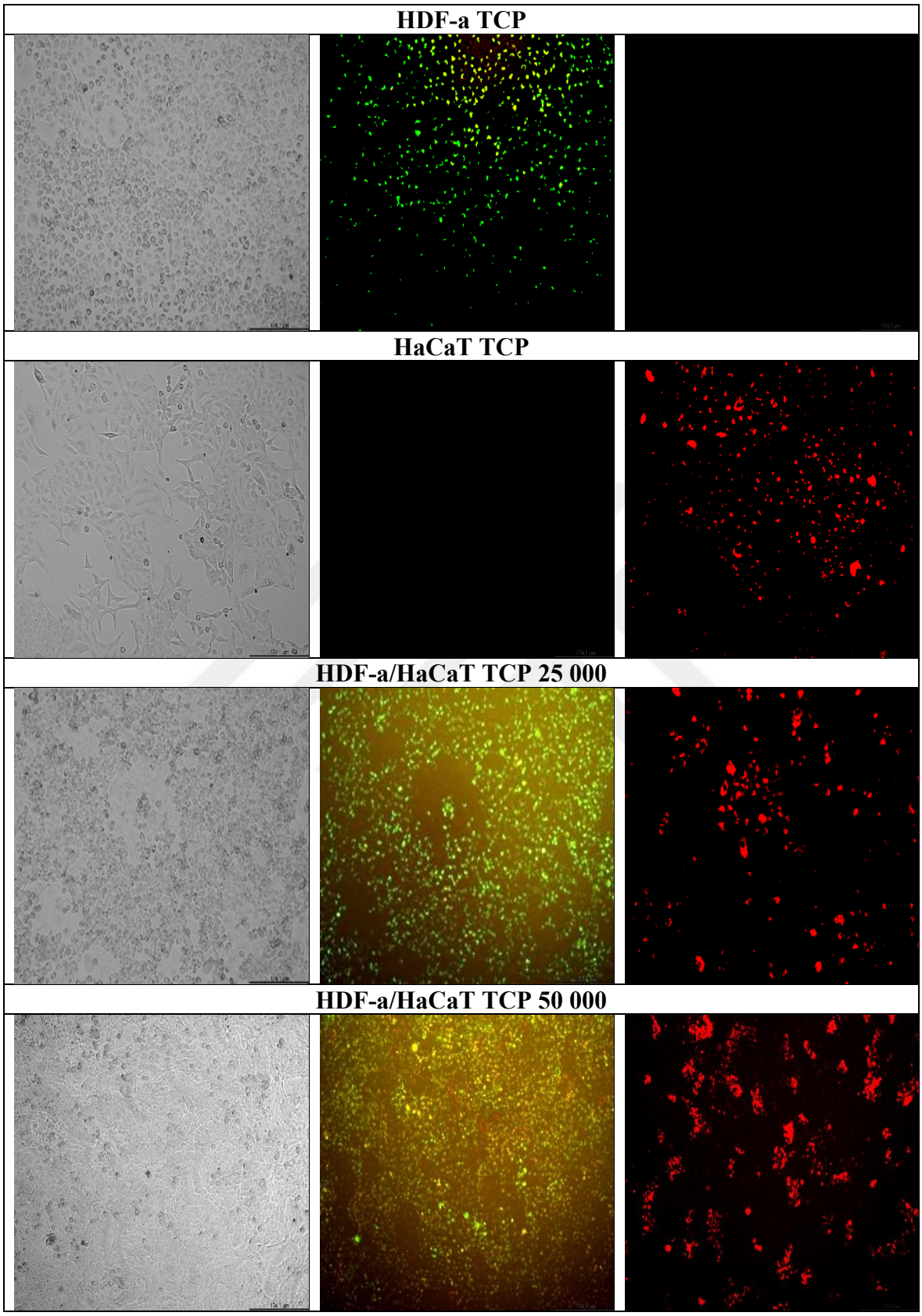

Figure 4.18. Fluorescence images of TCP groups at the end of Day 4

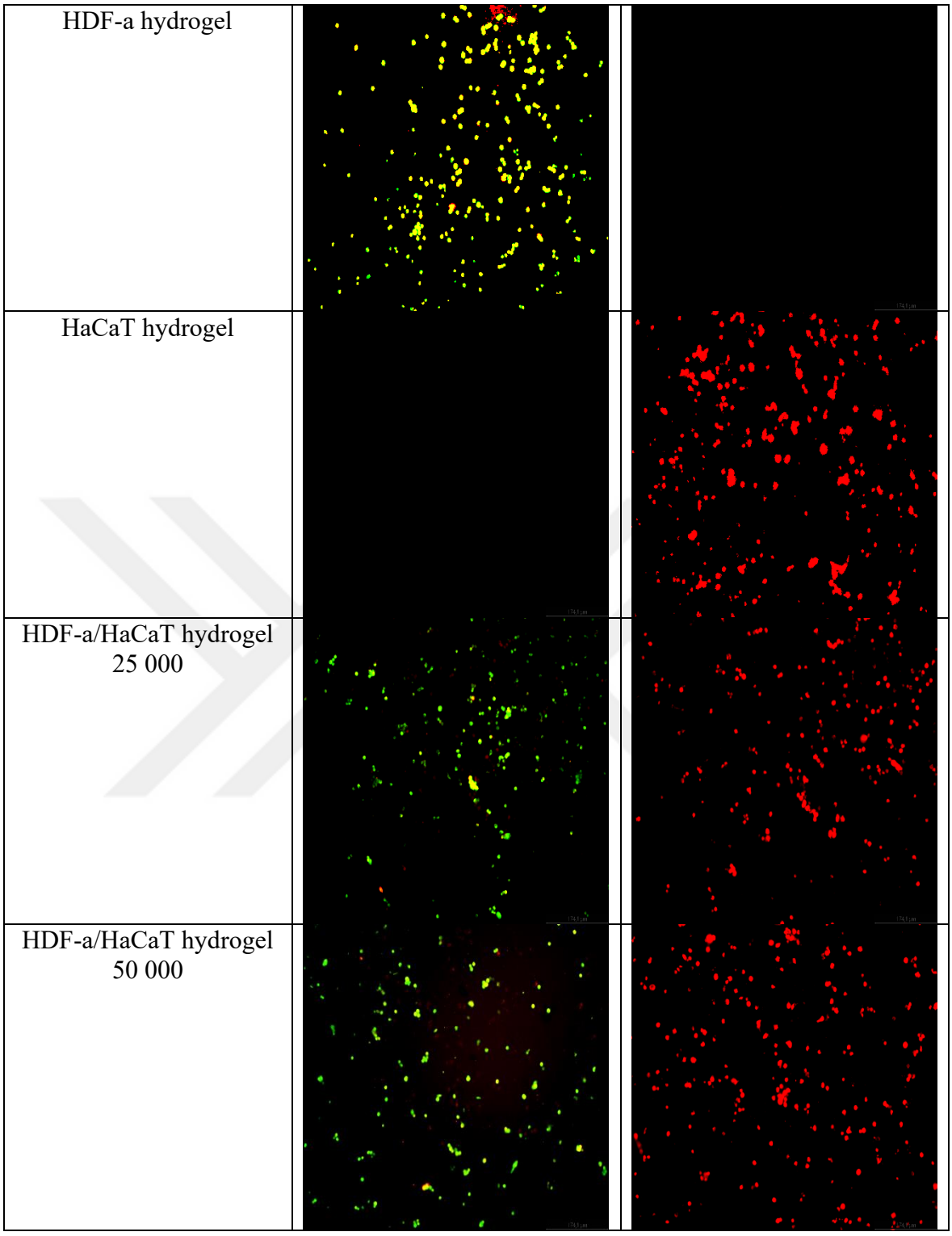

Figure 4.19. Fluorescence images of hydrogel groups at the end of Day 4

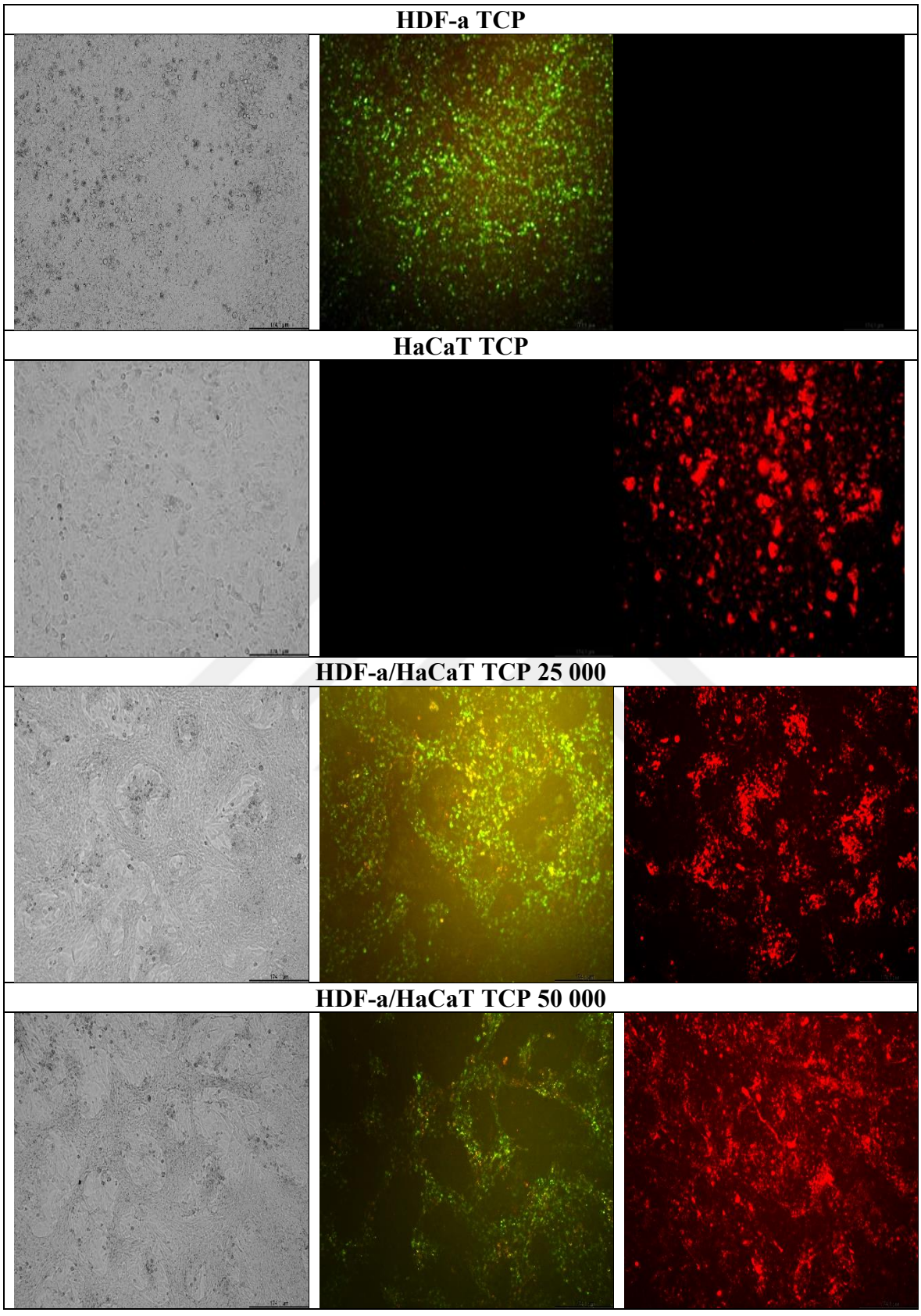

Figure 4.20. Fluorescence images of TCP groups at the end of Day 7

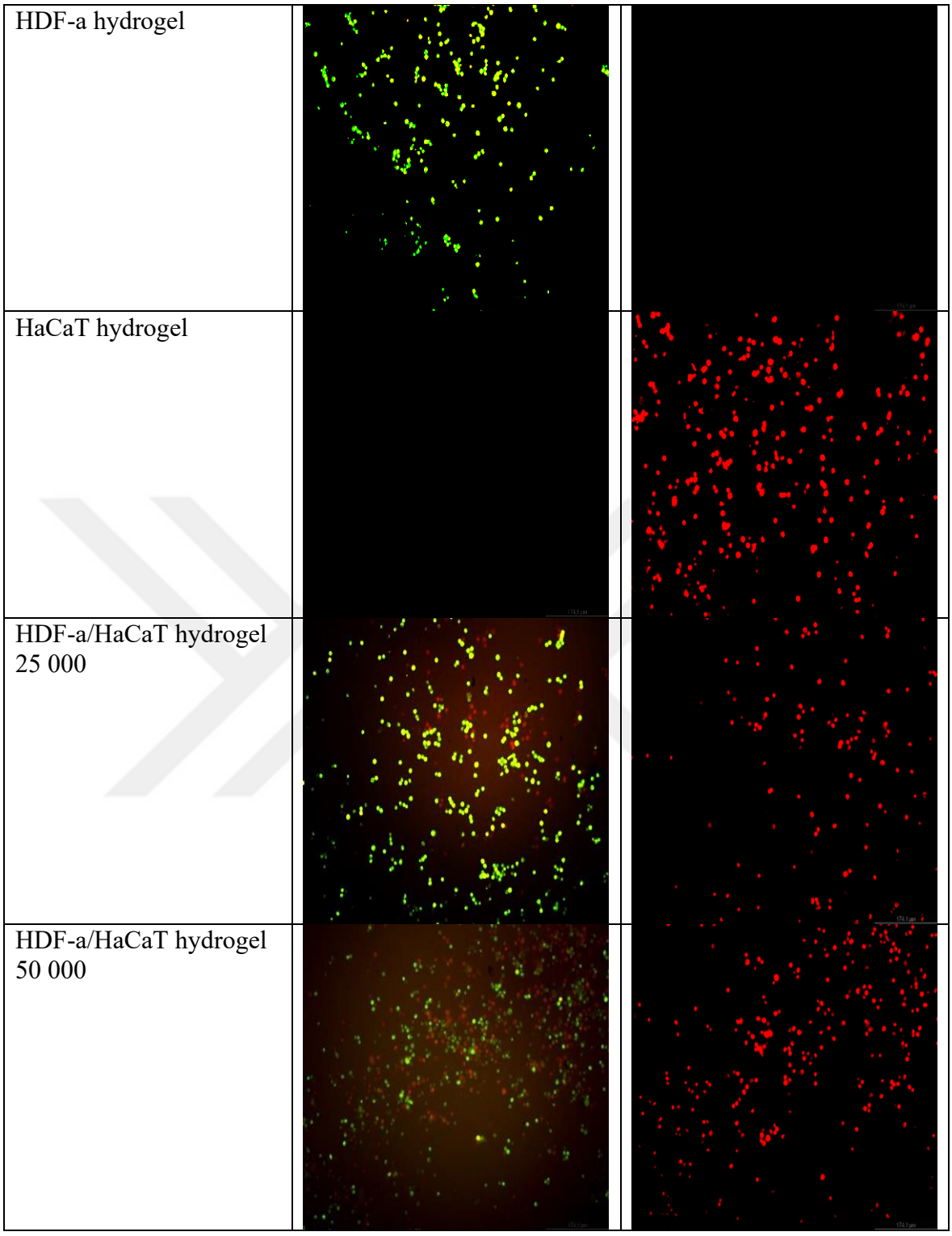

Figure 4.21. Fluorescence images of hydrogel groups at the end of Day 7

5. CONCLUSION

Tissue engineering is a revolutionary method in regenerative medicine that overcomes major challenges of conventional medicine therapies like organ transplantation and prosthetic implantation. One of the significant needs in this area has been to create a bioengineered scaffold to guide the regeneration of functional tissue, both in terms of the mechanical and physical requirements. As such, this thesis adds to this expanding field, with a focus on exploration of Collagen/Keratin/Alginate hydrogel system for a 3D co-culture environment of fibroblasts and keratinocytes. The achievement of extraction and characterization of collagen and keratin, as well as the preparation and evaluation of hydrogels, lays the groundwork for strategies to improve skin regeneration through biomaterials.

The objective of this study was to develop and fully characterize a Collagen/Keratin/Alginate (Col/Ker/Alg) hydrogel, and to evaluate the hydrogel characteristics in a 3D co-culture model of human dermal fibroblasts (HDF-a) and keratinocytes (HaCaT). The physicochemical and biological properties of the hydrogels were optimized as an efficacy characteristic of scaffolds for skin tissue engineering. Data acquired from profuse analytics emphasizes the capacity of these hydrogels for translation into developable biomimetic scaffolds that enable supported cell viability, proliferation and interaction for a restoration period. Such properties become especially pertinent for tissue engineering applications, such as in skin regeneration, where the cellular microenvironment should be the most favorable for efficient tissue repair and restoration. The developed hydrogel system provides a novel and extremely promising approach to access the limitations of current regenerative therapies as it mimics the ECM closely and promotes cell adhesion and differentiation.

Bovine *Achilles* tendon collagen and human hair waste keratin were extracted, and the proteins were characterized by Fourier transformation infrared spectrometry (FTIR) and sodium dodecyl sulfate-polyacrylamide gel electrophoresis (SDS-PAGE), to affirm their chemical structure and molecular composition. Outputs of results showed that extracted collagen keratin showed the characteristic SDS-PAGE bands. The structural features of the

extracted biomolecules verified their suitability for utilization in biomaterial applications. The incorporation of these structural proteins into the hydrogel matrix contributes to the biocompatibility of the material and closely mimics the native ECM of the skin.

The synthesized Col/Ker/Alg hydrogels were systematically characterized in terms of their structural, morphological and physicochemical characteristics. Extensive material characterization, including FTIR and scanning electron microscopy (SEM), successfully verified fabrication of the hydrogels, demonstrating that high structural integrity, optimal porosity, and a suitable surface for cellular adhesion and proliferation were all maintained. A broadly porous morphology suitable for cell infiltration and nutrient diffusion, which is beneficial for tissue engineering, was verified using the SEM. In water absorption and *in vitro* degradation experiments, the Col/Ker/Alg hydrogels remained sufficiently hydrated and underwent controllable biodegradation over time, suggesting the potential of these hydrogels as an effective support system for growing tissues, and ensuring their proper biodegradation, which are important characteristics for long-term tissue engineering implementations. Furthermore, the protein release kinetics ascertained a sustained and gradual release of bioactive molecules possibly leading to cellular proliferation and differentiation over prolonged periods of time. This property for controlled release is especially helpful in wound healing applications, as it releases the growth-promoting factors over time, which are needed for supporting tissue regeneration. This controlled degradation is also beneficial in tissue engineering since it allows new tissue to grow into the scaffold while the scaffold supports the tissue during the early stages of regeneration.

Formulation and optimization of these Col/Ker/Alg hydrogels are important for balancing the mechanical stability, biocompatibility, and biodegradability. The SEM examination of the hydrogels revealed their porous structure that strongly promoted cellular infiltration and tissue formation. To examine how the cross-linking conditions affected the hydrogel properties, a range of conditions were evaluated using calcium chloride ($CaCl_2$) (0.10 M, 0.50 M, 1.0 M). Among these, 0.50 M $CaCl_2$ cross-linked hydrogels exhibited the best performance by balanced combination of optimal physicochemical characteristics, mechanical stability, water uptake capacity, degradation behavior, and porosity. The findings indicate that $CaCl_2$ concentration significantly influences the morphological, swelling, and degradation properties of Col/Ker/Alg hydrogels. While higher cross-linker

concentrations (1.0 M $CaCl_2$) improve structural stability and reduce degradation, they also result in increased brittleness and reduced porosity. Moderate cross-linking (0.50 M $CaCl_2$) appears to offer the best balance between porosity, water uptake, and degradation resistance which makes it a promising option for biomedical applications that demand controlled swelling and mechanical stability. Indeed, swelling studies demonstrated that hydrogels had a sufficient hydration level to sustain cell viability and mimic the ECM. In addition, the *in vitro* degradation studies demonstrated that the hydrogels offered a controlled release of proteins which supported their possible potential for biomimetic scaffold. These properties are critical for scaffold-based tissue engineering because they allow the transport of nutrients, oxygen, and waste products while providing structural support for cellular growth.

Hydrogels were also evaluated for biological factors. Results from the resazurin assay revealed that, particularly in the early phases of incubation, both HDF-a and HaCaT cells cultured inside the hydrogels displayed considerable metabolic activity. In contrast to standard tissue culture polystyrene (TCP) substrates, the hydrogels promoted increased cell attachment and initial proliferation, supporting their enhanced ability to create a physiologically relevant microenvironment. Upon a longer incubation process, TCP cell groups displayed a marginally elevated metabolic activity, which could relate to improved monolayer spreading typically seen in a 2D system; however, the hydrogel groups still possessed a significant degree of viability, illustrating the capacity of the materials for long-term use in 3D co-culture systems.

A key element of this study was the development of a 3D co-culture environment formed with fibroblasts and keratinocytes. Micro-patterned hydrogels fabricated by 3D printing stamps ultimately resulted in distinct deep and superficial channels per cell type, resembling the organization of native skin layers. The resazurin assay showed viability for 21 days and confirmed significantly upregulated metabolic activity of 3D cultures when compared to 2D cultures.

In order to confirm the performance of hydrogel-based system the cell distribution and organization in 3D co-culture was studied using fluorescence microscopy. Fluorescence microscopy demonstrated that cell adhesion and proliferation were successful, with

fibroblasts found in the deeper regions of the hydrogel and keratinocytes forming an epithelial-like layer at the hydrogel surface. The spatial organization of fibroblasts and keratinocytes within the hydrogels suggested that produced scaffolds could support separate cell layers, a necessary feature for skin tissue engineering. The formation of deep and superficial channels specifically enabled the separation of these two cell types, similarly to the dermal-epidermal interface found in healthy skin. These results highlight the benefits of 3D culture systems in creating a more physiologically relevant environment that promotes cellular interactions and facilitates functional tissue development.

The combination of collagen, keratin, and alginate has several benefits, such as biocompatibility, bioactivity, structural stability, and controlled degradation, which are essential for tissue remodeling. Moreover, the capacity of these hydrogels to enable improved cell–cell crosstalk between fibroblasts and keratinocytes emphasizes their promise as potential skin substitutes for regenerative medicine. The incorporation of biomimetic hydrogels to support cell signaling and enable tissue integration may help create more bioengineered skin constructs that possess full donor-site specificity like native tissue.

Further study must be done to enhance the applicability of Col/Ker/Alg hydrogels by addressing key challenges such as vascularization, mechanical reinforcement, and long-term biocompatibility in *in vivo* models, as a powerful tool to use in different research areas. Moreover, the native skin consists of an intricate combination of biochemicals and mechanical properties, and thus further refining hydrogel formulations to better tap into these will be critical for their widespread adoption in wound healing applications. Scalability and standardization should be investigated further to ensure consistent production of these biomaterials and their regulatory approval for clinical translation. In addition, these hydrogels should be applied for developing advanced *in vitro* skin disease models that mimic pathological conditions.

The insights generated from this research could ultimately contribute to our knowledge about engineered tissue development and lead to more clinically relevant applications. Moreover, further studies are needed so that this can be considered a tool for application in other fields beyond skin tissue engineering and regenerative medicine, such as implementation on *in vitro* skin disease models. Through their ability to provide a 3D co-

culture environment, these biomimetic scaffolds provide a valuable tool to study disease pathology further, particularly skin diseases such as chronic wounds, burns, and genetic disorders. Moreover, these types of hydrogels may be useful for drug screening and testing of cosmetic products, providing an ethical and physiologically relevant alternative to animal testing. As advancements in tissue engineering and biomaterials continue to progress, integrating these hydrogel systems into broader research and industrial applications will further enhance their impact.

REFERENCES

[1] M. Mirshafiei, H. Rashedi, F. Yazdian, A. Rahdar, and F. Baino, "Advancements in tissue and organ 3D bioprinting: Current techniques, applications, and future perspectives," *Mater. Des.*, vol. 240, p. 112853, Apr. 2024, doi: 10.1016/j.matdes.2024.112853.

[2] S. Tajvar, A. Hadjizadeh, and S. S. Samandari, "Scaffold degradation in bone tissue engineering: An overview," *Int. Biodeterior. Biodegrad.*, vol. 180, p. 105599, May 2023, doi: 10.1016/j.ibiod.2023.105599.

[3] M. Krishani, W. Y. Shin, H. Suhaimi, and N. S. Sambudi, "Development of Scaffolds from Bio-Based Natural Materials for Tissue Regeneration Applications: A Review," *Gels*, vol. 9, no. 2, 2023, doi: 10.3390/gels9020100.

[4] H. Liu *et al.*, "Biomimetic fabrication bioprinting strategies based on decellularized extracellular matrix for musculoskeletal tissue regeneration: Current status and future perspectives," *Mater. Des.*, vol. 243, p. 113072, Jul. 2024, doi: 10.1016/j.matdes.2024.113072.

[5] N. Mahajan, S. Soker, and S. V. Murphy, "Regenerative Medicine Approaches for Skin Wound Healing: from Allografts to Engineered Skin Substitutes," *Curr. Transplant. Rep.*, vol. 11, no. 4, pp. 207–221, Dec. 2024, doi: 10.1007/s40472-024-00453-5.

[6] J. Dean *et al.*, "Advancements in bioengineered and autologous skin grafting techniques for skin reconstruction: a comprehensive review," *Front. Bioeng. Biotechnol.*, vol. 12, 2025, doi: 10.3389/fbioe.2024.1461328.

[7] C.-M. Moysidou, C. Barberio, and R. M. Owens, "Advances in Engineering Human Tissue Models," *Front. Bioeng. Biotechnol.*, vol. 8, 2021, doi: 10.3389/fbioe.2020.620962.

[8] P. Lu *et al.*, "Harnessing the potential of hydrogels for advanced therapeutic applications: current achievements and future directions," *Signal Transduct. Target. Ther.*, vol. 9, no. 1, p. 166, Jul. 2024, doi: 10.1038/s41392-024-01852-x.

[9] C. Bertsch *et al.*, “Biomimetic Bilayered Scaffolds for Tissue Engineering: From Current Design Strategies to Medical Applications,” *Adv. Healthc. Mater.*, vol. 12, no. 17, p. 2203115, Jul. 2023, doi: 10.1002/adhm.202203115.

[10] F. Wang *et al.*, “Effect of natural-based biological hydrogels combined with growth factors on skin wound healing,” vol. 11, no. 1, pp. 2493–2512, 2022, doi: 10.1515/ntrev-2022-0122.

[11] C. Gao, S. Peng, P. Feng, and C. Shuai, “Bone biomaterials and interactions with stem cells,” *Bone Res.*, vol. 5, no. 1, p. 17059, Dec. 2017, doi: 10.1038/boneres.2017.59.

[12] F. Yue *et al.*, “Induce Differentiation of Embryonic Stem Cells by Co-Culture System,” in *Regenerative Medicine and Tissue Engineering*, Rijeka: IntechOpen, 2013, p. Induce Differentiation of Embryonic Stem Cells by Co-Culture System. doi: 10.5772/56000.

[13] C. Li, W. He, Y. Song, X. Zhang, J. Sun, and Z. Zhou, “Advances of 3D Cell Co-Culture Technology Based on Microfluidic Chips,” *Biosensors*, vol. 14, no. 7, 2024, doi: 10.3390/bios14070336.

[14] Á. Sierra-Sánchez, K. H. Kim, G. Blasco-Morente, and S. Arias-Santiago, “Cellular human tissue-engineered skin substitutes investigated for deep and difficult to heal injuries,” *Npj Regen. Med.*, vol. 6, no. 1, p. 35, Jun. 2021, doi: 10.1038/s41536-021-00144-0.

[15] T. A. M. Andrade, V. A. da Silva, K. Scheck, T. Garay, R. Sharma, and S. M. Willerth, “3D Bioprinting a Novel Skin Co-Culture Model Using Human Keratinocytes and Fibroblasts,” *J. Biomed. Mater. Res. A*, vol. 113, no. 1, p. e37831, Jan. 2025, doi: 10.1002/jbm.a.37831.

[16] R. M. Quigley, M. Kearney, O. D. Kennedy, and H. F. Duncan, “Tissue engineering approaches for dental pulp regeneration: The development of novel bioactive materials using pharmacological epigenetic inhibitors,” *Bioact. Mater.*, vol. 40, pp. 182–211, Oct. 2024, doi: 10.1016/j.bioactmat.2024.06.012.

[17] S. Tripathi, S. S. Mandal, S. Bauri, and P. Maiti, “3D bioprinting and its innovative approach for biomedical applications,” *MedComm*, vol. 4, no. 1, p. e194, Feb. 2023, doi: 10.1002/mco2.194.

[18] P. K. Chandra, S. Soker, and A. Atala, “Chapter 1 - Tissue engineering: current status and future perspectives,” in *Principles of Tissue Engineering (Fifth Edition)*, R. Lanza, R. Langer, J. P. Vacanti, and A. Atala, Eds., Academic Press, 2020, pp. 1–35. doi: 10.1016/B978-0-12-818422-6.00004-6.

[19] A. Alghuwainem, A. T. Alshareeda, and B. Alsowayan, “Scaffold-Free 3-D Cell Sheet Technique Bridges the Gap between 2-D Cell Culture and Animal Models,” *Int. J. Mol. Sci.*, vol. 20, no. 19, 2019, doi: 10.3390/ijms20194926.

[20] A. Ovsianikov, A. Khademhosseini, and V. Mironov, “The Synergy of Scaffold-Based and Scaffold-Free Tissue Engineering Strategies,” *Trends Biotechnol.*, vol. 36, no. 4, pp. 348–357, Apr. 2018, doi: 10.1016/j.tibtech.2018.01.005.

[21] I. Yoshito, “Challenges in tissue engineering,” *J R Soc Interface*, vol. 3, pp. 589–601, 2006.

[22] A. Ostadfar, “Chapter 9 - Tissue Engineering of Cardiovascular System,” in *Biofluid Mechanics*, A. Ostadfar, Ed., Academic Press, 2016, pp. 323–339. doi: 10.1016/B978-0-12-802408-9.00009-0.

[23] L. G. Griffith and G. Naughton, “Tissue Engineering--Current Challenges and Expanding Opportunities,” *Science*, vol. 295, no. 5557, pp. 1009–1014, Feb. 2002, doi: 10.1126/science.1069210.

[24] E. Carletti, A. Motta, and C. Migliaresi, “Scaffolds for Tissue Engineering and 3D Cell Culture,” in *3D Cell Culture: Methods and Protocols*, J. W. Haycock, Ed., Totowa, NJ: Humana Press, 2011, pp. 17–39. doi: 10.1007/978-1-60761-984-0_2.

[25] F. Berthiaume, T. J. Maguire, and M. L. Yarmush, “Tissue Engineering and Regenerative Medicine: History, Progress, and Challenges,” *Annual Review of Chemical and Biomolecular Engineering*, vol. 2, no. Volume 2, 2011. Annual Reviews, pp. 403–430, 2011.

[26] J. L. Olson, A. Atala, and J. J. Yoo, “Tissue Engineering: Current Strategies and Future Directions,” *Chonnam Med J*, vol. 47, no. 1, pp. 1–13, Apr. 2011.

[27] A. Curtis and M. Riehle, “Tissue engineering: the biophysical background,” *Phys. Med. Biol.*, vol. 46, no. 4, p. R47, Apr. 2001, doi: 10.1088/0031-9155/46/4/201.

[28] P. Gentile, V. Chiono, I. Carmagnola, and P. V. Hatton, “An Overview of Poly(lactic-co-glycolic) Acid (PLGA)-Based Biomaterials for Bone Tissue Engineering,” *Int. J. Mol. Sci.*, vol. 15, no. 3, pp. 3640–3659, 2014, doi: 10.3390/ijms15033640.

[29] I. N. Amirrah, Y. Lokanathan, I. Zulkiflee, M. F. M. R. Wee, A. Motta, and M. B. Fauzi, “A Comprehensive Review on Collagen Type I Development of Biomaterials for Tissue Engineering: From Biosynthesis to Bioscaffold,” *Biomedicines*, vol. 10, no. 9, 2022, doi: 10.3390/biomedicines10092307.

[30] K. Athanasiou, C. Agrawal, F. Barber, and S. Burkhart, “Orthopaedic applications for PLA-PGA biodegradable polymers,” *Arthrosc. J. Arthrosc. Relat. Surg.*, vol. 14, no. 7, pp. 726–737, Oct. 1998, doi: 10.1016/S0749-8063(98)70099-4.

[31] H. Choi, W.-S. Choi, and J.-O. Jeong, “A Review of Advanced Hydrogel Applications for Tissue Engineering and Drug Delivery Systems as Biomaterials,” *Gels*, vol. 10, no. 11, 2024, doi: 10.3390/gels10110693.

[32] A. I. Caplan, “Adult mesenchymal stem cells for tissue engineering versus regenerative medicine,” *J. Cell. Physiol.*, vol. 213, no. 2, pp. 341–347, Nov. 2007, doi: 10.1002/jcp.21200.

[33] J. Ringe, C. Kaps, G.-R. Burmester, and M. Sittinger, “Stem cells for regenerative medicine: advances in the engineering of tissues and organs,” *Naturwissenschaften*, vol. 89, no. 8, pp. 338–351, Aug. 2002, doi: 10.1007/s00114-002-0344-9.

[34] A. C. Mitchell, P. S. Briquez, J. A. Hubbell, and J. R. Cochran, “Engineering growth factors for regenerative medicine applications,” *Acta Biomater.*, vol. 30, pp. 1–12, Jan. 2016, doi: 10.1016/j.actbio.2015.11.007.

[35] K. Jakab, C. Norotte, F. Marga, K. Murphy, G. Vunjak-Novakovic, and G. Forgacs, “Tissue engineering by self-assembly and bio-printing of living cells,” *Biofabrication*, vol. 2, no. 2, p. 022001, Jun. 2010, doi: 10.1088/1758-5082/2/2/022001.

[36] K. Vig *et al.*, “Advances in Skin Regeneration Using Tissue Engineering,” *Int. J. Mol. Sci.*, vol. 18, no. 4, 2017, doi: 10.3390/ijms18040789.

[37] P. A. J. Kolarsick, M. A. Kolarsick, and C. Goodwin, “Anatomy and Physiology of the Skin,” *J. Dermatol. Nurses Assoc.*, vol. 3, no. 4, 2011, [Online].

[38] J. A. McGrath, R. A. J. Eady, and F. M. Pope, “Anatomy and Organization of Human Skin,” in *Rook’s Textbook of Dermatology*, 2004, pp. 45–128. doi: 10.1002/9780470750520.ch3.

[39] A. Baroni, E. Buommino, V. De Gregorio, E. Ruocco, V. Ruocco, and R. Wolf, “Structure and function of the epidermis related to barrier properties,” *Epidermal Barrier Funct. Clin. Implic. Ther. Relev.*, vol. 30, no. 3, pp. 257–262, May 2012, doi: 10.1016/j.clindermatol.2011.08.007.

[40] G.-E. Costin and V. J. Hearing, “Human skin pigmentation: melanocytes modulate skin color in response to stress,” *FASEB J.*, vol. 21, no. 4, pp. 976–994, Apr. 2007, doi: 10.1096/fj.06-6649rev.

[41] N. PALASTANGA, D. FIELD, and R. SOAMES, “Skin and its appendages,” in *Anatomy and Human Movement*, N. PALASTANGA, D. FIELD, and R. SOAMES, Eds., Butterworth-Heinemann, 1989, pp. 40–49. doi: 10.1016/B978-0-433-00032-7.50008-5.

[42] W. Montagna and P. F. Parakkal, “4 - The Dermis**Written largely by Jeffrey Pinto, University of Oregon Medical School, Portland.,” in *The Structure & Function of Skin (Third Edition)*, W. Montagna and P. F. Parakkal, Eds., Academic Press, 1974, pp. 96–141. doi: 10.1016/B978-0-12-505263-4.50009-1.

[43] D. J. Tobin, “Introduction to skin aging,” *J. Tissue Viability*, vol. 26, no. 1, pp. 37–46, Feb. 2017, doi: 10.1016/j.jtv.2016.03.002.

[44] R. V. Shevchenko, S. R. James, and E. S. James, “A review of tissue-engineered skin bioconstructs available for skin reconstruction,” *J R Soc Interface*, vol. 7, pp. 229–258.

[45] F. Groeber, M. Holeiter, M. Hampel, S. Hinderer, and K. Schenke-Layland, “Skin tissue engineering — In vivo and in vitro applications,” *TISSUE Eng. Regen. Med. - POTENTIAL PITFALLS*, vol. 63, no. 4, pp. 352–366, Apr. 2011, doi: 10.1016/j.addr.2011.01.005.

[46] B. Dhandayuthapani, Y. Yoshida, T. Maekawa, and D. S. Kumar, “Polymeric Scaffolds in Tissue Engineering Application: A Review,” *Int. J. Polym. Sci.*, vol. 2011, no. 1, p. 290602, Jan. 2011, doi: 10.1155/2011/290602.

[47] F. Chogan, Y. Chen, F. Wood, and M. G. Jeschke, “Skin Tissue Engineering Advances in Burns: A Brief Introduction to the Past, the Present, and the Future Potential,” *J. Burn Care Res.*, vol. 44, no. Supplement_1, pp. S1–S4, Jan. 2023, doi: 10.1093/jbcr/irac127.

[48] M. M. Godoi, E. M. Reis, J. Koepp, and J. Ferreira, “Perspective from developers: Tissue-engineered products for skin wound healing,” *Int. J. Pharm.*, vol. 660, p. 124319, Jul. 2024, doi: 10.1016/j.ijpharm.2024.124319.

[49] J. M. Granjeiro, P. G. M. Borchio, I. P. B. Ribeiro, and K. B. S. Paiva, “Bioengineering breakthroughs: The impact of stem cell models on advanced therapy medicinal product development.,” *World J. Stem Cells*, vol. 16, no. 10, pp. 860–872, 2024, doi: doi.org/10.4252/wjsc.v16.i10.860.

[50] Md. S. Islam, S. Tahsin, R. Jahir, M. Rahman, M. Shariyar, and M. Rahman, *Journey of Biomaterials: An Emerging Field in Materials Science - (An Academic Report)*. 2024. doi: 10.13140/RG.2.2.23976.48647.

[51] P. S. Kowalski, C. Bhattacharya, S. Afewerki, and R. Langer, “Smart Biomaterials: Recent Advances and Future Directions,” *ACS Biomater. Sci. Eng.*, vol. 4, no. 11, pp. 3809–3817, Nov. 2018, doi: 10.1021/acsbiomaterials.8b00889.

[52] T. Weng *et al.*, “3D bioprinting for skin tissue engineering: Current status and perspectives,” *J. Tissue Eng.*, vol. 12, p. 20417314211028574, Jan. 2021, doi: 10.1177/20417314211028574.

[53] E. Radzikowska-Büchner, I. Łopuszyńska, W. Flieger, M. Tobiasz, R. Maciejewski, and J. Flieger, “An Overview of Recent Developments in the Management of Burn Injuries,” *Int. J. Mol. Sci.*, vol. 24, no. 22, 2023, doi: 10.3390/ijms242216357.

[54] X. Ding *et al.*, “Current application of tissue-engineered dermal scaffolds mimicking the extracellular matrix microenvironment in wound healing,” *Regen. Ther.*, vol. 28, pp. 371–382, Mar. 2025, doi: 10.1016/j.reth.2024.12.018.

[55] P. Pleguezuelos-Beltrán, S. Herráiz-Gil, D. Martínez-Moreno, I. Medraño-Fernandez, C. León, and S. Guerrero-Aspizua, “Regenerative Cosmetics: Skin Tissue Engineering for Anti-Aging, Repair, and Hair Restoration,” *Cosmetics*, vol. 11, no. 4, 2024, doi: 10.3390/cosmetics11040121.

[56] J. R. Yu *et al.*, “Current and Future Perspectives on Skin Tissue Engineering: Key Features of Biomedical Research, Translational Assessment, and Clinical Application,” *Adv. Healthc. Mater.*, vol. 8, no. 5, p. 1801471, Mar. 2019, doi: 10.1002/adhm.201801471.

[57] D. Chouhan, N. Dey, N. Bhardwaj, and B. B. Mandal, “Emerging and innovative approaches for wound healing and skin regeneration: Current status and advances,” *Biomaterials*, vol. 216, p. 119267, Sep. 2019, doi: 10.1016/j.biomaterials.2019.119267.

[58] C. Dieckmann, R. Renner, L. Milkova, and J. C. Simon, “Regenerative medicine in dermatology: biomaterials, tissue engineering, stem cells, gene transfer and beyond,” *Exp. Dermatol.*, vol. 19, no. 8, pp. 697–706, Aug. 2010, doi: 10.1111/j.1600-0625.2010.01087.x.

[59] R. H. Harrison, J.-P. St-Pierre, and M. M. Stevens, “Tissue Engineering and Regenerative Medicine: A Year in Review,” *Tissue Eng. Part B Rev.*, vol. 20, no. 1, pp. 1–16, Feb. 2014, doi: 10.1089/ten.teb.2013.0668.

[60] P. K. Upputuri, K. Sivasubramanian, C. S. K. Mark, and M. Pramanik, “Recent Developments in Vascular Imaging Techniques in Tissue Engineering and Regenerative Medicine,” *BioMed Res. Int.*, vol. 2015, no. 1, p. 783983, Jan. 2015, doi: 10.1155/2015/783983.

[61] J.-F. Stoltz *et al.*, “Introduction to regenerative medicine and tissue engineering,” *Biomed. Mater. Eng.*, vol. 22, no. 1–3, pp. 3–16, 2012, doi: 10.3233/BME-2012-0684.

[62] M. B. Fisher and R. L. Mauck, “Tissue Engineering and Regenerative Medicine: Recent Innovations and the Transition to Translation,” *Tissue Eng. Part B Rev.*, vol. 19, no. 1, pp. 1–13, Feb. 2013, doi: 10.1089/ten.teb.2012.0723.

[63] A. L. Strong, M. W. Neumeister, and B. Levi, “Stem Cells and Tissue Engineering: Regeneration of the Skin and Its Contents,” *Burn Care Rescue Resusc. Resurfacing*, vol. 44, no. 3, pp. 635–650, Jul. 2017, doi: 10.1016/j.cps.2017.02.020.

[64] J. Saji Joseph, S. Teboga Malindisa, and M. Ntwasa, “Two-Dimensional (2D) and Three-Dimensional (3D) Cell Culturing in Drug Discovery,” in *Cell Culture*, Rijeka: IntechOpen, 2018, p. Two-Dimensional (2D) and Three-Dimensional (3D) Cell Culturing in Drug Discovery. doi: 10.5772/intechopen.81552.

[65] B. D. Riehl, J.-H. Park, I. K. Kwon, and J. Y. Lim, “Mechanical Stretching for Tissue Engineering: Two-Dimensional and Three-Dimensional Constructs,” *Tissue Eng. Part B Rev.*, vol. 18, no. 4, pp. 288–300, Aug. 2012, doi: 10.1089/ten.teb.2011.0465.

[66] A. Abbott, “Biology’s new dimension,” *Nature*, vol. 424, no. 6951, pp. 870–872, Aug. 2003, doi: 10.1038/424870a.

[67] K. Duval *et al.*, “Modeling Physiological Events in 2D vs. 3D Cell Culture,” *Physiology*, vol. 32, no. 4, pp. 266–277, Jul. 2017, doi: 10.1152/physiol.00036.2016.

[68] M. Ravi, V. Paramesh, S. R. Kaviya, E. Anuradha, and F. D. P. Solomon, “3D Cell Culture Systems: Advantages and Applications,” *J. Cell. Physiol.*, vol. 230, no. 1, pp. 16–26, Jan. 2015, doi: 10.1002/jcp.24683.

[69] H. Page, P. Flood, and E. G. Reynaud, “Three-dimensional tissue cultures: current trends and beyond,” *Cell Tissue Res.*, vol. 352, no. 1, pp. 123–131, Apr. 2013, doi: 10.1007/s00441-012-1441-5.

[70] S. Caddeo, M. Boffito, and S. Sartori, “Tissue Engineering Approaches in the Design of Healthy and Pathological In Vitro Tissue Models,” *Front. Bioeng. Biotechnol.*, vol. 5, 2017, doi: 10.3389/fbioe.2017.00040.

[71] F. Pampaloni, E. G. Reynaud, and E. H. K. Stelzer, “The third dimension bridges the gap between cell culture and live tissue,” *Nat. Rev. Mol. Cell Biol.*, vol. 8, no. 10, pp. 839–845, Oct. 2007, doi: 10.1038/nrm2236.

[72] M. Sun *et al.*, “3D Cell Culture—Can It Be As Popular as 2D Cell Culture?,” *Adv. NanoBiomed Res.*, vol. 1, no. 5, p. 2000066, May 2021, doi: 10.1002/anbr.202000066.

[73] J. Klangprapan, G. R. Souza, and J. N. Ferreira, “Bioprinting salivary gland models and their regenerative applications,” *BDJ Open*, vol. 10, no. 1, p. 39, May 2024, doi: 10.1038/s41405-024-00219-2.

[74] Y. Imamura *et al.*, “Comparison of 2D- and 3D-culture models as drug-testing platforms in breast cancer,” *Oncol. Rep.*, vol. 33, no. 4, pp. 1837–1843, Apr. 2015, doi: 10.3892/or.2015.3767.

[75] V.-M. Le, M.-D. Lang, W.-B. Shi, and J.-W. Liu, “A collagen-based multicellular tumor spheroid model for evaluation of the efficiency of nanoparticle drug delivery,” *Artif. Cells Nanomedicine Biotechnol.*, vol. 44, no. 2, pp. 540–544, Feb. 2016, doi: 10.3109/21691401.2014.968820.

[76] C. Jensen and Y. Teng, “Is It Time to Start Transitioning From 2D to 3D Cell Culture?,” *Front. Mol. Biosci.*, vol. 7, 2020, doi: 10.3389/fmolb.2020.00033.

[77] Y. Park, K. M. Huh, and S.-W. Kang, “Applications of Biomaterials in 3D Cell Culture and Contributions of 3D Cell Culture to Drug Development and Basic Biomedical Research,” *Int. J. Mol. Sci.*, vol. 22, no. 5, 2021, doi: 10.3390/ijms22052491.

[78] J. Martin, “Seeing the Full Picture: Advances in 3D Cell Culture Microscopy,” *BioTechniques*, vol. 69, no. 2, pp. 77–79, Aug. 2020, doi: 10.2144/btn-2020-0094.

[79] R. Edmondson, J. J. Broglie, A. F. Adcock, and L. Yang, “Three-Dimensional Cell Culture Systems and Their Applications in Drug Discovery and Cell-Based Biosensors,” *ASSAY Drug Dev. Technol.*, vol. 12, no. 4, pp. 207–218, May 2014, doi: 10.1089/adt.2014.573.

[80] K. G. Battiston, J. W. C. Cheung, D. Jain, and J. P. Santerre, “Biomaterials in co-culture systems: Towards optimizing tissue integration and cell signaling within scaffolds,”

Biomaterials, vol. 35, no. 15, pp. 4465–4476, May 2014, doi: 10.1016/j.biomaterials.2014.02.023.

[81] N. K. Paschos, W. E. Brown, R. Eswaramoorthy, J. C. Hu, and K. A. Athanasiou, "Advances in tissue engineering through stem cell-based co-culture," *J. Tissue Eng. Regen. Med.*, vol. 9, no. 5, pp. 488–503, May 2015, doi: 10.1002/term.1870.

[82] J. Baldwin *et al.*, "In vitropre-vascularisation of tissue-engineered constructs A co-culture perspective.," *Vasc. Cell*, vol. 6, no. 1, p. 13, 2014, doi: doi:10.1186/2045-824X-6-13.

[83] M. Bi, K. Yang, T. Yu, G. Wu, and Q. Li, "Cell-based mechanisms and strategies of co-culture system both in vivo and vitro for bone tissue engineering," *Biomed. Pharmacother.*, vol. 169, p. 115907, Dec. 2023, doi: 10.1016/j.biopha.2023.115907.

[84] Y. Liu, J. K. Y. Chan, and S.-H. Teoh, "Review of vascularised bone tissue-engineering strategies with a focus on co-culture systems," *J. Tissue Eng. Regen. Med.*, vol. 9, no. 2, pp. 85–105, Feb. 2015, doi: 10.1002/term.1617.

[85] M. Bahram, N. Mohseni, and M. Moghtader, "An Introduction to Hydrogels and Some Recent Applications," in *Emerging Concepts in Analysis and Applications of Hydrogels*, Rijeka: IntechOpen, 2016. doi: 10.5772/64301.

[86] M. C. Catoira, L. Fusaro, D. Di Francesco, M. Ramella, and F. Boccafoschi, "Overview of natural hydrogels for regenerative medicine applications," *J. Mater. Sci. Mater. Med.*, vol. 30, no. 10, p. 115, Oct. 2019, doi: 10.1007/s10856-019-6318-7.

[87] X. Tang *et al.*, "Chapter 21 - Polymeric Biomaterials in Tissue Engineering and Regenerative Medicine," in *Natural and Synthetic Biomedical Polymers*, S. G. Kumbar, C. T. Laurencin, and M. Deng, Eds., Oxford: Elsevier, 2014, pp. 351–371. doi: 10.1016/B978-0-12-396983-5.00022-3.

[88] E. M. Ahmed, "Hydrogel: Preparation, characterization, and applications: A review," *J. Adv. Res.*, vol. 6, no. 2, pp. 105–121, Mar. 2015, doi: 10.1016/j.jare.2013.07.006.

[89] A. Gupta, M. Kowalczuk, W. Heaselgrave, S. T. Britland, C. Martin, and I. Radecka, "The production and application of hydrogels for wound management: A review," *Eur. Polym. J.*, vol. 111, pp. 134–151, Feb. 2019, doi: 10.1016/j.eurpolymj.2018.12.019.

[90] H. Cao, L. Duan, Y. Zhang, J. Cao, and K. Zhang, "Current hydrogel advances in physicochemical and biological response-driven biomedical application diversity," *Signal Transduct. Target. Ther.*, vol. 6, no. 1, p. 426, Dec. 2021, doi: 10.1038/s41392-021-00830-x.

[91] T.-C. Ho *et al.*, "Hydrogels: Properties and Applications in Biomedicine," *Molecules*, vol. 27, no. 9, 2022, doi: 10.3390/molecules27092902.

[92] D. Kang *et al.*, "3D bioprinting of a gelatin-alginate hydrogel for tissue-engineered hair follicle regeneration," *Biofabrication Spheroid Organoid Mater.*, vol. 165, pp. 19–30, Jul. 2023, doi: 10.1016/j.actbio.2022.03.011.

[93] J. Venkatesan, R. Jayakumar, E. Chalisserry, R. Pallela, and S.-K. Kim, "Development of Alginate-Chitosan-Collagen Based Hydrogels for Tissue Engineering," *J. Biomater. Tissue Eng.*, vol. 5, pp. 458–464, 2015.

[94] K. Yue *et al.*, "Visible light crosslinkable human hair keratin hydrogels," *Bioeng. Transl. Med.*, vol. 3, no. 1, pp. 37–48, Jan. 2018, doi: 10.1002/btm2.10077.

[95] D. Min, W. Lee, I.-H. Bae, T. R. Lee, P. Croce, and S.-S. Yoo, "Bioprinting of biomimetic skin containing melanocytes," *Exp. Dermatol.*, vol. 27, no. 5, pp. 453–459, May 2018, doi: 10.1111/exd.13376.

[96] S. Saghati, R. Rahbarghazi, A. Baradar Khoshfetrat, K. Moharamzadeh, H. Tayefi Nasrabadi, and L. Roshangar, "Phenolated alginate-collagen hydrogel induced chondrogenic capacity of human amniotic mesenchymal stem cells," *J. Biomater. Appl.*, vol. 36, no. 5, pp. 789–802, Nov. 2021, doi: 10.1177/08853282211021692.

[97] J. Zhu and R. E. Marchant, "Design properties of hydrogel tissue-engineering scaffolds," *Expert Rev. Med. Devices*, vol. 8, no. 5, pp. 607–626, Sep. 2011, doi: 10.1586/erd.11.27.

[98] J. Elisseeff, C. Puleo, F. Yang, and B. Sharma, “Advances in skeletal tissue engineering with hydrogels,” *Orthod. Craniofac. Res.*, vol. 8, no. 3, pp. 150–161, Aug. 2005, doi: 10.1111/j.1601-6343.2005.00335.x.

[99] Z. Li and J. Guan, “Hydrogels for Cardiac Tissue Engineering,” *Polymers*, vol. 3, no. 2, pp. 740–761, 2011, doi: 10.3390/polym3020740.

[100] J. H. Min, M. Patel, and W.-G. Koh, “Incorporation of Conductive Materials into Hydrogels for Tissue Engineering Applications,” *Polymers*, vol. 10, no. 10, 2018, doi: 10.3390/polym10101078.

[101] S. Bashir *et al.*, “Fundamental Concepts of Hydrogels: Synthesis, Properties, and Their Applications,” *Polymers*, vol. 12, no. 11, p. 2702, Nov. 2020, doi: 10.3390/polym12112702.

[102] A. Khandan, H. Jazayeri, M. D. Fahmy, and M. Razavi, “Hydrogels: Types, Structure, Properties, and Applications,” in *Frontiers in Biomaterials Biomaterials for Tissue Engineering*, vol. 4, Bentham Science Publisher, 2017, p. 143. [Online].

[103] X. Xue, Y. Hu, Y. Deng, and J. Su, “Recent Advances in Design of Functional Biocompatible Hydrogels for Bone Tissue Engineering,” *Adv. Funct. Mater.*, vol. 31, no. 19, p. 2009432, May 2021, doi: 10.1002/adfm.202009432.

[104] M. D. Shoulders and R. T. Raines, “Collagen Structure and Stability,” *Annual Review of Biochemistry*, vol. 78, no. Volume 78, 2009. Annual Reviews, pp. 929–958, 2009.

[105] N. Davari *et al.*, “Protein-Based Hydrogels: Promising Materials for Tissue Engineering,” *Polymers*, vol. 14, no. 5, 2022, doi: 10.3390/polym14050986.

[106] M. Cherim, A. Mustafa, E. Cadar, N. Lupaşcu, S. Paris, and R. Sirbu, “Collagen Sources and Areas of Use,” *Eur. J. Med. Nat. Sci.*, vol. 2, no. 2, pp. 8–13, 2019.

[107] D. Coppola *et al.*, “Marine Collagen from Alternative and Sustainable Sources: Extraction, Processing and Applications,” *Mar. Drugs*, vol. 18, no. 4, 2020, doi: 10.3390/md18040214.

[108] M. Ansari, A. Darvishi, and A. Sabzevari, “A review of advanced hydrogels for cartilage tissue engineering,” *Front. Bioeng. Biotechnol.*, vol. 12, 2024, doi: 10.3389/fbioe.2024.1340893.

[109] M. Kempf *et al.*, “A denatured collagen microfiber scaffold seeded with human fibroblasts and keratinocytes for skin grafting,” *Biomaterials*, vol. 32, no. 21, pp. 4782–4792, Jul. 2011, doi: 10.1016/j.biomaterials.2011.03.023.

[110] B. Wang, W. Yang, J. McKittrick, and M. A. Meyers, “Keratin: Structure, mechanical properties, occurrence in biological organisms, and efforts at bioinspiration,” *Prog. Mater. Sci.*, vol. 76, pp. 229–318, Mar. 2016, doi: 10.1016/j.pmatsci.2015.06.001.

[111] H. H. Bragulla and D. G. Homberger, “Structure and functions of keratin proteins in simple, stratified, keratinized and cornified epithelia,” *J. Anat.*, vol. 214, no. 4, pp. 516–559, Apr. 2009, doi: 10.1111/j.1469-7580.2009.01066.x.

[112] J. McKittrick, P.-Y. Chen, S. G. Bodde, W. Yang, E. E. Novitskaya, and M. A. Meyers, “The Structure, Functions, and Mechanical Properties of Keratin,” *JOM*, vol. 64, no. 4, pp. 449–468, Apr. 2012, doi: 10.1007/s11837-012-0302-8.

[113] S. Feroz, N. Muhammad, J. Ratnayake, and G. Dias, “Keratin - Based materials for biomedical applications,” *Bioact. Mater.*, vol. 5, no. 3, pp. 496–509, Sep. 2020, doi: 10.1016/j.bioactmat.2020.04.007.

[114] P. Hill, H. Brantley, and M. Van Dyke, “Some properties of keratin biomaterials: Kerateines,” *Biomaterials*, vol. 31, no. 4, pp. 585–593, Feb. 2010, doi: 10.1016/j.biomaterials.2009.09.076.

[115] L. N. Jones, M. Simon, N. R. Watts, F. P. Booy, A. C. Steven, and D. A. D. Parry, “Intermediate filament structure: hard α-keratin,” *12th Int. Biophys. Congr.*, vol. 68, no. 1, pp. 83–93, Oct. 1997, doi: 10.1016/S0301-4622(97)00013-6.

[116] L. R. Burnett *et al.*, “Hemostatic properties and the role of cell receptor recognition in human hair keratin protein hydrogels,” *Biomaterials*, vol. 34, no. 11, pp. 2632–2640, Apr. 2013, doi: 10.1016/j.biomaterials.2012.12.022.

[117] S. Reichl, M. Borrelli, and G. Geerling, “Keratin films for ocular surface reconstruction,” *Biomaterials*, vol. 32, no. 13, pp. 3375–3386, May 2011, doi: 10.1016/j.biomaterials.2011.01.052.

[118] S. Reichl, “Films based on human hair keratin as substrates for cell culture and tissue engineering,” *Biomaterials*, vol. 30, no. 36, pp. 6854–6866, Dec. 2009, doi: 10.1016/j.biomaterials.2009.08.051.

[119] S. Ye, C. Xie, O. T. Agar, C. J. Barrow, F. R. Dunshea, and H. A. R. Suleria, “Alginates from Brown Seaweeds as a Promising Natural Source: A Review of Its Properties and Health Benefits,” *Food Rev. Int.*, vol. 40, no. 9, pp. 2682–2710, Nov. 2024, doi: 10.1080/87559129.2023.2279583.

[120] J. Tan *et al.*, “Development of alginate-based hydrogels: Crosslinking strategies and biomedical applications,” *Int. J. Biol. Macromol.*, vol. 239, p. 124275, Jun. 2023, doi: 10.1016/j.ijbiomac.2023.124275.

[121] D. R. Sahoo and T. Biswal, “Alginate and its application to tissue engineering,” *SN Appl. Sci.*, vol. 3, no. 1, p. 30, Jan. 2021, doi: 10.1007/s42452-020-04096-w.

[122] R. M. Jarrah *et al.*, “Alginate hydrogels: A potential tissue engineering intervention for intervertebral disc degeneration,” *J. Clin. Neurosci.*, vol. 113, pp. 32–37, Jul. 2023, doi: 10.1016/j.jocn.2023.05.001.

[123] K. Y. Lee and D. J. Mooney, “Alginate: Properties and biomedical applications,” *Prog. Polym. Sci.*, vol. 37, no. 1, pp. 106–126, Jan. 2012, doi: 10.1016/j.progpolymsci.2011.06.003.

[124] R. Abka-khajouei, L. Tounsi, N. Shahabi, A. K. Patel, S. Abdelkafi, and P. Michaud, “Structures, Properties and Applications of Alginates,” *Mar. Drugs*, vol. 20, no. 6, 2022, doi: 10.3390/md20060364.

[125] M. Beata Łabowska, I. Michalak, and J. Detyna, “Methods of extraction, physicochemical properties of alginates and their applications in biomedical field – a review,” vol. 17, no. 1, pp. 738–762, 2019, doi: 10.1515/chem-2019-0077.

[126] L. Xia *et al.*, “Hierarchical macro-/meso-/microporous oxygen-doped carbon derived from sodium alginate: A cost-effective biomass material for binder-free supercapacitors,” *Mater. Des.*, vol. 182, p. 108048, Nov. 2019, doi: 10.1016/j.matdes.2019.108048.

[127] A. M. E. Matinong, Y. Chisti, K. L. Pickering, and R. G. Haverkamp, “Collagen Extraction from Animal Skin,” *Biology*, vol. 11, no. 6, 2022, doi: 10.3390/biology11060905.

[128] Ö. Erdemli, B. Yilmaz, İ. G. Saran, and E. Serin, “Sustainable biomaterials for tissue engineering: electrospun polycaprolactone fibers enriched with freshwater snail calcium carbonate and waste human hair keratin,” *Polym. Int.*, vol. 73, no. 10, pp. 833–843, Oct. 2024, doi: 10.1002/pi.6667.

[129] U. K. LAEMMLI, “Cleavage of Structural Proteins during the Assembly of the Head of Bacteriophage T4,” *Nature*, vol. 227, no. 5259, pp. 680–685, Aug. 1970, doi: 10.1038/227680a0.

[130] N. Jabeen, M. Sohail, A. Mahmood, S. Ahmed Shah, A. H. Mohammad Qalawlus, and T. Khaliq, “Nanocrystals loaded collagen/alginate-based injectable hydrogels: A promising biomaterial for bioavailability improvement of hydrophobic drugs,” *J. Drug Deliv. Sci. Technol.*, vol. 91, p. 105291, Jan. 2024, doi: 10.1016/j.jddst.2023.105291.

[131] M. Siaghi *et al.*, “Luteolin-incorporated fish collagen hydrogel scaffold: An effective drug delivery strategy for wound healing,” *Int. J. Pharm.*, vol. 657, p. 124138, May 2024, doi: 10.1016/j.ijpharm.2024.124138.

[132] A. Abou-Okeil and G. M. Taha, “Investigation and kinetics of hydrogel scaffold with sustained release ciprofloxacin hydrochloride,” *Polym. Bull.*, vol. 81, no. 18, pp. 17393–17411, Dec. 2024, doi: 10.1007/s00289-024-05495-4.

[133] B. Yilmaz, “Additive manufacturing and characterization of mathematically designed bone scaffolds based on triply periodic minimal surface lattices,” *Mech. Adv. Mater. Struct.*, vol. 31, no. 15, pp. 3492–3502, Aug. 2024, doi: 10.1080/15376494.2023.2177913.

[134] A. Pangjantuk, P. Kaokaen, P. Kunhorm, N. Chaicharoenaudomrung, and P. Noisa, "3D culture of alginate-hyaluronic acid hydrogel supports the stemness of human mesenchymal stem cells," *Sci. Rep.*, vol. 14, no. 1, p. 4436, Feb. 2024, doi: 10.1038/s41598-024-54912-1.

[135] X. Gong, Z. Liang, Y. Yang, H. Liu, J. Ji, and Y. Fan, "A resazurin-based, nondestructive assay for monitoring cell proliferation during a scaffold-based 3D culture process," *Regen. Biomater.*, vol. 7, no. 3, pp. 271–281, Jun. 2020, doi: 10.1093/rb/rbaa002.

[136] B. Barzaghini *et al.*, "Bone Marrow Mesenchymal Stem Cells Expanded Inside the Nichoid Micro-Scaffold: a Focus on Anti-Inflammatory Response," *Regen. Eng. Transl. Med.*, vol. 9, no. 4, pp. 494–505, Dec. 2023, doi: 10.1007/s40883-023-00296-z.

[137] Y. Li *et al.*, "Comparison of collagens extracted from swim bladder and bovine Achilles tendon," *Mater. Res. Express*, vol. 10, no. 5, p. 055403, May 2023, doi: 10.1088/2053-1591/acd379.

[138] S. N. Oslan, R. Shapawi, R. A. Mokhtar, W. N. Md. Noordin, and N. Huda, "Characterization of Acid- and Pepsin-Soluble Collagen Extracted from the Skin of Purple-Spotted Bigeye Snapper," *Gels*, vol. 8, no. 10, 2022, doi: 10.3390/gels8100665.

[139] L. Salvatore *et al.*, "An insight on type I collagen from horse tendon for the manufacture of implantable devices," *Int. J. Biol. Macromol.*, vol. 154, pp. 291–306, Jul. 2020, doi: 10.1016/j.ijbiomac.2020.03.082.

[140] E. M. Yelkuvan, Ö. Erdemli, B. Yilmaz, and Ö. Aktürk, "Evaluation of photochemically cross-linked collagen/gold nanoparticle composites as potential skin tissue scaffolds," *Turk. J. Chem.*, vol. 47, no. 1, p. Article 12, 2023.

[141] G. K. Pal and P. V. Suresh, "Physico-chemical characteristics and fibril-forming capacity of carp swim bladder collagens and exploration of their potential bioactive peptides by in silico approaches," *Int. J. Biol. Macromol.*, vol. 101, pp. 304–313, Aug. 2017, doi: 10.1016/j.ijbiomac.2017.03.061.

[142] A. Shubha, G. Sharmita, and L. Anita, “Production and characterization of human hair keratin bioplastic films with novel plasticizers,” *Sci. Rep.*, vol. 14, no. 1, p. 1186, Jan. 2024, doi: 10.1038/s41598-023-44905-x.

[143] J. Wang *et al.*, “Feather keratin hydrogel for wound repair: Preparation, healing effect and biocompatibility evaluation,” *Colloids Surf. B Biointerfaces*, vol. 149, pp. 341–350, Jan. 2017, doi: 10.1016/j.colsurfb.2016.10.038.

[144] O. A. Silva *et al.*, “Synthesis of Keratin Nanoparticles Extracted from Human Hair through Hydrolysis with Concentrated Sulfuric Acid: Characterization and Cytotoxicity,” *Materials*, vol. 17, no. 15, 2024, doi: 10.3390/ma17153759.

[145] J. M. Mohamed *et al.*, “Human Hair Keratin Composite Scaffold: Characterisation and Biocompatibility Study on NIH 3T3 Fibroblast Cells,” *Pharmaceuticals*, vol. 14, no. 8, 2021, doi: 10.3390/ph14080781.

[146] H. Zhang, F. Carrillo-Navarrete, M. López-Mesas, and C. Palet, “Use of Chemically Treated Human Hair Wastes for the Removal of Heavy Metal Ions from Water,” *Water*, vol. 12, no. 5, 2020, doi: 10.3390/w12051263.

[147] L. Hou and P. Wu, “Exploring the hydrogen-bond structures in sodium alginate through two-dimensional correlation infrared spectroscopy,” *Carbohydr. Polym.*, vol. 205, pp. 420–426, Feb. 2019, doi: 10.1016/j.carbpol.2018.10.091.

[148] H. Daemi and M. Barikani, “Synthesis and characterization of calcium alginate nanoparticles, sodium homopolymannuronate salt and its calcium nanoparticles,” *Sci. Iran.*, vol. 19, no. 6, pp. 2023–2028, Dec. 2012, doi: 10.1016/j.scient.2012.10.005.

[149] Helmiyati and M. Aprilliza, “Characterization and properties of sodium alginate from brown algae used as an ecofriendly superabsorbent,” *IOP Conf. Ser. Mater. Sci. Eng.*, vol. 188, no. 1, p. 012019, Apr. 2017, doi: 10.1088/1757-899X/188/1/012019.

[150] A. Belhachem *et al.*, “Study of the antibacterial activity of hybrid nanocomposites ‘metal oxide/alginate’ synthesized for therapeutic purposes,” *Discov. Med.*, vol. 1, no. 1, p. 145, Dec. 2024, doi: 10.1007/s44337-024-00147-y.

[151] Z. Belattmania *et al.*, "Isolation and FTIR-ATR and 1H NMR Characterization of Alginates from the Main Alginophyte Species of the Atlantic Coast of Morocco," *Molecules*, vol. 25, no. 18, 2020, doi: 10.3390/molecules25184335.

[152] H. Ju, X. Liu, G. Zhang, D. Liu, and Y. Yang, "Comparison of the Structural Characteristics of Native Collagen Fibrils Derived from Bovine Tendons Using Two Different Methods: Modified Acid-Solubilized and Pepsin-Aided Extraction," *Materials*, vol. 13, no. 2, 2020, doi: 10.3390/ma13020358.

[153] P. Hartrianti *et al.*, "Modulating Mesenchymal Stem Cell Behavior Using Human Hair Keratin-Coated Surfaces," *Stem Cells Int.*, vol. 2015, no. 1, p. 752424, Jan. 2015, doi: 10.1155/2015/752424.

[154] J. Gao *et al.*, "Human hair keratins promote the regeneration of peripheral nerves in a rat sciatic nerve crush model," *J. Mater. Sci. Mater. Med.*, vol. 30, no. 7, p. 82, Jul. 2019, doi: 10.1007/s10856-019-6283-1.

[155] A. Mukherjee, Y. H. Kabutare, and P. Ghosh, "Dual crosslinked keratin-alginate fibers formed via ionic complexation of amide networks with improved toughness for assembling into braids," *Polym. Test.*, vol. 81, p. 106286, Jan. 2020, doi: 10.1016/j.polymertesting.2019.106286.

[156] A. Sionkowska, K. Kulka-Kamińska, P. Brudzyńska, K. Lewandowska, and Ł. Piwowarski, "The Influence of Various Crosslinking Conditions of EDC/NHS on the Properties of Fish Collagen Film," *Mar. Drugs*, vol. 22, no. 5, 2024, doi: 10.3390/md22050194.

[157] M. Yan *et al.*, "Effects of cross-linking with EDC/NHS and genipin on characterizations of self-assembled fibrillar gel prepared from tilapia collagen and alginate," *Polym. Degrad. Stab.*, vol. 200, p. 109929, Jun. 2022, doi: 10.1016/j.polymdegradstab.2022.109929.

[158] Y. D. Nokoorani, A. Shamloo, M. Bahadoran, and H. Moravvej, "Fabrication and characterization of scaffolds containing different amounts of allantoin for skin tissue engineering," *Sci. Rep.*, vol. 11, no. 1, p. 16164, Aug. 2021, doi: 10.1038/s41598-021-95763-4.

[159] I. M. Savić Gajić, I. M. Savić, and Z. Svirčev, “Preparation and Characterization of Alginate Hydrogels with High Water-Retaining Capacity,” *Polymers*, vol. 15, no. 12, 2023, doi: 10.3390/polym15122592.

[160] N. Tuancharoensri *et al.*, “Porous Poly(2-hydroxyethyl methacrylate) Hydrogel Scaffolds for Tissue Engineering: Influence of Crosslinking Systems and Silk Sericin Concentration on Scaffold Properties,” *Polymers*, vol. 15, no. 20, 2023, doi: 10.3390/polym15204052.

[161] J. L. Holloway, H. Ma, R. Rai, and J. A. Burdick, “Modulating hydrogel crosslink density and degradation to control bone morphogenetic protein delivery and in vivo bone formation,” *Elev. Int. Nanomedicine Drug Deliv. Symp.*, vol. 191, pp. 63–70, Oct. 2014, doi: 10.1016/j.jconrel.2014.05.053.

[162] A. Wierzbicka, M. Bartniak, J. Waśko, B. Kolesińska, J. Grabarczyk, and D. Bociaga, “The Impact of Gelatin and Fish Collagen on Alginate Hydrogel Properties: A Comparative Study,” *Gels*, vol. 10, no. 8, 2024, doi: 10.3390/gels10080491.

[163] Y. Jing *et al.*, “The Synthesis, Characterization, and Protein-Release Properties of Hydrogels Composed of Chitosan-Zingiber offcinale Polysaccharide,” *Foods*, vol. 11, no. 18, 2022, doi: 10.3390/foods11182747.

[164] T. Jiao *et al.*, “Properties of Collagen/Sodium Alginate Hydrogels for Bioprinting of Skin Models,” *J. Bionic Eng.*, vol. 20, no. 1, pp. 105–118, Jan. 2023, doi: 10.1007/s42235-022-00251-8.

[165] J. Skopinska-Wisniewska, M. Tuszynska, Ł. Kaźmierski, M. Bartniak, and A. Bajek, “Gelatin–Sodium Alginate Hydrogels Cross-Linked by Squaric Acid and Dialdehyde Starch as a Potential Bio-Ink,” *Polymers*, vol. 16, no. 18, 2024, doi: 10.3390/polym16182560.

[166] H. Chavda and C. Patel, “Effect of crosslinker concentration on characteristics of superporous hydrogel,” *Int. J. Pharm. Investig.*, vol. 1, no. 1, p. 17.

[167] C. G. Gomez, C. I. Alvarez Igarzabal, and M. C. Strumia, “Effect of the crosslinking agent on porous networks formation of hema-based copolymers,” *Polymer*, vol. 45, no. 18, pp. 6189–6194, Aug. 2004, doi: 10.1016/j.polymer.2004.06.053.

[168] J. G. Rheinwatd and H. Green, “Seria cultivation of strains of human epidemal keratinocytes: the formation keratinizin colonies from single cell is,” *Cell*, vol. 6, no. 3, pp. 331–343, Nov. 1975, doi: 10.1016/S0092-8674(75)80001-8.

[169] C. M. Gabbott and T. Sun, “Comparison of Human Dermal Fibroblasts and HaCat Cells Cultured in Medium with or without Serum via a Generic Tissue Engineering Research Platform,” *Int. J. Mol. Sci.*, vol. 19, no. 2, 2018, doi: 10.3390/ijms19020388.

[170] K. Iyer, Z. Chen, T. Ganapa, B. M. Wu, B. Tawil, and C. S. Linsley, “Keratinocyte Migration in a Three-Dimensional In Vitro Wound Healing Model Co-Cultured with Fibroblasts,” *Tissue Eng. Regen. Med.*, vol. 15, no. 6, pp. 721–733, Dec. 2018, doi: 10.1007/s13770-018-0145-7.

[171] T. P. Lehmann *et al.*, “Co-culture of human nucleus pulposus cells with multipotent mesenchymal stromal cells from human bone marrow reveals formation of tunnelling nanotubes,” *Mol. Med. Rep.*, vol. 9, no. 2, pp. 574–582.

APPENDICES

A. SDS-PAGE BUFFERS AND SOLUTIONS

Laemmli Sample Loading Buffer (4x)	**10 mL**
1 M Tris-HCl, pH 6.8	2.50 mL
20% Glycerol	4.00 mL
10% 2-mercaptoethanol	2.00 mL
4% SDS	0.800 g
Bromophenol blue	0.001 g
Distilled Water (dH_2O)	1.50 mL
7.5 % Separating Gel for Collagen	**10 mL**
30% Acrylamide/2% Bisacrylamide solution	2.48 mL
1.5 M Tris, pH 8.7-8.8	2.50 mL
10% SDS	100 µL
dH_2O	4.80 mL
10% Ammonium persulfate (APS)	100 µL
TEMED	10.0 µL
10% Separating Gel for Keratin	**10 mL**
30% Acrylamide/2% Bisacrylamide solution	3.33 mL
1.5 M Tris, pH 8.7-8.8	2.50 mL
10% SDS	100 µL
Distilled Water (dH_2O)	4.10 mL
10% APS	100 µL
TEMED	10 µL

4% Stacking Gel for Both	**10 mL**
30% Acrylamide/2%Bisacrylamide solution	650 µL
0.5 M Tris, pH 6.7-6.8	1.25 mL
10% SDS	50 µL
dH_2O	3.10 mL
10% APS	50 µL
TEMED	5 µL
Gel Staining Solution	**500 mL**
0.25 g Coomassie Bright Blue R250	125 mL in isopropanol
Glacial Acetic Acid	50 mL
dH2O	325 mL
De-Staining Solution	**300 mL**
10% Isopropanol	30 mL
5% Acetic Acid	15 mL
dH2O	255 mL

B. CALIBRATION CURVE OF THE BCA ASSAY